Systematic understanding of chemical process in solution

Kenji Iida

2012

Preface

Chemical process in solution is ubiquitous, but this ubiquitous process yet remains unclear in many respects. Although a variety of computational methods to describe the process in solution have been developed so far, it is difficult to understand the process only by the calculation. While an enormous amount of numerical data becomes available by the methods, it is not straightforward to find out the main factor governing the process at the molecular-level without appropriate analysis or consideration. Because of the complexity of the computational procedure, it is often difficult to understand the cause-and-effect relationship. Further theoretical consideration of the obtained data is therefore indispensable to systematically understand the process.

In this thesis, the author wishes to systematically understand the chemical process in solution based on molecular orbital in solution phase as well as on solvation structure. From chapter 1 to 3, chemical reactions in solution are studied. The mechanism is discussed in terms of solvation structure and the change of electronic structure by solvation. The electronic structure is characterized by orbital energy and resonance structure. In chapter 4, the orbital energy shift by solvation is studied. The mechanism of the shift is systematically understood with the aid of the dielectric continuum theory. In chapter 5, the ionization in aqueous solution is studied. The change of ionization energy by solvation and the spectral width of vertical ionization are discussed in terms of the solute size, its charge, and the solvation structure. In chapter 6, the solvation structure near the solid-liquid interface is studied. A new theory based on the integral equation theory is developed, focusing on the distinguishing feature of the interface from bulk phase, namely, the anisotropy of solvation structure.

The studies presented in this thesis were carried out at the Department of Molecular Engi-

neering, Graduate School of Engineering, Kyoto University from 2006 to 2012. The author would like to express his deepest appreciation to Professor Hirofumi Sato for his helpful discussion, interesting suggestions, and encouragement. His various comments based on theoretical and physical chemistries were invaluable for this study. The author wishes to express his sincere gratitude to Prof. Shigeyoshi Sakaki for his helpful discussion and suggestions. The author also expresses gratitude to Associate Professor Yoshihide Nakao for his technical supports.

The author is very much thankful to Dr. Atsushi Ikeda, and Dr. Daisuke Yokogawa for their kind helps and cooperation. The author is also grateful to Mr. Hideo Ando, Mr. Kentaro Kido, and Mr. Seigo Hayaki. Scientific talks with them on various occasions were very enjoyable and fruitful to him. Acknowledgement is also made to all members of the research group of Prof. Shigeyoshi Sakaki and Prof. Hirofumi Sato. The discussion with them was stimulative and exciting for him to induce and activate the motivation of the studies.

The author thanks Japan Society for the Promotion of Science (JSPS) for financial support (Grant-in-Aid for JSPS Fellows).

Finally, the author sincerely thanks his parents, Koji and Hiroko Iida, for their understanding, encouragement, and continuous support.

Kenji Iida

January, 2012

Contents

General introduction

1 Problems to understand chemical process in solution

Chemical process in solution is ubiquitous, but this ubiquitous process yet remains unclear in many respects.[1,2] For molecular system in the gas phase, a variety of chemical process is in general understood based on the property of each molecule alone. However, it is difficult to understand the process in the solution phase in a similar manner.

One of the problems to understand the process is its complexity. Solution consists of vast number of fluctuating molecules that interact with each other. The interaction and fluctuation characterize the solution as being completely different from the gas and solid phase. However, it is in practice impossible to investigate all of each molecule dealing with the interaction with other molecules. Another problem is the variety of solution. The property of solution variates dependent on the solvent molecule, the concentration, the combination of solute and solvent and so on. It is thus indispensable to reveal common characteristic among a variety of solution by finding out a factor governing the process at the molecular-level and thereon by systematically understanding how the factor governs the process.

2 Theory for chemical process in solution

In the field of solution chemistry, solution is often treated by separating into two components. One is solute molecule, which is the core of chemical process and the other is solvent molecules surrounding the solute. Both of them are treated using well-established theoretical formula, respectively. The property of solute molecule is characterized by the electronic structure because chemical processes, such as chemical reaction, photo absorption and emission, are

attributed to the change of electronic structure. In quantum chemistry, the electronic structure is described by wave function. Ab-initio electronic structure calculations (e.g. Hartree-Fock, B3LYP) have been established as a tool to obtain the wave function, and have successfully contributed to obtain the knowledge of molecular property (e.g. polarity) and molecular structure. Recently, highly-accurate quantum chemical calculations such as a post Hartree-Fock method (e.g. CCSD(T), CASSCF) are extensively performed according to the development of computational resource. The accuracy allows to obtain the reliable knowledge of molecular stability.[3,4] These methods have successfully applied to complicated molecules such as organometallic compounds.[5]

On the other hand, there is no unique way to treat solvent, which consists of vast number of molecules. In the dielectric continuum theory, solvent is macroscopically treated as continuum medium with dielectric permittivity ϵ. The solvent is represented only by this one parameter ϵ, and this simplicity makes the consideration of the solvation effect easy. Born's equation for solvation free energy (ΔG) of ion is the representative of the theory,[6,7]

$$\Delta G = -\frac{1}{2}\left(1 - \frac{1}{\epsilon}\right)\frac{Q^2}{a}, \tag{1}$$

where Q is the solute charge and a is ionic radius. Eq. (1) describes the dependency of ΔG on solute size (a) and its charge (Q). However, the dielectric continuum theory cannot describe solvent at the molecular-level.

The treatment based on the statistical mechanics allows us to describe solvent at the molecular-level. Molecular simulation and reference interaction site model (RISM) are the representative methods to obtain the insight based on statistical mechanics. In these methods, the structural property of solvent is commonly characterized with pair correlation function (PCF), which describes the one-dimensional density distribution of solvent molecules. Fig. 1 is PCF of water oxygens calculated with molecular dynamics simulation.[8] PCF well describes the structural feature of fluctuating molecules: the peak top represents the relative distance of oxygen atoms, and the peak width reflects the thermal fluctuation. Unifying the insights by the dielectric continuum theory and the statistical mechanics, solvation effect is understood associated with molecular properties of solute and solvent.

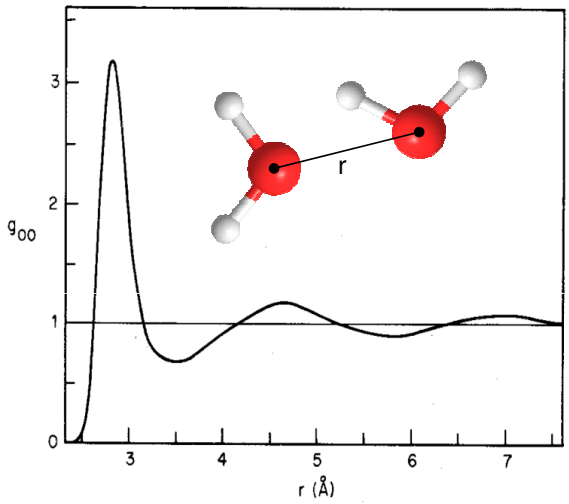

Figure 1: Pair correlation function between water oxygens (O-O) calculated with molecular dynamics simulation.[8]

Chemical processes in solution are studied by combining the aforementioned electronic structure theory and the method for solvation. Fig. 2 shows the representative methods. In polarizable continuum theory (PCM, Fig. 2(a)), solvent is treated with the dielectric continuum theory.[1,6,7] Quantum Mechanics/Molecular Mechanics (QM/MM, Fig. 2(b)) is another representative.[3] In this method, solvent molecules are explicitly treated with molecular simulation. RISM-SCF (Fig. 2(c)) is recognized as an alternative to QM/MM.[2,9,10] In this theory, solvent is treated by RISM, which analytically yields PCFs.[2,11,12] All these methods have been successfully applied to a variety of chemical processes in solution.[13–15]

While an enormous amount of numerical data becomes available by the methods, it is not straightforward to find out the main factor governing the process at the molecular-level. Appropriate analysis or consideration is indispensable in order to select the relevant data to describing the factor from such an enormous amount of data. To obtain the systematic understanding is not also straightforward because of the complexity of computational procedure. The methods to solve Shrödinger equation and/or RISM equation usually consist of several iterative calculations. The numerical solution is given only after the complicated computation. It is thus difficult to understand why such a result is obtained by the calculation, namely the cause-and-effect relationship. Further theoretical consideration of the numerical data is therefore

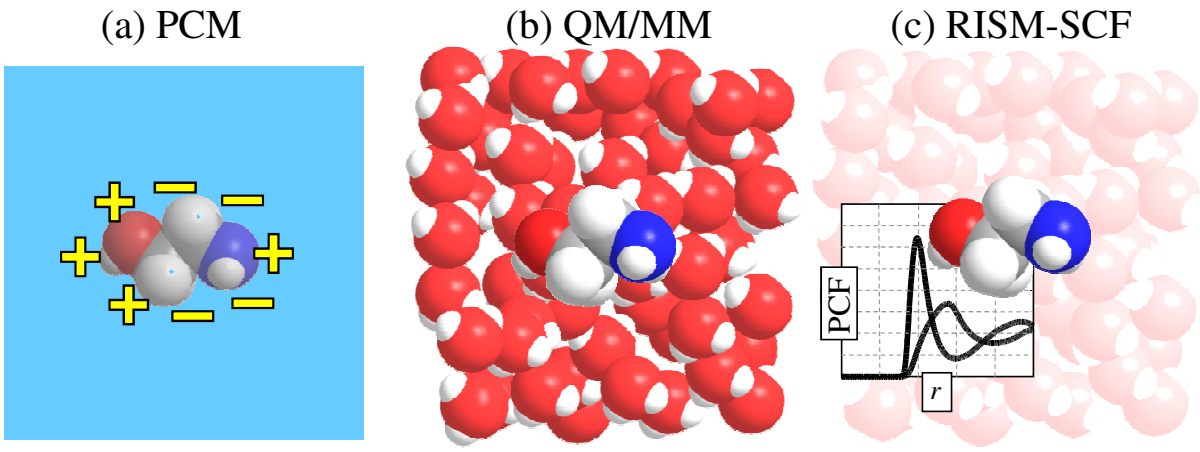

Figure 2: Methods to treat chemical process in solution. (a): PCM; (b): QM/MM; (c): RISM-SCF.

indispensable to understand the chemical process in solution.

3 To systematically understand chemical process in solution

Many-electron wave function of solute molecule is commonly represented based on one-electron wave function called molecular orbital (MO). The properties of molecule described with many-electron wave function can be separately described with each one-electron wave function. In particular, the highest occupied molecular orbital (HOMO) and lowest unoccupied molecular orbital (LUMO) are responsible for a variety of chemical phenomena. According to the frontier orbital theory, the reactivity is attributed to the energy difference between these orbitals and phases.[16] Many of photo absorption and emission processes are also systematically understood using these orbitals. Within the framework of Hartree-Fock theory, MO of isolated molecule is defined as follows:[17]

$$\hat{F}\left|\psi_i\right\rangle = \varepsilon_i \left|\psi_i\right\rangle , \tag{2}$$

where $\hat{F}$ is the Fock operator, $|\psi_i\rangle$ and ε_i are respectively i-th MO and its orbital energy.

Since MO is a fundamental concept, it would be natural to utilize the same concept in order to understand the chemical process in solution phase. Since the solvation effect is recognized as "external field" generated by the surrounding solvent, the extended formula of Hartree-Fock

equation incorporating the field is given as follows:[2,6]

$$\left[\hat{F} + \hat{V}\right] |\psi_i^s\rangle = \varepsilon_i^s \, |\psi_i^s\rangle \, , \tag{3}$$

where $\hat{V}$ is the filed due to the surrounding solvent. Eq. (3) provides MO ($|\psi_i^s\rangle$) and orbital energy (ε_i^s) in *solution phase*. Of course, they have the same physical meaning as those in the isolated state, and chemical process in solution should be understood in a similar manner. The change of MO and its energy shift by solvation, $|\psi_i^s\rangle - |\psi_i\rangle$ and $\varepsilon_i^s - \varepsilon_i$, would be regarded as the factors characterizing the role of solvation in chemical process.

Notice that $\hat{V}$ is not yet explicitly defined. Since the change of MO and its energy shift by solvation are determined by $\hat{V}$, it is essentially important to clarify the dependency of $\hat{V}$ on molecular properties of solute and solvent in order to understand the process in solution.

For example, $\hat{V}$ can be described by utilizing PCFs between solute atom A and solvent site s, $g_{As}(r)$, as follows:

$$\hat{V}^{\mathrm{PCF}} \;=\; \sum_A \hat{b}_A \sum_s \rho \int_0^\infty 4\pi r^2 g_{As}(r) \frac{q_s}{r} dr, \tag{4}$$

where $\hat{b}_A$ is an appropriate population operator on atom A, ρ is number density of solvent, and q_s is charge of atomic site of solvent molecule. Using Eqs. (3) and (4), solvation effect on MO and its energy is discussed associated with molecular level information of solvent distribution. It is noted, however, the relationship between ε_i^s and $\hat{V}$ (or $g_{As}(r)$) is not simple because of the complexity of computational procedure to solve Eq. (3)

Similarly, the dielectric continuum theory is also used to represent the field although it does not deal with the solute-solvent interaction at the molecular-level. For example, $\hat{V}$ for an ion with charge Q could be given as,[7]

$$\hat{V}^{\mathrm{Born}} = -\hat{b}_A \left(1 - \frac{1}{\epsilon}\right) \frac{Q}{a}. \tag{5}$$

4 Purpose in this thesis

The purpose in this thesis is to systematically understand the chemical process in solution based on molecular property of solute and solvent. The mechanism of the process is thus

discussed from the two point of view. One is the change of electronic structure of solute. To characterize the electronic structure, the molecular orbital in solution is employed. The other point is solvation structure, which reveals the role of solvent in the process at the molecular-level.

4.1 Chemical reaction in solution

From chapter 1 to 3, chemical reaction in solution is studied. The reaction between CO_2 and OH^- in aqueous solution,

$$CO_2 + OH^- \rightarrow HCO_3^-, \tag{6}$$

is found in various aspects of the earth's natural systems such as ocean and biological processes. It is known that there is no barrier to this reaction in the gas phase, whereas this reaction has 13.3 kcal mol^{-1} of the barrier in the aqueous solution.[18]

The purpose in chapter 1 is to clarify the barrier origin. According to the frontier orbital theory, the reactivity is well described by the orbital energy differences. The change of reactivity should thus be explained with the orbital energy shifts by solvation. The reaction mechanism is then investigated focusing on the change of PCF along the reaction.

In chapter 2 and 3, chemical reaction between monoethanol amine ($CH_2OHCH_2NH_2$; MEA) and CO_2 is studied. It is well known that this reaction proceeds in two steps. The first is the bond formation between MEA and CO_2,

$$CH_2OHCH_2NH_2 + CO_2 \rightarrow CH_2OHCH_2NH_2\text{-}CO_2. \tag{7}$$

Then a proton transfer occurs from the MEA-CO_2 complex to a base (B),

$$\begin{aligned} CH_2OHCH_2NH_2\text{-}CO_2 \;+\; & B \\ \rightarrow\; & CH_2OHCH_2NHCOO^- + BH^+ . \end{aligned} \tag{8}$$

The purpose in chapter 2 is to clarify the role of solvation in the bond formation step (7). The orbital analysis method for resonance structure[19] is performed to characterize the change of electronic structure. Based on the insight obtained from the resonance structure analysis, the

role of solvation in the reaction is discussed at the molecular-level, focusing on the change of PCF along the reaction.

In chapter 3, the proton transfer step (8) is studied. The purpose in chapter 3 is to clarify which MEA or H_2O acts as the base B, and thereon to clarify the origin of stabilization of final product. The stability is discussed in terms of the bonding nature and the solvation structure.

4.2 Electronic structure change by solvation

The purpose of chapter 4 is to clarify the mechanism of orbital energy shift by solvation effect. The mechanism have not been explained neither logically nor comprehensively in any literature. This is because of the complexity to evaluate the shift. As seen from Eqs. (3) and (4), $\hat{V}$ and orbital energy are dependent with each other. These equations are thus iteratively solved, and the shift of orbital energy is obtained only as the result of this iteration.

With the aid of the dielectric continuum theory, the simple theoretical framework for orbital energy shift is proposed. This framework allows to systematically understand the mechanism of orbital energy shift in terms of solvation structure and polarity of solute.

In chapter 5, ionization in solution phase is studied. Recently, vertical ionization energy in aqueous solution is measured, and it is shown that the energy is significantly different form gas-phase value.[20] It's also shown that the spectral width in the solution significantly broadens caused by thermal fluctuation of solvent molecule.[20] The purposes in chapter 5 is to understand the mechanism of the change of energy and that of the broadening by solvation. The role of solvent in ionization is discussed by using solvation structure in order to clarify the role of solute-solvent interaction at the molecular-level, comparing with the dielectric continuum theory. With the aid of the dielectric continuum theory, the simple formulas describing the change and broadening by solvation are then derived to discuss the ionization in terms of the property of solute molecule such as solute size and its charge.

4.3 Solvation near solid-liquid interface

While solvent is recognized as homogeneous liquid so far, solvation near the solid-liquid interface could also play the crucial role in various chemical process near electrode. Although there are commonly used theories in the basis of dielectric continuum theory (e.g. the electric double layer theory by Hermholtz, Gouy, and Chapman), more sophisticated theory to understand the molecular-level insight into solvent near the interface is required in relation to the necessity of developing new electrode system. Various experimental or theoretical methods are developed to obtain the molecular-level description of the solvent near the interface.[21–28]

In chapter 6, the solvation near the solid-liquid interface is investigated. The purpose is to develop the theory describing the feature of solvation near the interface. To describe the feature, the anisotropy of solvation structure near the interface is focused on. The developed equation in this study describes the anisotropic solvation structure as two-dimensional (2D) density distribution in a cylindrical coordinate system. The 2D distribution is along two directions, one of which is perpendicular to the interface and the other is parallel to the interface. Using the developed equation, solvation structure near the interface is discussed at the molecular-level.

Bibliography

[1] *Continuum Solvation Models in Chemical Physics*, eds. B. Mennucci and R. Cammi, John Wiley & Sons, Chichester, 2007.

[2] *Molecular Theory of Solvation, Understanding Chemical Reactivity*, ed. F. Hirata, Springer, 2003.

[3] F. Jensen, *Introduction to computational chemistry*, 2nd Ed. Wiley, Chichester, 2007.

[4] T. Helgaker, P. Jørgensen, J. Olsen, *Molecular Electronic-Structure Theory*, Wiley, Chichester, 2000.

[5] S. Sakaki, Y. Ohnishi, H. Sato, *Chem. Rec.*, **10**, 29 (2010).

[6] J. Tomasi, B. Mennucci, R. Cammi, Chem. Rev., **105**, 2999 (2005).

[7] C. J. F. Bottcher, *Theory of Electric Polarization*, Elsevier, Amsterdam (1983).

[8] F. H. Stilinger, A. Rahman, J. Chem. Phys., **60**, 1545 (1974).

[9] S. Ten-no, F. Hirata, S. Kato, J. Chem. Phys., **100**, 7443 (1994).

[10] H. Sato, F. Hirata, S. Kato, J. Chem. Phys., **105**, 1546 (1996).

[11] J. -P. Hansen, I. R. McDonald, *Theory of Simple Liquids*, 3nd Ed. Academic, London, 2006.

[12] C. G. Gray, K. E. Gubbins, *Theory of Molecular Fluids*, Vol. 1, Clarendon Press, Oxford, New York, 1984.

[13] J. Gao, Acc. Chem. Res., **29**, 298 (1996).

[14] S. Hayaki, K. Kido, D. Yokogawa, H. Sato, S. Sakaki, J. Phys. Chem. B, **113**, 8227 (2009).

[15] Y. Tateyama, J. Blumberger, T. Ohno, M. Sprik, J. Chem. Phys., **126**, 204506 (2007).

[16] K. Fukui, Science, **218**, 747 (1982).

[17] A. Szabo and N. S. Ostlund, *Modern Quantum Chemistry*.

[18] B.R.W. Pinsent, L. Pearson, F.J.W. Roughton, Trans. Faraday Soc., **52**, 1512 (1956).

[19] (a) A. Ikeda, Y. Nakao, H. Sato, S. Sakaki, J. Phys. Chem. A, **110**, 9028 (2006). (b) A. Ikeda, D. Yokogawa, H. Sato, S. Sakaki, Chem. Phys. Lett., **424**, 499 (2006). (c) A. Ikeda, D. Yokogawa, H. Sato, S. Sakaki, Int. J. Quantum. Chem., **107**, 3132 (2007). (d) A. Ikeda, Y. Nakao, H. Sato, S. Sakaki, J. Chem. Theory Comp., **5**, 1741 (2009).

[20] B. Winter, M. Faubel, Chem. Rev., **106**, 1176 (2006).

[21] T. Fukuma, K. Kobayashi, K. Matsushige, H. Yamada, Appl. Phys. Lett., **87**, 034101 (2005).

[22] Z. D. Schultz, S. K. Shaw, A. A. Gewirth, J. Am. Chem. Soc., **127**, 15916 (2005).

[23] H. Noguchi, T. Okada, K. Uosaki, Faraday Discuss., **140**, 125 (2008).

[24] M. F. Toney, J. N. Howard, J. Richer, G. L. Borges, J. G. Gordon, O. R. Melroy, D. G. Wiesler, D. Yee, L. B. Sorensen, Nature, **368**, 444 (1994).

[25] S. K. Reed, O. J. Lanning, P. A. Madden, J. Chem. Phys., **126**, 084704 (2007).

[26] E. Spohr, J. Phys. Chem., **93**, 6171 (1989).

[27] A. Kovalenko, F. Hirata, Chem. Phys. Lett., **290**, 237 (1998).

[28] J. J. Howard, J. S. Peryns, B. M. Pettitt, J. Phys. Chem. B, **114**, 6074 (2010).

Chapter 1

The barrier origin on the reaction of CO_2 + OH^- in aqueous solution

1.1 Introduction

The reaction of carbon dioxide with hydroxide anion in aqueous solution,

$$CO_2 + OH^- \rightarrow HCO_3^- \tag{1.1}$$

is found in various aspects of the earth's natural systems such as ocean and biological processes. It is known that there is no barrier to this reaction in the gas phase, whereas 13.3 kcal mol^{-1} of the barrier height is observed in the aqueous solution.[1] In this regard, it is the solvation effect that governs the characteristic of this ubiquitous reaction.

As a benchmark system of the solvation effect, several theoretical studies on this reaction have so far been reported.[2–4] For example, Davidson et al. show that the dielectric continuum model with density functional theory (DFT) can yield acceptable estimation of the energy change along the reaction pathway.[2] However, detailed information on the solvation phenomenon is yet unknown since the solvation process is oversimplified in this model.

Since solvation free energy is closely related to the solvation structure, explicit treatment of the structure in molecular level is often essential to understand chemical reactions. Generally speaking, however, the evaluation of the free energy based on molecular simulation methods such as QM/MM requires high cost of computations. Moreover, the electronic polarization effect on the solute molecule is indispensable because the electron clouds of OH^- is considered to be sensitive to the electrostatic environment.[5,6] An accurate evaluation on the polarization

effect by quantum chemical calculation is necessary to understand the mechanism of the reaction. During our work, Leung et al. reported ab initio molecular dynamics (AIMD) study with the similar purpose to ours.[7]

In this Letter, we study the origin of the barrier by using the RISM-SCF method.[8,9] Since the reference interaction site model (RISM)[10,11] deals with the solvation process in analytical description based on the statistical mechanics for molecular liquids, the solvation structure and free energy can be evaluated with a reasonable cost of computations. It is another advantage, in comparison with widely used molecular simulation methods such as MD, the analytical treatment in RISM enables us to analyze the free energy in terms of atomic or spatial contributions. Furthermore RISM-SCF, in which RISM is coupled with quantum molecular orbital theory, provides an accurate treatment on the electronic polarization effect on the reaction system. Now this combinational method can shed a new light on the understanding of the reaction both from quantum chemistry and from statistical mechanics.

1.2 Method

The details of the RISM-SCF method have been reported in previous papers.[8,9] In the present study, we employ the new-generation of RISM-SCF, in which the spatial electron density distribution (SEDD) is explicitly treated, RISM-SCF-SEDD.[12] This method removes the dependency on the grid required in the charge fitting procedure in the original version of RISM-SCF. It is also noted that the RISM-SCF-SEDD is much more robust in the connection between RISM and MO calculation. It was very difficult to obtain the RISM-SCF solution for the present system by using the original version.

All calculations were carried out at MP2 level using 6-311++G** basis set. For the results reported in the previous study,[2] this level of computation is considered to provide the energy curve with reliable accuracy. RISM-SCF calculation was performed by GAMESS program.[13] The Lennard-Jones parameters of the solute were taken from Refs.[14,15] ($\sigma_{\mathrm{C}} = 3.296$ Å, $\sigma_{\mathrm{O}} = 3.166$ Å, $\sigma_{\mathrm{H}} = 1.000$ Å, $\epsilon_{\mathrm{C}} = 0.120$ kcal/mol, $\epsilon_{\mathrm{O}} = 0.155$ kcal/mol, $\epsilon_{\mathrm{H}} = 0.056$ kcal/mol) and SPC-like water was assumed for the solvent[16] ($\sigma_{\mathrm{O}} = 3.166$ Å, $\sigma_{\mathrm{H}} = 1.000$ Å, $\epsilon_{\mathrm{O}} = 0.155$ Å,

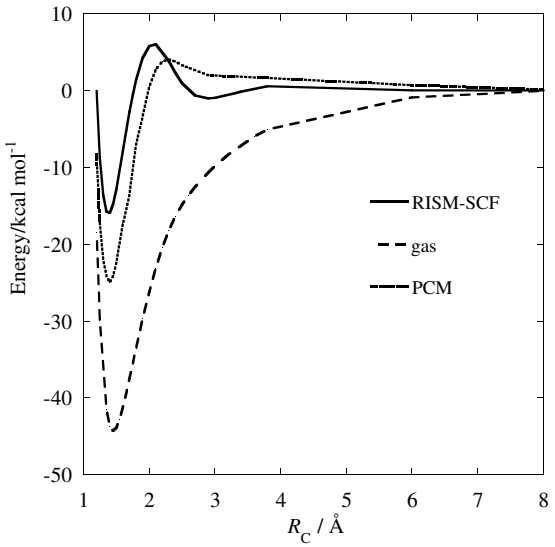

Figure 1.1: Total energy along the reaction coordinate in gas (dashed line) and in solute calculated by RISM-SCF (solid line), PCM (dotted line).

$\epsilon_{\mathrm{H}} = 1.000$ Å). The solvent water density was set to 1 g/cm^3 at T =298.15 K. The RISM equation was solved with HNC closure.[17] Polarization continuum model (PCM) calculations were also performed by using Gaussian03 program package[18] for comparison. The cavity radii were set equal to those used in RISM-SCF calculation.

The distance between the carbon atom and the oxygen atom of hydroxide anion was taken as the reaction coordinate (R_{C}) to focus on the bond-making process in the reaction. The potential energy curve in the gas phase was computed along R_{C} by optimizing all of the other degrees of freedom by using the standard MP2/6-311++G**. Computations in the aqueous solution phase were then carried out with the RISM-SCF-SEDD and PCM methods with these gas-phase geometries, because we wished to exclude the contribution of the geometrical difference to the electronic structure.

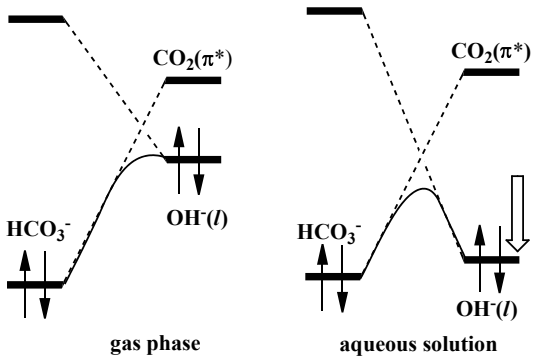

Figure 1.2: Change in the energy gap of reactant and product in gas and in aqueous solution.

1.3 Results and discussion

1.3.1 Total energy profile of the reaction

Figure 1.1 shows the energy profile along R_{C} calculated by the standard MP2/6-311++G** (gas phase), RISM-SCF and PCM (aqueous phase) methods. As the reaction proceeds from the reactant (CO_2+OH^-; right-hand side) to the product (HCO_3^-; left-hand side), the total energy monotonically decreases without barrier in the gas phase. On the other hand, both RISM-SCF and PCM calculations surely show the barrier around $R_{\mathrm{C}} = 2.1$Å in aqueous phase. The height of the barrier in aqueous solution is 6.1 kcal mol^{-1} (RISM-SCF) and 4.1 kcal mol^{-1} (PCM). The RISM-SCF value is close to 7.1 kcal mol^{-1} obtained by AIMD,[7] which corresponds to the present model. The profile of the barrier looks sharper in the RISM-SCF result than that in PCM, which should be related to the explicit treatment of the solvent in the RISM-SCF method such as hydrogen bonding. The free energy change of the reaction in aqueous solution is also quite different, and the great stabilization observed in the gas phase (more than 40 kcal/mol^{-1}) is significantly reduced. The free energy of the reaction is -15.9 kcal mol^{-1} by RISM-SCF, and -24.9 kcal mol^{-1} by PCM. The RISM-SCF value is very close to the experimental one, -12.5 kcal mol^{-1}.[1,19]

The appearance of the barrier can also be understood in terms of the orbital energy gap. Since the mechanism of the reaction is essentially interpreted by the charge transfer from

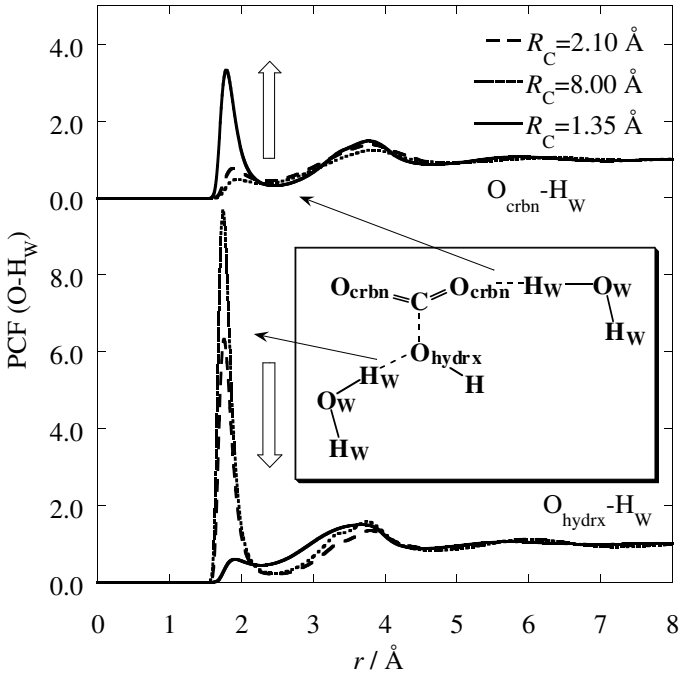

Figure 1.3: Pair correlation functions between O_{hydrx} and H_W (upper), O_{crbn} and H_W (lower) at $R_C = 8.00$ Å(dotted line), $R_C = 2.10$ Å(dashed line) and $R_C = 1.35$ Å (solid line).

OH^- to CO_2 within the framework of the frontier orbital theory, the orbital energy changes are primarily important. Figure 1.2 illustrates the energy levels of the related orbitals in the gas phase and in aqueous solution. In the gas phase, the energy gap between the π^* orbital of carbon dioxide and the lone pair orbital (l) of hydroxide anion is 1.96 eV. The energy of the π^* orbital is not affected by the solvation so much, while that of OH^- orbital is considerably lowered. In consequence the energy gap increases in solution than that in the gas phase, causing the reduction of the reactivity. The energy gap calculated by PCM (3.89 eV) is slightly smaller than by RISM-SCF (4.17 eV), being consistent with the result that the barrier of PCM is lower than the RISM-SCF calculation.

Solvation structure

Figure 1.3 shows the representative site-site PCFs (pair correlation functions) along the reaction. The upper panel is the PCF between the CO_2 oxygen atom (O_{crbn}) and water hydrogen atom (H_W), while the lower one is that between the OH^- oxygen (O_{hydrx}) and H_W. The sharp

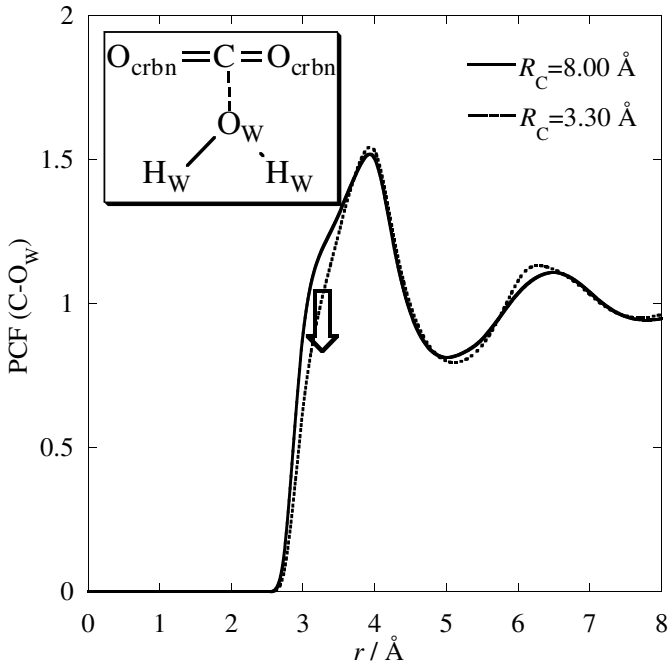

Figure 1.4: Pair correlation functions between C and O_W at $R_C = 8.0$ Å(solid line) and $R_C = 3.3$ Å(dotted line).

peak found in $r = 1.8$ Å corresponds to the hydrogen bonding by surrounding water molecules. The peak heights dramatically change as the reaction progresses: the peak of O_{hydrx}–H_W is rapidly lowered and that of O_{crbn}–H_W is enhanced as the two species approach each other. This indicates that the solvation structure in the microscopic level is quite different from either of the two oxygen atoms. The hydroxide moiety is desolvated while O_{crbn} attracts solvent water molecules with decreasing R_C. As the reaction proceeds, the O–C–O angle bends from 180° and the excess electron is shared by all the oxygen atoms, i.e. the electron population on the O_{crbn} considerably increases. At the initial state of the reaction, the charge on this atom is -0.43 $|e|$, which becomes almost -1.00 $|e|$ at the bond-making situation. In contrast, the charge on O_{hydrx} changes from -1.52 $|e|$ to -0.82 $|e|$. These changes are comparable with that in PCFs.

The PCF between the carbon and O_W shows no significant change along the reaction as shown in Fig. 1.4. The solid line indicating the PCF at $R_C = 8.0$ Å can be regarded as the reactant, while the dotted line at $R_C = 3.3$ Å corresponds to the nascent state of the C–O bond. One of the remarkable differences between these two PCFs is the absence of the shoulder in the

region from $r = 2.5$ Å to $r = 3.5$ Å. This change suggests the desolvation around the carbon atom. Although the change looks negligible, the free energy change associated this depression of the shoulder is indispensable for the barrier formation. This point will be discussed later. It is noted that the depression has no relation to the change of the CO_2 structure, i.e., the bending of O–C–O angle because the angle-change occurs at $R_{\mathrm{C}} < 3.0$ Å.

1.3.2 Solvation energy along the reaction pathway

The total energy of the system ($\mathscr{A}$) defined by the sum of the solute potential energy and the solvation free energy can be written as follows:

$$\mathscr{A} = \langle \Psi_0 | H_0 | \Psi_0 \rangle + E_{\mathrm{reorg}} + \Delta\mu^{(\mathrm{HNC})}, \tag{1.2}$$

where Ψ_0 and H_0 are the wave function and the standard Hamiltonian of the solute molecule in gas phase. The reorganization energy E_{reorg} is associated with the solute electronic polarization and defined by

$$E_{\mathrm{reorg}} = \left\langle \Psi^{\mathrm{solute}} \middle| H_0 \middle| \Psi^{\mathrm{solute}} \right\rangle - \langle \Psi_0 | H_0 | \Psi_0 \rangle . \tag{1.3}$$

Ψ^{solute} is obtained by solving the equation with the modified Fock operator.

In the RISM framework, the solvation free energy using the HNC closure equation[17] can be "formally" divided into the contributions ($\Delta\mu_\alpha^{(\mathrm{HNC})}$) from respective atom labeled α.

$$\Delta\mu_\alpha^{(\mathrm{HNC})} = \frac{\rho}{2\beta} \sum_{\gamma}^{\mathrm{solvent}} \int_0^\infty 4\pi r^2 (h_{\alpha\gamma}^2 - 2c_{\alpha\gamma} - h_{\alpha\gamma}c_{\alpha\gamma}) \mathrm{d}r. \tag{1.4}$$

It should be emphasized here that $\Delta\mu_\alpha^{(\mathrm{HNC})}$ is not equal to the solvation free energy of an atom α isolated in the solvent, since all the correlation functions related to this atom are determined by the RISM theory under the perturbation by the existence of the other atoms composing the solute. In this regard, this division is rather formal but useful for systematic understanding of the solvation processes.

Figure 1.5 plots $\Delta\mu^{(\mathrm{HNC})}$, $\Delta\mu_\alpha^{(\mathrm{HNC})}$ and E_{reorg} as the function of the reaction coordinate, R_{C}. $\Delta\mu^{(\mathrm{HNC})}$ shows a peak around $R_{\mathrm{C}} = 2$Å where the barrier of the reaction is also found.

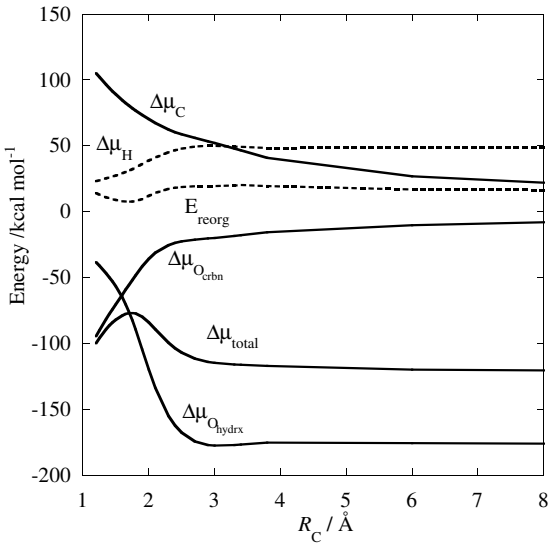

Figure 1.5: Electronic reorganization energy E_{reorg}, solvation free energy $\Delta\mu$ and its components along the reaction coordinate.

The change of E_{reorg} is smaller than $\Delta\mu^{(\mathrm{HNC})}$, meaning that it is the solvation free energy that governs the energy profile of the reaction. The change of $\Delta\mu_{\mathrm{O_{hydrx}}}$, $\Delta\mu_{\mathrm{O_{crbn}}}$ and $\Delta\mu_{\mathrm{C}}$ show great contributions to the total solvation free energy. As smaller R_{C}, both of $\Delta\mu_{\mathrm{O_{hydrx}}}$ and $\Delta\mu_{\mathrm{C}}$ increase while $\Delta\mu_{\mathrm{O_{crbn}}}$ decreases. All of them are consistent with the change in PCFs discussed in Sec. 1.3.1. Namely, while the $\mathrm{O_{crbn}}$ is solvated, both of $\mathrm{O_{hydrx}}$ and the carbon are desolvated as the reaction proceeds. These changes in the solvation structure and their interplay cause a barrier of the reaction.

It is noteworthy that the gross change in $\Delta\mu_{\mathrm{C}}$ is nearly 50 kcal/mol from the reactant to the bond-making region, although the change in PCF looks very small. Thanks to its analytical treatment in the RISM framework, it is possible to analyze the solvation free energy in terms of the spatial contribution. In other words, we can compute the "partial" solvation free energy related to a particular region around the solute atom α by,

$$\Delta\mu_{\alpha}^{(\mathrm{partial})}(r_{\mathrm{min}}, r_{\mathrm{max}}) = \frac{\rho}{2\beta}\sum_{\gamma}^{\mathrm{solvent}}\int_{r_{\mathrm{min}}}^{r_{\mathrm{max}}} 4\pi r^2(h_{\alpha\gamma}^2 - 2c_{\alpha\gamma} - h_{\alpha\gamma}c_{\alpha\gamma})\mathrm{d}r. \tag{1.5}$$

Since $\Delta\mu^{(\mathrm{HNC})}$ is the functional of the reaction coordinate R_{C}, we then define

$$\Delta\Delta\mu_{\alpha}^{(\mathrm{partial})}$$

$$= \Delta\mu_{\alpha}^{(\mathrm{partial})}(r_{\min}, r_{\max}; R_{\mathrm{C}} = 3.3\ \text{Å}) - \Delta\mu_{\alpha}^{(\mathrm{partial})}(r_{\min}, r_{\max}; R_{\mathrm{C}} = 8.0\ \text{Å}),$$

where $r_{\min} = 2.5$ Å and $r_{\max} = 3.5$ Å were used because the change of PCF is distinct in this area (see Figure 1.4). The free-energy raise on the reaction attributed to the carbon atom ($\Delta\Delta\mu_{\mathrm{C}}^{(\mathrm{partial})}$) is calculated to be 36 kcal mol^{-1}. The result clearly shows that the change in C-O_{W} PCF, which looks tiny, considerably contributes to the solvation free energy. The distance between the carbon and the oxygen ($R_{\mathrm{C}} \sim 3.0$ Å) is close to the sum of their radius, $\sigma_{\mathrm{C}}/2 + \sigma_{\mathrm{O}}/2$. Solvent water molecules existing between these atoms get expelled from the interatomic region by the new bond making process, which leads to the significant increase in the solvation free energy and to make the barrier. As decreasing R_{C} less than 3.0 Å, the electronic structure on the carbon atom is significantly changed by this bond formation. In other words, the change in the solvation structure is strongly coupled with that in the electronic structure. This is the reason why $R_{\mathrm{C}} \geq 3.3$ Å, where the change in the solvation structure solely contributes the energy change, has been chosen in the above discussion. It should also be noted that the contribution from carbon is important, but the sum of all contributions including oxygen atoms determines the position of the barrier (see Figure 1.5).

In the present study, the effect of counterion is not taken into account. Since the system of an infinitely dilute solution is treated, the effect is expected to be small enough.

1.4 Conclusion

We have studied the origin of the reaction barrier between carbon dioxide and hydroxide anion using the RISM-SCF method. A detailed analysis of the solvation structure and the free energy change have shown that the desolvation in the oxygen site of hydroxide anion and solvation in the oxygen site of carbon dioxide play important roles in the formation of the barrier. It is also found that the desolvation due to the formation of a new bond making between carbon and oxygen is another main origin of the barrier. We emphasize that an analytical treatment in the RISM theory enables formulation of the solvation free energy in terms of the spatial or atomic contribution. This is the unique advantage of the integral equation theory for liquids, which is quite different from methods based on the molecular simulation technique.

Bibliography

[1] B.R.W. Pinsent, L. Pearson, F.J.W. Roughton, Trans. Faraday Soc., **52**, 1512 (1956).

[2] M.M. Davidson, I.H. Hillier, R.J. Hall, N.A. Burton, Mol. Phys., **83**, 327 (1994).

[3] Z. Peng, K.M. Merz Jr., J. Am. Chem. Soc., **115**, 9640 (1993).

[4] A.V. Nemukin, I.A. Topol, B.L. Grigorenko, S.K. Burt, J. Phys. Chem. B, **106**, 1734 (2002).

[5] H. Sato, F. Hirata, J. Phys. Chem. B, **103**, 6596 (1999).

[6] H. Sato, F. Hirata, J. Phys. Chem. A, **102**, 2603 (1998).

[7] K. Leung, I.M.B. Nielsen, I. Kurtz, J. Phys. Chem. B, **111**, 4453 (2007).

[8] S. Ten-no, F. Hirata, S. Kato, J. Chem. Phys., **100**, 7443 (1994).

[9] H. Sato, F. Hirata, S. Kato, J. Chem. Phys., **105**, 1546 (1996).

[10] H.C. Andersen, D. Chandler, J. Chem. Phys., **57**, 1930 (1972).

[11] F. Hirata, P. Rossky, Chem. Phys. Lett., **83**, 329 (1981).

[12] D. Yokogawa, H. Sato, S. Sakaki, J. Chem. Phys., **126**, 244504 (2007).

[13] M. W. Schmidt, K. K. Baldridge, J.A . Boatz, S. T. Elbert, M. S. Gordon, J. H. Jensen, S. Koseki, N. Matsunaga, K. A. Nguyen, S. Su, T. L. Windus, M. Dupuis, J. A. Montgomery, J. Chem. Phys., **73**, 1347 (1993).

[14] S. J. Weiner, P. A. Kollman, D. A. Case, U. C. Singh, C. Ghio, G. Alagona, S. Profeta, Jr, P. Weiner, J. Am. Chem. Soc., **106**, 765 (1984).

[15] S.J. Weiner, P.A. Kollman, D.T. Nguyen, D.A. Case, J. Comput. Chem., **7**, 230 (1986).

[16] H.J.C. Berendsen, J.P.M. Postma, W.F. van Gunsteren, J. Hermans, in B. Pullman (Ed.), *Intermolecular Forces*, Reidel, Dordrecht, 1981.

[17] S.J. Singer, D. Chandler, Mol. Phys., **55**, 621 (1985).

[18] Gaussian 03, Revision C.02; Gaussian Inc., Wallingford, CT, 2004.

[19] M.J. Welch, J. Phys. Chem., **73**, 3351 (1969).

Chapter 2

Carbon dioxide capture at the molecular level

2.1 Introduction

Carbon dioxide is recognized as a typical greenhouse gas and drastic reduction of CO_2 emissions from industrial process is becoming more and more important in relation to global warming. Aqueous amine systems have been widely used for the removal from flue gases and the following process operates in these systems:

$$CO_2 + NHR_2 \rightarrow CO_2NR_2^- + H^+. \tag{2.1}$$

Among several factors controlling the capability of the absorption, a molecular characteristic of the amine is of primary importance. To develop a more efficient system, understanding of the mechanism is indispensable. Monoethanolamine (MEA) is one of the representative substances utilized for such a purpose. Thanks to intensive experimental studies,[1–5] it becomes clear that the rate-determining step of the process is the bond formation between amine nitrogen and CO_2 carbon.

$$CO_2 + NH_2CH_2CH_2OH \rightarrow CO_2\text{-}NH_2CH_2CH_2OH. \tag{2.2}$$

A theoretical approach is expected to offer precious information that is difficult to be accessed by experimental research. Several studies based on standard molecular orbital theory as well as molecular simulation have been reported.[6–8] However, interplay between aqueous water and the bond formation –which is nothing but the changing of electronic structure in MEA-CO_2 system– has not been studied so far though it is essential for addressing the heart of the

capture. Therefore, a simultaneous treatment of quantum chemistry and ensemble of solvent molecules is necessary, namely only QM/MM or its equivalent theory can touch the essence of the process. An explicit treatment of solvent water is crucial to deal with hydrogen bonding that governs the intermolecular interaction.

In the present study, the reaction mechanism of this bond formation between MEA and CO_2 is investigated by means of RISM-SCF-SEDD.[9–11] Since reference interaction site model (RISM)[12,13] is a statistical mechanics for molecular liquids, wealth of information including solvation structure, free energy change can be obtained efficiently. RISM-SCF-SEDD, in which RISM is coupled with molecular orbital theory, is recognized as an alternative to QM/MM. One of the big differences is the capability to compute accurate free energy with reasonable computational time due to the advantage of RISM, allowing us to use highly sophisticated electronic structure theory cooperated with solvation effect. The emphasis is on the free energy that describes the system in reality, which is difficult to elucidate only by considering a few water molecules. Now, this combinational method can afford the heart of the mechanism of the reaction.

2.2 Method

RISM is a statistical mechanics theory for molecular liquids developed by Chandler and Andersen.[12] The theory was then extended to treat electrostatic interaction (XRISM) by Rossky and Hirata.[13] The main equation of the theory is as follows,

$$\boldsymbol{\rho}\mathbf{h}\boldsymbol{\rho} = \boldsymbol{\omega} * \mathbf{c} * \boldsymbol{\omega} + \boldsymbol{\omega} * \mathbf{c} * \boldsymbol{\rho}\mathbf{h}\boldsymbol{\rho}. \tag{2.3}$$

Here, '*' denotes convolution integral, $\boldsymbol{\rho}$ is number of density, $\boldsymbol{\omega}$ is intramolecular correlation function defining the molecular geometry. $\mathbf{h}$ and $\mathbf{c}$ are total and direct correlation function, respectively. In the present study very standard hyper-netted chain (HNC) closure was employed to solve the equation.

$$\begin{aligned} c_{\alpha s}(r) &= \exp\left[-\beta u_{\alpha s}(r) + \gamma_{\alpha s}(r)\right] - \gamma_{\alpha s}(r) - 1, \\ \gamma_{\alpha s}(r) &= h_{\alpha s}(r) - c_{\alpha s}(r), \end{aligned} \tag{2.4}$$

where $u_{\alpha s}(r)$ is interaction between site α and s, $h_{\alpha s}(r)$ and $c_{\alpha s}(r)$ correspond to the matrix element appearing in Eq. (2.3), and $\beta = 1/k_{\mathrm{B}}T$. Free energy of solvation ($\Delta\mu$) is then readily computed by using obtained $h_{\alpha s}(r)$ and $c_{\alpha s}(r)$.[14]

$$\Delta\mu = -\frac{\rho}{\beta}\sum_{\alpha s}\int \mathrm{d}\mathbf{r}\left[c_{\alpha s}(r) - \frac{1}{2}h_{\alpha s}^2(r) + \frac{1}{2}h_{\alpha s}(r)c_{\alpha s}(r)\right]. \tag{2.5}$$

Some selected features and advantages of RISM are summarized as following: (1) the theory provides adequate thermodynamic ensemble and is free from statistical error or so-called sampling problem. It deals with an infinite number of solvent molecules and requires no 'simulation box'. (2) Since it is written in algebraic equation, computational cost is dramatically reduced compared to standard molecular simulation method. (3) The inputs of the computation are the same as those of simulations, and the outputs are very similar, too.

In RISM-SCF,[9,10] total energy of the system is defined as,

$$\mathscr{A} = E_{\mathrm{solute}} + \Delta\mu, \tag{2.6}$$

where E_{solute} is total energy of the solute molecule described by standard *ab initio* molecular orbital theory, corresponding to MEA and/or CO_2 in the present study. By using variational principle, a set of equations describing solution system is obtained.[10] Hence, the electronic structure of the solute and solvation structure are obtained in a self-consistent manner. RISM-SCF has been successfully applied to a wide range of chemical reactions in solution. It is our intent here to only describe the brief summary of the theory and assume the readers' familiarity of RISM-SCF as well as the statistical mechanics of molecular liquids. Some examples of recent studies are found in refs.[15–18] More lengthly discussions can be found in the literature.[19–21]

2.3 Computational detail

The distance between the carbon atom of CO_2 and the nitrogen atom of MEA was taken as the reaction coordinate (R_{C}) to focus on the bond-making process in the reaction. The geometry optimisation was carried out at B3LYP/6-311++G** level in gas phase under the restriction of C_s structure, in which CO_2 and N-C-C-O-H are in the same plane. This treatment

Table 2.1: Lennard-Jones parameters.

	σ /Å	ϵ /kcal mol^{-1}
Solute		
N	3.300	0.170
C(methyl)	3.500	0.066
C(CO_2)	3.296	0.120
O(OH)	3.070	0.170
O(CO_2)	2.850	0.200
H(methyl)	2.500	0.030
H(HO)	1.000	0.0560
Solvent		
O	3.166	0.1550
H	1.000	0.0560

was necessary to exclude trivial intramolecular hydrogen-bonding structure that is unstable in aqueous solution. In fact, even starting from a low symmetry structure at meta-stable state (**III**; see below), optimisation in aqueous solution leads to the same C_s structure. In C_s symmetry, there is another conformation in which CO_2 is perpendicular to the N-C-C-O-H plane. But its total energy was only slightly higher ($\simeq$0.1 kcal/mol) and the rotation about the axis of N(MEA)–C(CO_2) bond was virtually free. All the energy was evaluated with CCSD(T)/6-311++G**. The present basis set is considered among the best, especially in combination with the highly sophisticated CCSD(T) theory and its dependency seems to be negligible. Computations in aqueous solution phase were then carried out with the RISM-SCF-SEDD by GAMESS package[23] modified by us and PCM methods by Gaussian 03 program[24] with these gas-phase geometries. We have also performed the optimisation in aqueous solution and found that the structure were almost unchanged. The barrier height is only 0.4 kcal mol^{-1} less than that in gas phase. Note that the aqueous-solution geometry by PCM is also different, and thus we decided to use the gas phase geometry to exclude the contribution of the geometrical difference between our method and PCM with the aim of focusing on the interplay between bond formation and solvation effect. The Lennard-Jones parameters of the solute were taken from refs.[25–28] and SPC-like water was assumed for the solvent.[29] All of them are summarized in Table. 2.1. To compute the weight of resonance structure, Pipek-Mezey localization[30] was

utilized to separate valence orbitals. Unfortunately, π orbital and lone-pair orbital at oxygen were mixed together and four equivalent localized orbitals were obtained. Hence, these four orbitals were chosen to evaluate the weights using the standard Löwdin-type operator.[31] Then the contributions from two lone-pair orbitals, corresponding to O^- C^{2+} O^-, were eliminated to represent the resonance structure.

2.4 Results and discussion

2.4.1 Free energy profile in aqueous solution

Figure 2.1 shows the energy profile along the reaction coordinate, R_{C}. CO_2 approaches to MEA from the right hand side of the figure. In gas phase, the energy is continuously decreasing as the reaction proceeds, then the stable structure is found at R_{C} = 3.0 Å (**I**). Obviously it does not correspond to the capturing because of too long bond length as well as barrier-free approaches that are not consistent with experimental knowledge. The energy monotonically increases at shorter regions ($R_{\mathrm{C}} < 3.0$Å) due to the repulsive interaction derived from *Pauli*'s principle. In aqueous solution, energy profiles change drastically. Besides the minimum at $R_{\mathrm{C}} \simeq 3.0$ Å corresponding to **I**, another meta-stable structure appears at $R_{\mathrm{C}} < 2.0$ Å(**III**), which is followed by a fast proton dissociation step to reach the final product. The barrier height from **I** to **III** calculated by RISM-SCF-SEDD is 6.9 kcal mol^{-1}, being slightly higher (2.7 kcal mol^{-1}) than by PCM. Presumably the difference comes from strong stabilization of **I** due to the hydrogen bonding that is properly treated in RISM-SCF-SEDD. Since the experimentally obtained data is the activation enthalpy $\Delta H^{\ddagger}$, the free energy change mentioned above should be converted as following,

$$\Delta H^{\ddagger} = \Delta G^{\ddagger} + T\Delta S^{\ddagger}, \tag{2.7}$$

where activation entropy $\Delta S^{\ddagger}$ was calculated by difference formula, and standard corrections such as zero point energy are taken into account. Our activation enthalpy $\Delta H^{\ddagger}$ is 9.3 kcal mol^{-1} (The zero point and vibration contribution: 0.8 kcal mol^{-1}), which is in good agreement with experimental results (11.2,[2] 9.8,[3] 11.7,[4] and 11.1[5] kcal mol^{-1}). Although the free energy

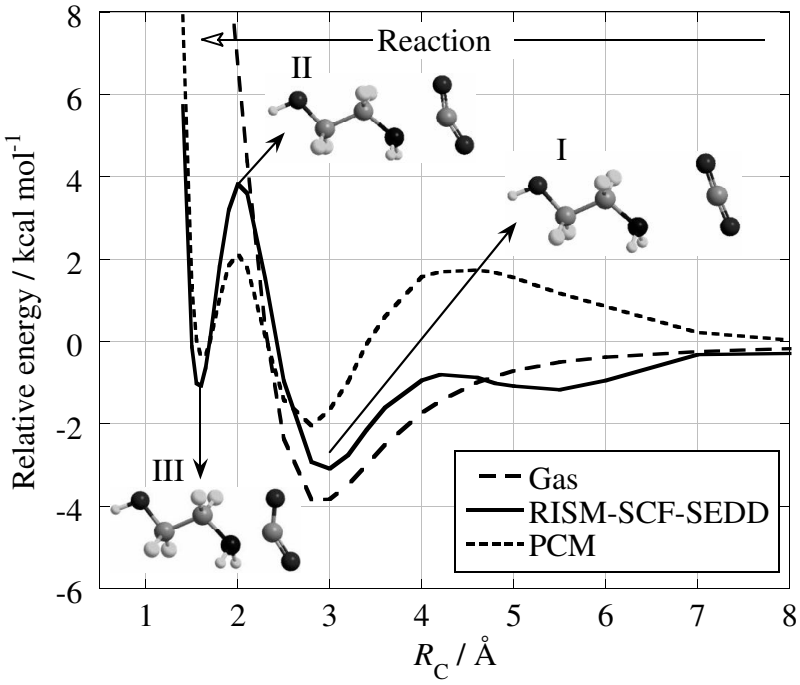

Figure 2.1: Potential energy curve for the C–N bond formation in gas phase (dashed line) and free energy curves in aqueous solution calculated by RISM-SCF-SEDD (solid line) and PCM (dotted line) along the reaction coordinate (R_C). The inset structures are at R_C = 3.0 Å (I), 2.0 Å (II), 1.6 Å (III), respectively.

profile and the activation enthalpy are obtained using one of the most accurate theoretical methods available at the present time, further calibration would be desired because the results may depend on Lennard-Jones parameters, basis sets, the closure and so on.

2.4.2 Resonance structure

MEA–CO_2 bonding complex is formed at $R = 1.6$ Å caused by the charge migration from MEA nitrogen to CO_2 carbon (C_{cdx}). The change of electronic structure may be nicely analyzed in terms of resonance structure embedded in molecular orbital by using the recently developed analysis based on the second quantization of singlet-coupling.[31] Fig. 2.2 shows the dominative weight of CO_2 moiety both in gas and aqueous phases. Supposably, the largest contribution to the electronic structure contains one ionic bond and one double bond. The doubly ionic structure is also important and the sum of three main contributions (**2**, **4** and **5**) is about 60%. In isolated CO_2, the change in electronic structure is negligibly small upon

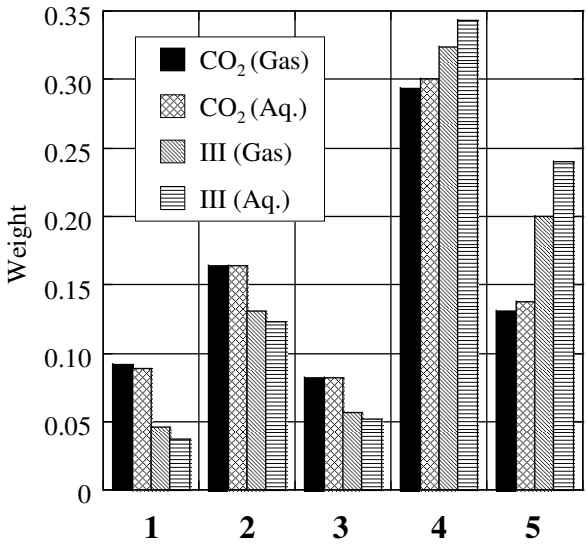

Figure 2.2: Change of selected resonance Weights of CO_2 moiety from the isolated state (CO_2) to the complex. **1**: O=C$^-$ $\equiv$O$^+$, **2**: O=C=O, **3**: O$^-$C$\equiv$O$^+$, **4**: O$^-$$-C^+$ =O, **5**: O$^-$$-C^{2+}-O^-$. Note that symmetrically equivalent contributions are summed up, *e.g.*, **4** comprises both of O$^-$$-C^+$ =O and O=C$^+$$-O^-$.

transferring from gas phase to aqueous solution. However, the bond formation significantly affects the electronic structure: the contribution from **5** is especially enhanced more than 10% while the double bond character (**2**) is considerably reduced. This may be simply attributed to the change of bond angle, O–C–O. The angle changes from 177° (**I**) to 141° (**II**; $R_{\mathrm{C}} = 2.0$ Å), suggesting that the π conjugation is substantially suppressed and electron tends to be isolated at oxygen atoms. In terms of molecular orbital, the change corresponds to the electron transfer from N lone pair to CO_2 π^* orbital. In fact, natural population charge of N changes as $-0.95|e| \rightarrow -0.68|e|$ and that of O_{cdx} as $-0.62|e| \rightarrow -0.83|e|$. The same trends can be found in the resonance structure on C$\cdots$N bond at **III**: 38%(C–N), 10%(C$^+$ N $^-$) and 37%(C $^-$ N $^+$), respectively (corresponding gas phase values are 34%, 42%, 7%).

2.4.3 Solvation structure and solvation free energy change

Because of the large charge migration, solvation structure around them drastically changes as the reaction proceeds. Fig. 2.3 shows the change of pair correlation functions (PCFs). The left panel exhibits PCF between N and solvent-water hydrogen (H_{W}), while the right one is that

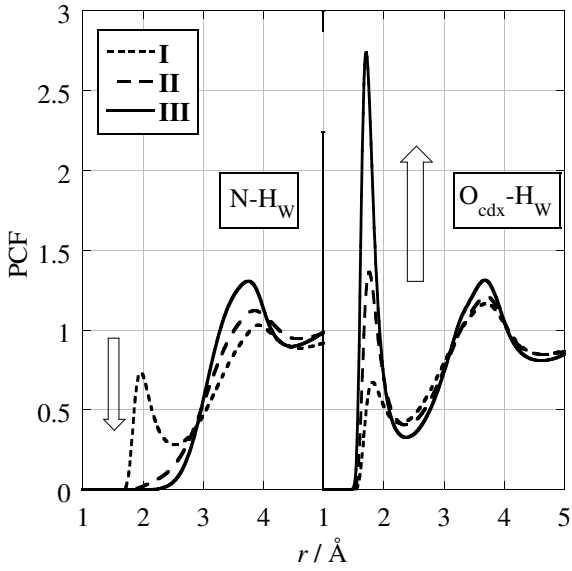

Figure 2.3: Pair correlation function of N-H_W (left side) and O_{cdx}-H_W (right side) of R_C=3.0 Å (I, dotted line), R_C=2.0 Å (II, dashed line), and R_C=1.6 Å (III, solid line).

between O_{cdx}-H_W. The sharp peaks found at $r = 2.0$ Å in both panels correspond to hydrogen bonding. At first, MEA is weakly hydrated around N atom at **I**, and the peak completely disappears in the transition state (**II**). This is, of course, caused by the steric hindrance by approaching CO_2 and the solvation structure hardly changes after passing through **T**. PCF around CO_2 oxygen also shows weak hydrogen bonding at **I**, but the peak is contrastively increasing as the reaction proceeding, indicating that CO_2 moiety strongly attracts solvent water even at $R_C < 2.0$ Å. The development of hydrogen bonding is attributed to the above mentioned increasing of O_{cdx} charge.

Both of these changes in hydration structure affect the free energy change in this bond-forming region. Solvation free energy $\Delta\mu$ (Eq. (2.5)) can be "formally" divided into the contribution from each atom labeled α.

$$\Delta\mu = \sum_{\alpha} \Delta\mu_{\alpha}, \tag{2.8}$$

and

$$\Delta\mu_{\alpha} = -\frac{\rho}{\beta} \sum_{s} \int \mathrm{d}\mathbf{r} \left[c_{\alpha s}(r) - \frac{1}{2} h_{\alpha s}^2(r) + \frac{1}{2} h_{\alpha s}(r) c_{\alpha s}(r) \right]. \tag{2.9}$$

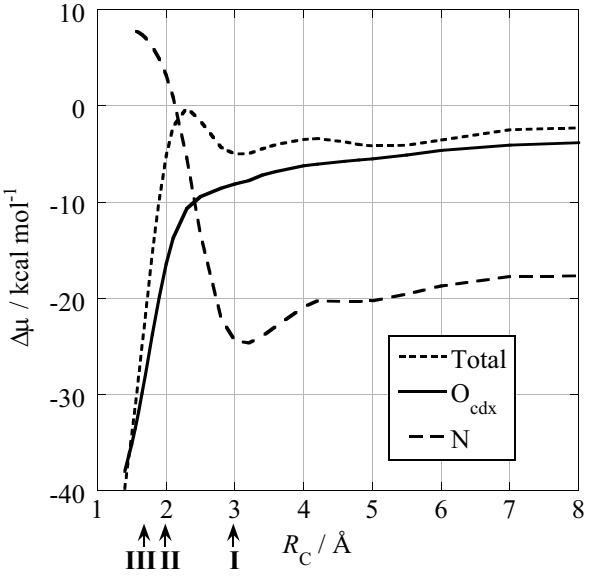

Figure 2.4: Selected solvation free energy components along R_{C} calculated by RISM-SCF-SEDD.

This quantity represents how much the contribution from each site is. Fig. 2.4 shows the change of total solvation free energy ($\Delta\mu_{total}$) and the main elements, $\Delta\mu_{total}$, $\Delta\mu_{\mathrm{N}}$ and $\Delta\mu_{\mathrm{O_{cdx}}}$, along R_{C}. $\Delta\mu_{\mathrm{N}}$ increases along the reaction coordinate from I to III region, whereas $\Delta\mu_{\mathrm{O_{cdx}}}$ decreases around the same region. Namely, while $\mathrm{O_{cdx}}$ is solvated, nitrogen atom is desolvated as the reaction proceeds. At the region from **I** to **II**, the hydration-development around $\mathrm{O_{cdx}}$ and de-hydration around N are virtually canceled out, and thus the total free energy change in aqueous solution eventually looks very similar to the energy change in the gas phase. However, at the region from **II** to **III**, $\mathrm{O_{cdx}}$ hydration becomes dominative and the total free energy decreases to establish the meta-stable intermediate. These are consistent with the change of the solvation structure. In other words, the barrier and stability of the state in aqueous solution are understood as an interplay of the dehydration around N and hydration around $\mathrm{O_{cdx}}$. Note that many previous works indicate that a proton is released from this meta-stable intermediate as the second step of the absorption.

2.5 Conclusion

In summary, we first report the bonding mechanism between carbon dioxide and monoethanolamine at molecular level. In gas phase, an ordinary single minimum is formed at R_{C} = 3.0 Å without barrier. On the other hand, in aqueous solution, after the formation of intermediates similar to the gas phase, a stable structure is found at the bonding region (R_{C} = 1.6 Å) *via* the transition state at R_{C} = 2.0 Å with activation enthalpy of 9.3 kcal/mol, which shows good agreement with experimental knowledge. The hybrid method that can describe both electronic structure change and hydrogen bonding is a promising tool to understand the CO_2 capture. This understanding would lead to a more tactical search for amines with higher absorption capability.

Bibliography

[1] P. D. Vaidya, E. Y. Kenig, Chem. Eng. Tech., **30**, 1467 (2007).

[2] E. Alper, Ind. Eng. Chem. Res., **29**, 1725 (1990).

[3] H. Hikita, S. Asai, H. Ishikawa, M. Honda, *Chem. Eng. J.*, **13**, 7 (1977).

[4] J. E. Crooks, J. P. Donnellan, J. Chem. Soc. Perkin. Trans. 2, **4**, 331 (1989).

[5] S. H. Ali, Int. J. Chem. Kinet, **37**, 391 (2005).

[6] E. F. da Silva, H. F. Svendsen, Ind. Eng. Chem. Res., **43**, 3413 (2004).

[7] E. F. da Silva, T. Kuznetsova, B. Kvamme, K. M. Merz Jr., J. Phys. Chem. B, **111**, 3695 (2007).

[8] B. Arstad, R. Blom, O. Swang, J. Phys. Chem. A, **111**, 1222 (2007).

[9] S. Ten-no, F. Hirata, S. Kato, J. Chem. Phys., **100**, 7443 (1994).

[10] H. Sato, F. Hirata, S. Kato, J. Chem. Phys., **105**, 1546 (1996).

[11] D. Yokogawa, H. Sato, S. Sakaki, J. Chem. Phys., **126**, 244504 (2007).

[12] H. C. Andersen, D. Chandler, J. Chem. Phys., **57**, 1930 (1972).

[13] F. Hirata, P. J. Rossky, Chem. Phys. Lett., **83**, 329 (1981).

[14] S. J. Singer, D. Chandler, Mol. Phys., **55**, 621 (1985).

[15] H. Sato, S. Sakaki, J. Phys. Chem. A, **108**, 1629 (2004).

[16] N. Minezawa, S. Kato, J. Phys. Chem. A, **109**, 5445 (2005).

[17] K. Iida, D. Yokogawa, S. Sato, S. Sakaki, Chem. Phys. Lett., **443**, 264 (2007).

[18] S. Hayaki, D. Yokogawa, S. Sato, S. Sakaki, Chem. Phys. Lett., **458**, 329 (2008).

[19] *Continuum Solvation Models in Chemical Physics*, eds. B. Mennucci and R. Cammi, John Wiley & Sons, Chichester, 2007.

[20] *Molecular Theory of Solvation, Understanding Chemical Reactivity*, ed. F. Hirata, Springer, 2003.

[21] *Computational Biochemistry and Biophysics*, eds. O. M. Becker, A. D. MacKerell, Jr., B. Roux and K. Watanabe, Marcel Dekker, New York, 2001.

[22] J. Tomasi, B. Mennucci, R. Cammi, Chem. Rev., **105**, 2999 (2005).

[23] M. W. Schmidt, K. K. Baldridge, J. A. Boatz, S. T. Elbert, M.S. Gordon, J. H. Jensen, S. Koseki, N. Matsunaga, K. A. Nguyen, S. Su, T. L. Windus, M. Dupuis, J. A. Montgomery, J. Comput. Chem., **14**, 1347 (1993).

[24] Gaussian 03, Revision C.02; Gaussian Inc., Wallingford, CT, 2004.

[25] R. C. Rizzo, W. L. Jorgensen, J. Am. Chem. Soc., **121**, 4827 (1999).

[26] W. L. Jorgensen, J. Phys. Chem., **90**, 1276 (1986).

[27] S.J. Weiner, P.A. Kollman, D.A. Case, U.C. Singh, C. Ghio, G. Alagona, S. Profeta, Jr, P. Weiner, J. Am. Chem. Soc., **106**, 765 (1984).

[28] S.J. Weiner, P.A. Kollman, D.T. Nguyen, D.A. Case, J. Comput. Chem., **7**, 230 (1986).

[29] H. J. C. Berendsen, J. P. M. Postma, W. F. van Gunsteren, J. Hermans, in *Intermolecular Forces*, ed. B. Pullman, Reidel, Dordrecht, 1981.

[30] J. Pipek and P. G. Mezey, J. Chem. Phys., **90**, 4916 (1989).

[31] (a) A. Ikeda, Y. Nakao, H. Sato, S. Sakaki, J. Phys. Chem. A, **110**, 9028 (2006). (b) A. Ikeda, D. Yokogawa, H. Sato, S. Sakaki, Chem. Phys. Lett., **424**, 499 (2006). (c) A. Ikeda, D. Yokogawa, H. Sato, S. Sakaki, *Int. J. Quantum Chem.*, **107**, 3132 (2007). (d) A. Ikeda, Y. Nakao, H. Sato, S. Sakaki, *J. Chem. Theory Comp.*, **5**, 1741 (2009).

Chapter 3

Proton Transfer Step in the Carbon Dioxide Capture by Monoethanol Amine: A Theoretical Study at the Molecular Level

3.1 Introduction

In relation to global warming, chemical absorption of CO_2 by amine attracts much attention as the industrial process for CO_2 removal from flue gases. Monoetanolamine ($CH_2OHCH_2NH_2$; MEA) is one of the representative absorbents. Although MEA absorbs CO_2 sufficiently fast, the formed N–C bond is too strong to be broken under a mild condition. In other words, an excess amount of energy is necessary to reproduce MEA solution. A more efficient amine is thus highly desired, and the search for new amine is extensively performed.

To find a more efficient amine, knowledge about the mechanism of CO_2 adsorption by MEA should be valuable. On the basis of experimental studies, it is known that two steps are involved in the process.[1–6] The first step is the bond formation between MEA (**1a**) and CO_2 (**1b**) ,

$$CH_2OHCH_2NH_2\ (\mathbf{1a}) + CO_2\ (\mathbf{1b}) \rightarrow CH_2OHCH_2NH_2\text{-}CO_2\ (\mathbf{3}). \tag{3.1}$$

Then a proton transfer occurs from the MEA-CO_2 complex (**3**) to a base (B),

$$\begin{aligned} CH_2OHCH_2NH_2\text{-}CO_2\ (\mathbf{3}) \quad &+ \quad B \\ &\rightarrow \quad CH_2OHCH_2NHCOO^-\ (\mathbf{4}) + BH^+\ (\mathbf{5}). \end{aligned} \tag{3.2}$$

Whereas the step (3.1) is already established as the rate-determining step, the step (3.2) is not fully understood. For example, it still remains an open question which MEA or H_2O acts as

the base. Because the amount of required energy for reproducing MEA solution is mainly determined by the relative stability of the final products (**4** + **5**) to the reactants (**1a** + **1b**), it is essentially important to clarify the mechanism of the step (3.2). Note that the solvation effect plays a central role in this reaction because it does not proceed in the gas phase. It is thus indispensable to treat both quantum chemistry and an ensemble of solvent molecules to grasp essence of the reaction. RISM-SCF-SEDD[7–9] is a hybrid method of RISM theory[10,11] and *ab initio* molecular orbital theory. Different from QM/MM, which is a popular method to treat chemical reaction in the solution phase, RISM-SCF-SEDD utilizes RISM theory to treat solvent. The RISM theory is expressed as an algebraical equation in statistical mechanics for an ensemble of an infinite number of solvent molecules. With RISM-SCF-SEDD, we can obtain a wealth of knowledge about the electronic structure and solvation structure in a self-consistent manner.

Recently we studied the bond formation step (1) using RISM-SCF-SEDD.[12] We have clarified that the solvation effect governs the free energy profile. The interplay between the hydration around oxygen of CO_2 and the dehydration around the nitrogen is essential for the mechanism of the bond formation. A solvation effect is considered to be also crucial in the second step (*i.e.*, proton transfer), but the role of solvent is still unclear. Only few studies based on the dielectric continuum model and cluster model just considering a few water molecules nearby have been reported so far.[13–15] In this study, we would like to accomplish a full understanding of the chemical absorption of CO_2 by MEA using RISM-SCF-SEDD, especially focusing on the proton transfer step.

3.2 Method

Here we briefly summarize RISM-SCF-SEDD. A more detailed explanation of the theory can be found in the previous articles.[7–11] RISM-SCF-SEDD utilizes RISM theory to treat solvent. The main equation is as follows.[10,11]

$$\mathbf{h} = \boldsymbol{\omega} * \mathbf{c} * \boldsymbol{\omega} + \boldsymbol{\omega} * \mathbf{c} * \boldsymbol{\rho}\mathbf{h}, \tag{3.3}$$

where '*' denotes a convolution integral and all the quantities are matrices whose element corresponds to a pair of interaction sites; $\boldsymbol{\rho}$ is the number of density, $\boldsymbol{\omega}$ is intramolecular correlation function defining the molecular geometry. In Eq. (3.3), $\mathbf{h}$ (total correlation function) and $\mathbf{c}$ (direct correlation function) are unknown functions to be solved. Hyper-netted chain (HNC) closure is a well-known equation to be coupled with the equation,

$$\begin{aligned} c_{\alpha s}(r) &= \exp\left[-\beta u_{\alpha s}(r) + \gamma_{\alpha s}(r)\right] - \gamma_{\alpha s}(r) - 1, \\ \gamma_{\alpha s}(r) &= h_{\alpha s}(r) - c_{\alpha s}(r), \end{aligned} \tag{3.4}$$

where α and s are respectively solute and solvent site; $u_{\alpha s}(r)$ is interaction potential between them; and $\beta = 1/k_{\mathrm{B}}T$. Solvation free energy ($\Delta\mu$) is readily evaluated by $h_{\alpha s}(r)$ and $c_{\alpha s}(r)$ with an HNC formula,[16]

$$\Delta\mu^{\mathrm{HNC}} = -\frac{1}{\beta}\sum_{\alpha,s}\int \mathrm{d}\mathbf{r}\rho_s \left[c_{\alpha s}(r) - \frac{1}{2}h_{\alpha s}^2(r) + \frac{1}{2}h_{\alpha s}(r)c_{\alpha s}(r)\right], \tag{3.5}$$

or with the gaussian fluctuation (GF) formula,[17]

$$\Delta\mu^{\mathrm{GF}} = -\frac{1}{\beta}\sum_{\alpha,s}\int \mathrm{d}\mathbf{r}\rho_s \left[c_{\alpha s}(r) + \frac{1}{2}h_{\alpha s}(r)c_{\alpha s}(r)\right]. \tag{3.6}$$

The GF evaluation (Eq. (3.6)) often shows better agreement with experimental result than the HNC evaluation (Eq. (3.5)), though the physical background of the HNC formula is considered to be clearer. More accurate free energy calculation methods based on RISM theory have recently developed, and the extensive studies with these methods also show that the GF evaluation provides better agreement than the HNC evaluation.[18–22]

Total free energy of the system with RISM-SCF-SEDD is defined as

$$\mathscr{A} = E_{\mathrm{solute}} + \Delta\mu, \tag{3.7}$$

where E_{solute} is the total energy of the solute molecule described by a standard *ab initio* molecular orbital theory and $\Delta\mu$ is given by Eq. (3.5) or (3.6). The change of free energy caused by solvation is given by

$$\Delta\mathscr{A} = \mathscr{A} - E_{\mathrm{gas}} = E_{\mathrm{reog}} + \Delta\mu, \tag{3.8}$$

Table 3.1: Lennard-Jones parameters.

	σ /Å	ϵ /kcal mol^{-1}
	Solute	
N	3.300	0.170
C(methyl)	3.500	0.066
C(CO_2)	3.296	0.120
O(OH)	3.070	0.170
O(CO_2)	2.850	0.200
H(methyl)	2.500	0.030
H(HO)	1.000	0.0560
	Solvent	
O	3.166	0.1550
H	1.000	0.0560

where E_{reog} is the energy difference of the solute molecule from its isolated state (E_{gas}) upon the solvation.

$$E_{\mathrm{reog}} \equiv E_{\mathrm{solute}} - E_{\mathrm{gas}} = \langle \Phi \left| H \right| \Phi \rangle - \langle \Phi_0 \left| H \right| \Phi_0 \rangle \,. \tag{3.9}$$

Here $|\Phi\rangle$ and $|\Phi_0\rangle$ are wave functions in the solution phase and in the gas phase, respectively.

3.3 Computational detail

Geometry optimizations were carried out with B3LYP/6-311++G** under the restriction of C_s symmetry, in which CO_2 and N-C-C-O-H are in the same plane. Energy calculations were then performed with CCSD(T)/6-311++G** at the obtained geometry. PCM[23] computation was also performed for comparison purposes. The RISM equation was solved with hypernetted chain (HNC) closure.[16] The Lennard-Jones parameters of the solute were taken from Refs.[24–27] and SPC-like water[28] was employed for the solvent. All of them are summarized in Tab. 3.1.

The resonance structure analysis developed by us was employed.[29] Pipek-Mezey localization[30] was utilized to separate valence orbitals, and the weight of resonance structure is evaluated with the standard Löwdin-type operator. Unfortunately, the π orbital and the lone-pair orbital in the carbon dioxide moiety were mixed together. These two orbitals were thus cho-

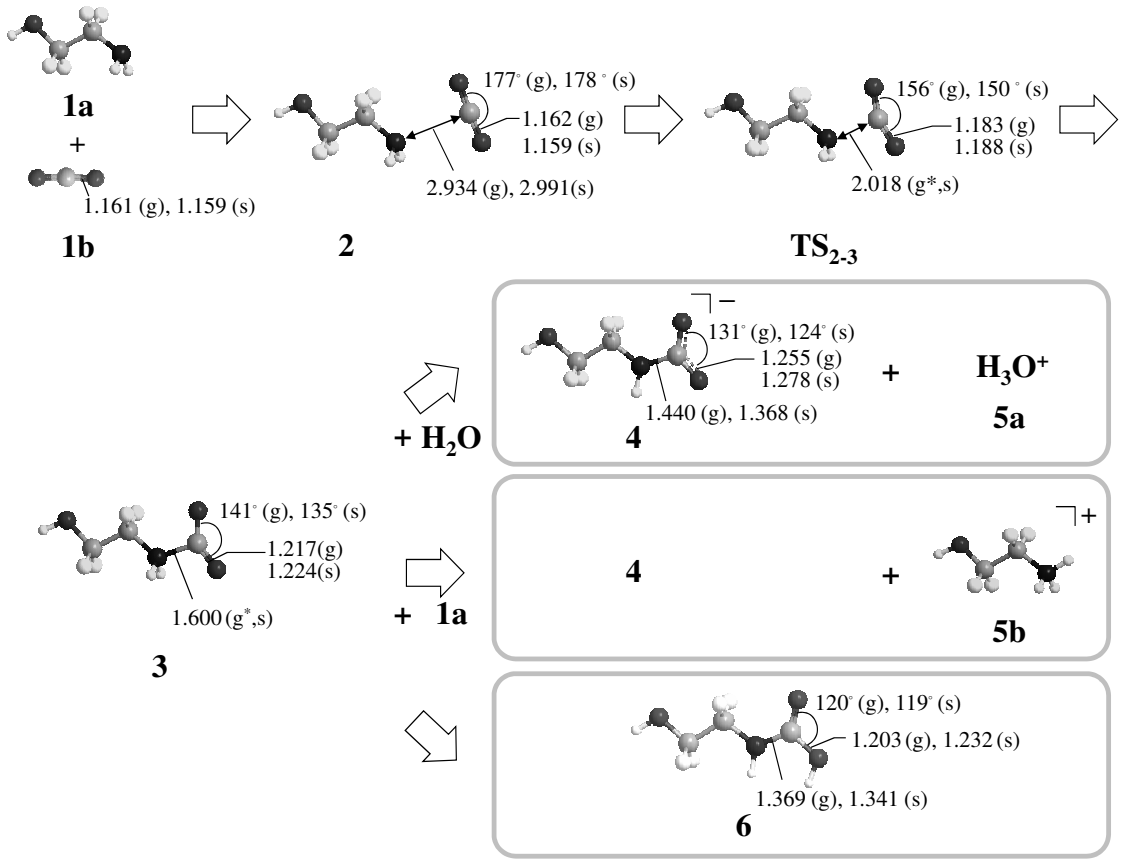

Figure 3.1: Reaction scheme of MEA and CO_2. Bond lengths of C_{cdx}-N and C_{cdx}-O in Å and the bond angle of O_{cdx}-C_{cdx}-O_{cdx} are shown. (g) and (s) mean that the structure is optimized in the gas phase and in aqueous solution with RISM-SCF-SEDD, respectively. Since $\mathbf{TS_{2-3}}$ and **3** are non-existent in the gas phase (marked with '*'), C_{cdx}-N bond length is fixed to that in aqueous solution, and all other degrees of freedom were optimized.

sen to evaluate the weight of the C–O bond, and then the contribution from lone-pair orbitals corresponding to C^+ O^- was subtracted to evaluate the resonance structure.[12]

Geometry optimizations in gas-phase and PCM computations were carried out by the Gaussian 03 program.[31] All other computations were performed with GAMESS package,[32] in which our developed methods were implemented.

3.4 Results and discussion

3.4.1 Reaction profile

The reaction profile is shown in Fig. 3.1. The geometry optimization in aqueous solution is performed for the step (1) in this study, and the obtained energy profile is mostly the same as that in the previous one.[12] **2** is an intermediate before the bond formation between CO_2 carbon (C_{cdx}) and the nitrogen. After passing though the transition state ($\mathbf{TS_{2-3}}$), another intermediate **3** is produced.

The proton transfer step proceeds from **3**, and three paths are possible. In the first path, H_2O acts as the base, then **4** and H_3O^+ (**5a**) are yielded. If another **1a** (MEA) acts as the base, **4** and the protonated MEA (**5b**) are produced (the second path). The third path is an intramolecular proton transfer from the nitrogen moiety to CO_2 oxygen (O_{cdx}) to form **6**. Although **6** has not been observed in experimental studies, an *ab initio* electronic structure calculation of the water-cluster model reported that **6** is stable.[14]

An anion (**4**) is produced in both the first and second paths. As expected, this species is notably affected by solvation, and the geometry in aqueous solution is substantially different from the gas phase one. For example, the O_{cdx}-C_{cdx}-O_{cdx} bond angle is changed from 131° (gas phase) to 124°(aqueous solution). The decrease of the angle should be related to the change in the electronic structure of the CO_2 moiety. As shown in the previous study, the double bond character is reduced when N–C bond is formed. The π conjugation in CO_2 is suppressed, and the electron tends to be isolated at oxygen atoms. In other words, the electron is shifted from the nitrogen lone pair to the CO_2 π^* orbital. The further bending in aqueous solution thus indicates that the solvation promotes the occupation of the π^* orbital. In fact, the natural charge on CO_2 moiety decreases from -0.73 |e| (gas phase) to -0.92 |e| (aqueous solution), and the C_{cdx}-O_{cdx} bond is lengthened. The bond length of C_{cdx}-N is also noticeably changed from 1.440 Å (gas phase) to 1.368 Å (aqueous solution). These geometry changes clearly indicate that solvation considerably affects the electronic structure. As shown below, this is deeply related to the strong hydration of the O_{cdx} site. In a different standpoint, the

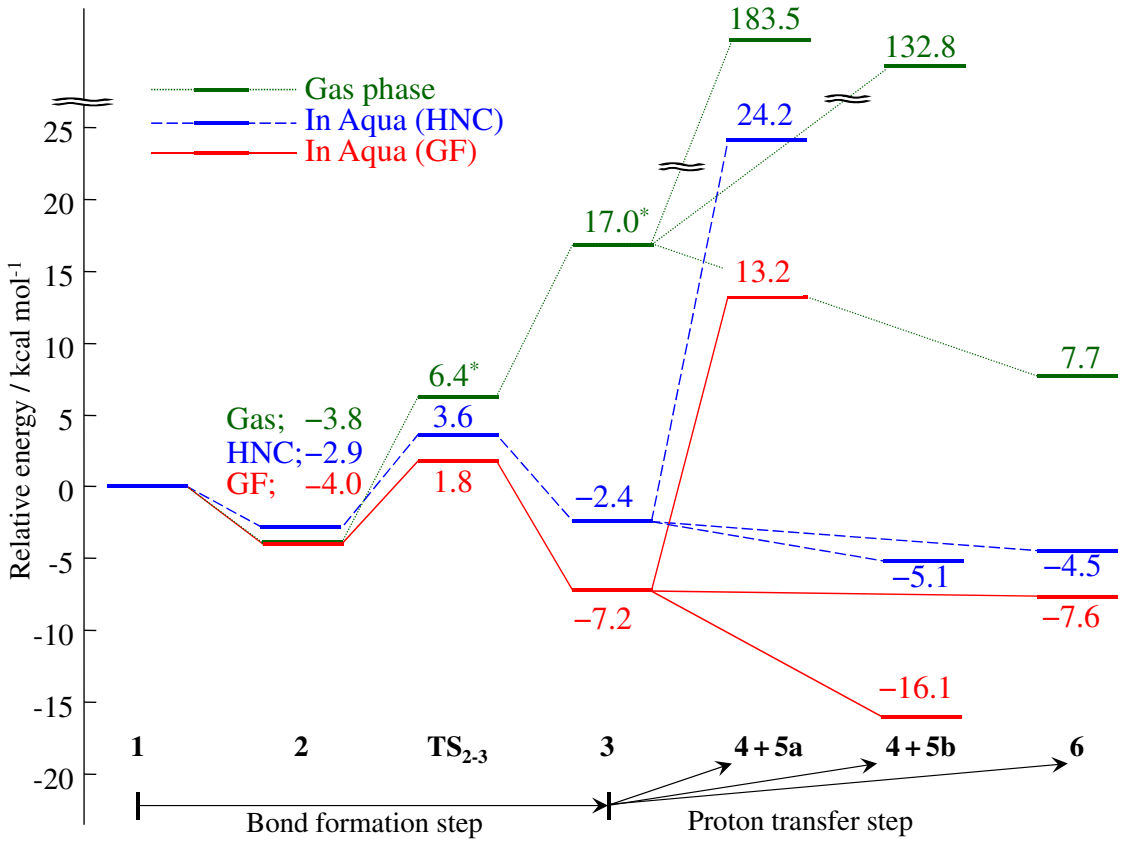

Figure 3.2: Total potential energy profile in the gas phase (green dotted line) and free energy profile in aqueous solution calculated by RISM-SCF-SEDD using HNC (blue dashed line), GF (red solid line). Concerning the '*' mark, see Fig. 3.1.

bond polarization in C_{cdx}-O_{cdx} by the solvation enhances the drawing of electron from MEA to CO_2.

3.4.2 Free energy profile

The free energy profile along the reaction is shown in Fig. 3.2. First, we briefly summarize the bond formation step. For the reaction in aqueous environment, both free energy profiles evaluated by HNC and GF methods are presented. In the gas phase, the potential energy is monotonically increased after the formation of the intermediate (**2**). However, in aqueous solution, the transition state ($\mathbf{TS_{2-3}}$) and an intermediate (**3**) are found. By analyzing the pair correlation functions (PCFs), it was revealed that the development of hydrogen bonding around

O_{cdx} and dehydration around nitrogen are virtually canceled out near the transition state, although the energy curve looks very similar to that in the gas phase.[12] The hydration of O_{cdx} then gradually becomes dominative to form stable **3**. In other words, the bond formation step is understood as an interplay between the solvation around O_{cdx} and the desolvation around the nitrogen.[12]

Let us then focus on the proton transfer step, which is the main subject of the present study. Among the three paths, the energy of the first path to give **4** + **5a**, in which H_2O acts as the base, is very high in the gas phase ($+183.5$ kcal mol^{-1}). Although this is dramatically stabilized in aqueous solution, the total free energy is still positive, $+24.2$ kcal mol^{-1} (HNC) and $+13.2$ kcal mol^{-1} (GF). For the second path, the reaction energy in the gas phase is lower than the first path by about 50 kcal mol^{-1} due to the stronger basicity of **1a** (MEA) than H_2O,[33] but the final product is still very unstable (+132.8 kcal mol^{-1}). However, the total free energy of **4** + **5b** in aqueous solution is definitely negative (-5.1 kcal mol^{-1} by HNC and -16.1 kcal mol^{-1} by GF) and the transfer becomes exothermic. Both of the formulae clearly shows that **4** + **5b** is more stable, indicating that MEA (**1a**) acts as the base in reality. **6** is much more stable than **4** + **5a** or **4** + **5b** in the gas phase, but the contribution from solvation is rather small. Consequently, **6** is slightly unstable compared to **4** + **5b** in an aqueous environment, but the difference between them is only 0.6 kcal mol^{-1} by HNC, and 8.5 kcal mol^{-1} by GF. The result suggests that the intramolecular proton transfer could occur to produce **6**, but the transferred proton is eventually abstracted by MEA. The details of the mechanism might be further clarified, for example, by changing the chemical composition of MEA (**1a**) in an experiment. In any of these cases, H_2O does not act as the base. It should be emphasized that it is the solvation effect that mainly determines the relative stability of the final products. The change of solvation structure reveals the role of solvation at the molecular level. Fig. 3.3 shows PCFs between O_{cdx}, to which the proton transfers, and water hydrogen (H_W) in **3** and **6**. The sharp peak at $r \simeq 2$Å in **3** corresponds to the hydrogen bond, showing the strong interaction before the intramolecular transfer. The peak hight is significantly decreased from 2.9 to 0.6 by completing the transfer. Actually, the de-solvation around O_{cdx} is consistent with the increase of $\Delta\mathscr{A}$ from **3** to **6**. In

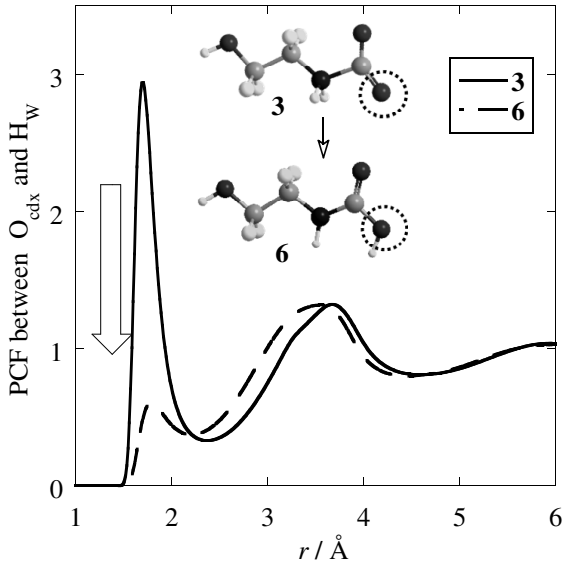

Figure 3.3: PCF between O_{cdx}-H_W of **3** (solid line) and **6** (dashed line).

other words, the solvation slightly prevents the protonation of O_{cdx} in **3**.

3.4.3 Origin of the stabilization of final products

Since the remarkable stabilization of **4** + **5b** by solvation is the origin of the exothermicity of the reaction, solvation energy is further analyzed. Hereafter, we discuss mainly with the GF evaluation for brevity, but the HNC evaluations gives qualitatively the same results. The great stabilization of the final product obtained by the present computation is consistent with the experimental knowledge. Fig. 3.4 displays $\Delta\mathscr{A}$ of the possible products of the reaction computed by RISM-SCF-SEDD as well as by PCM. Both RISM-SCF-SEDD and PCM computations show similar trend as a whole, but the difference in **4** is remarkable. $\Delta\mathscr{A}$ by RISM-SCF-SEDD (-117.6 kcal mol^{-1}) is noticeably lower than the other species (**5a**: -81.4 kcal mol^{-1}, **5b**: -67.9 kcal mol^{-1}, **6**: -34.6 kcal mol^{-1}). Note that $\Delta\mathscr{A}$ with the HNC evaluation is also lower than those of the other species. This distinct stabilization of **4** is the main source of the exothermicity of the reaction. This result may be interesting from the viewpoint of conventional solution chemistry because solvation free energy of the same-charged species is generally in inverse proportion to the radius of species according to the dielectric continuum

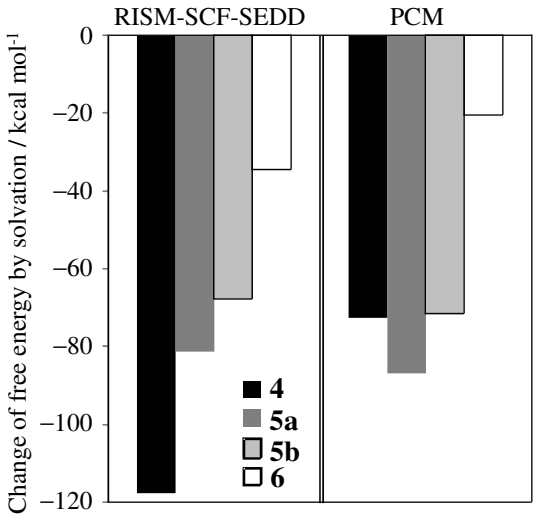

Figure 3.4: Change of free energy by solvation ($\Delta\mathscr{A}$) computed by RISM-SCF-SEDD (left) and PCM (right).

theory.[34] In fact, as shown in Fig. 3.4, $\Delta\mathscr{A}$ of **4** evaluated with PCM (-72.6 kcal mol^{-1}) is similar to that of **5b** (-71.3 kcal mol^{-1}) and higher than that of **5a** (H_3O^+) with a small volume (-86.9 kcal mol^{-1}).

The stabilization of **4** with RISM-SCF-SEDD thus comes from the solute-solvent specific interaction at the molecular-level, which is not adequately described by dielectric continuum model. The origin may be further analyzed by "formally" dividing $\Delta\mu^{\mathrm{GF}}$(Eq. (3.6)) into the contribution from each atom labeled α.

$$\Delta\mu_\alpha^{\mathrm{GF}} = -\frac{1}{\beta}\sum_s \int \mathrm{d}\mathbf{r}\rho_s \left[c_{\alpha s}(r) + \frac{1}{2}h_{\alpha s}(r)c_{\alpha s}(r)\right]. \tag{3.10}$$

As expected, the contribution from the CO_2 moiety is dominative (-102.2 kcal mol^{-1}), corresponding to 87% of the total stabilization. Further decomposition reveals that the solvation around O_{cdx} is essential to understand the stabilization. Fig. 3.5 illustrates the change of solvation structure around O_{cdx} and hydrogen in the amino moiety (H_{N}) that makes another hydrogen bond with solvent water. Both of them correspond to a change from a neutral species to a charged one; from **1a** (MEA) to **5b** (left hand side) and from **3** to **4** (right hand side). The peak at $r \simeq 2$ Å of PCFs between H_{N} and water oxygen (O_{W}) is obviously hydrogen bond, which remains mostly unchanged on the proton transfer (**1a**→**5b**). In contrast, the peak correspond-

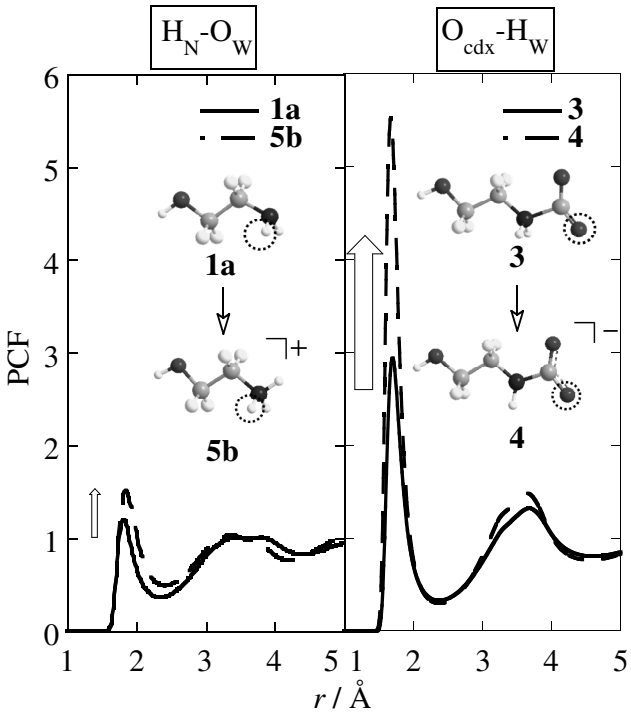

Figure 3.5: PCFs between H_N and O_W (left hand side) and between O_{cdx} and H_W (right hand side) before (solid line) and after (dashed line) the proton transfer.

ing to the hydrogen bond ($r \simeq 2$ Å) between O_{cdx} and water hydrogen (H_W) becomes much higher through the transfer, and the height increases from 3.0 (**3**) to 5.5 (**4**). This dramatic change of hydration is a key to understanding the stability of **4** and the driving force of the promotion of the proton transfer.

The strength of the hydrogen bond may be interpreted using the resonance structures. Concerning the N–H_N bond in **5b**, the covalent bond character (N-H_N) is the largest contribution (42%). However, the two ionic contributions are also considerably large (N^- H_N^+, 36% and N^+ H_N^-, 12%). In other words, the positive charge is not localized only on H_N but distributes over the whole NH_3 moiety. Accordingly, H_N does not strongly attract water oxygen (O_W). On the other hand, the ionic bond character (C_{cdx}^+ O_{cdx}^-) is evidently dominant (62%) in the $C_{cdx}O_{cdx}$ moiety in **4**, whereas the covalent character (C_{cdx}-O_{cdx}) is not significant (28%). The electron (negative charge) is strongly localized at O_{cdx}, which causes the strong interaction with solvent water.

3.5 Conclusion

In this work, the reaction between MEA and CO_2 is investigated using RISM-SCF-SEDD method, which deals with the solvation effect based on a molecular theory. It is shown that MEA acts as the base, and the following insights into the reaction are obtained.

In the bond formation step, the barrier height is determined by hydration around O_{cdx} in CO_2 moiety and dehydration around the nitrogen. The hydration around O_{cdx} then significantly drives the stabilization of the final product. In other words, the solvation around O_{cdx} mainly controls the reaction of MEA and CO_2. The strong interaction between O_{cdx} and H_W could be understood by the dominative resonance character of C^{+}_{cdx} O^{-}_{cdx}. These insights might indicate that the solvation around O_{cdx} could be a key to designing a new efficient amine for CO_2 absorption.

Bibliography

[1] P. D. Vaidya, E. Y. Kenig, Chem. Eng. Tech., **30**, 1467 (2007).

[2] E. Alper, Ind. Eng. Chem. Res., **29**, 1725 (1990).

[3] H. Hikita, S. Asai, H. Ishikawa, M. Honda, *Chem. Eng. J.*, **13**, 7 (1977).

[4] J. E. Crooks, J. P. Donnellan, J. Chem. Soc. Perkin. Trans. 2, **4**, 331 (1989).

[5] S. H. Ali, Int. J. Chem. Kinet, **37**, 391 (2005).

[6] D. Bonenfant, M. Mimeault, R. Hausler, Ind. Eng. Chem. Res., **42**, 3179 (2003).

[7] D. Yokogawa, H. Sato, S. Sakaki, J. Chem. Phys., **126**, 244504 (2007).

[8] S. Ten-no, F. Hirata, S. Kato, J. Chem. Phys., **100**, 7443 (1994).

[9] H. Sato, F. Hirata, S. Kato, J. Chem. Phys., **105**, 1546 (1996).

[10] H. C. Andersen, D. Chandler, J. Chem. Phys., **57**, 1930 (1972).

[11] F. Hirata, P. J. Rossky, Chem. Phys. Lett., **83**, 329 (1981).

[12] K. Iida, D. Yokogawa, A. Ikeda, H. Sato, S. Sakaki, *Phys. Chem. Chem. Phys.*, **11**, 8556 (2009).

[13] E. F. da Silva, H. F. Svendsen, Ind. Eng. Chem. Res., **43**, 3413 (2004).

[14] B. Arstad, R. Blom, O. Swang, J. Phys. Chem. A, **111**, 1222 (2007).

[15] J.-G. Shim, J.-H. Kim, Y. H. Jhon, J. Kim, K.-H. Cho, Ind. Eng. Chem. Res., **48**, 2172 (2009).

[16] S. J. Singer, D. Chandler, Mol. Phys., **55**, 621 (1985).

[17] D. Chandler, Y. Singh, D. M. Richardson J. Chem. Phys., **81**, 1975 (1984).

[18] E. L. Ratkova, G. N. Chuev, V. P. Sergiievskyi, M. V. Fedorov, J. Phys. Chem. B, **114**, 12068 (2010).

[19] Y. Karino, M. V. Fedorov, N. Matubayasi, Chem. Phys. Lett., **496**, 351 (2010).

[20] A. I. Frolov, E. L. Ratkova, D. S. Palmer, M. V. Fedorov, J. Phys. Chem. B, **115**, 6011 (2011).

[21] D. S. Palmer, V. P. Sergiievskyi, F. Jensen, M. V. Fedorov, J. Chem. Phys., **133**, 044104 (2010).

[22] S. Ten-no, J. Chem. Phys., **115**, 3724 (2001).

[23] J. Tomasi, B. Mennucci, R. Cammi, Chem. Rev., **105**, 2999 (2005).

[24] R. C. Rizzo, W. L. Jorgensen, J. Am. Chem. Soc., **121**, 4827 (1999).

[25] W. L. Jorgensen, J. Phys. Chem., **90**, 1276 (1986).

[26] S. J. Weiner, P. A. Kollman, D. A. Case, U. C. Singh, C. Ghio, G. Alagona, S. Profeta, Jr, P. Weiner, J. Am. Chem. Soc., **106**, 765 (1984).

[27] S. J. Weiner, P. A. Kollman, D. T. Nguyen, D. A. Case, J. Comput. Chem., **7**, 230 (1986).

[28] H. J. C. Berendsen, J. P. M. Postma, W. F. van Gunsteren, J. Hermans, in *Intermolecular Forces*, ed. B. Pullman, Reidel, Dordrecht, 1981.

[29] (a) A. Ikeda, Y. Nakao, H. Sato, S. Sakaki, J. Phys. Chem. A, **110**, 9028 (2006). (b) A. Ikeda, D. Yokogawa, H. Sato, S. Sakaki, Chem. Phys. Lett., **424**, 499 (2006). (c) A. Ikeda, D. Yokogawa, H. Sato, S. Sakaki, *Int. J. Quantum Chem.*, **107**, 3132 (2007). (d) A. Ikeda, Y. Nakao, H. Sato, S. Sakaki, *J. Chem. Theory Comp.*, **5**, 1741 (2009).

[30] J. Pipek and P. G. Mezey, J. Chem. Phys., **90**, 4916 (1989).

[31] Gaussian 03, Revision C.02; Gaussian Inc., Wallingford, CT, 2004.

[32] M. W. Schmidt, K. K. Baldridge, J. A. Boatz, S. T. Elbert, M. S. Gordon, J. H. Jensen, S. Koseki, N. Matsunaga, K. A. Nguyen, S. Su, T. L. Windus, M. Dupuis, J. A. Montgomery, J. Comput. Chem., **14**, 1347 (1993).

[33] D. D. Perrin, *Dissociation constants of organic bases in aqueous solution*, London, Butterworths,1972

[34] C. J. F. Bottcher, *Theory of Electric Polarization*, Elsevier, Amsterdam, 1983.

Chapter 4

A systematic understanding of orbital energy shift in polar solvent

4.1 Introduction

Orbital energy (ε) is one of the most important quantities to characterize electronic structure of molecule. For example, ε plays a crucial role to describe the reactivity in the *frontier orbital theory*. ε is also deeply related to the molecular property such as ionization potential (IP) through Koopmans' theorem,[1] though ε is not physical measurable. Recently, direct observation of ionization and excitation energy become experimentally available for solvated molecule,[2,3] and the observed values often exhibit significant change from gas phase ones. However, systematic understanding has not been established yet.

In fact, it is also well known that computed ε in solution phase is different from that in gas phase due to the interaction between solute and solvent.[4–7] The electronic structure of solvated molecule can be calculated using solvation theory such as the family of reference interaction site model-self-consistent field (RISM-SCF)[8–10] and porlalizable continuum model (PCM).[11] However, the obtained shifts look often random; ε sometimes increases and sometimes decreases. Figure 4.1 illustrates the shifts of orbital energies of acetamide in aqueous solution computed by PCM. It looks lacking in orderliness, namely, classifications such as core–valence or σ–π orbital seem nothing short of impossible. It is also noted that the shifts are obtained only after solving complicated modified Schrödinger equation. Unfortunately, we could not find any literatures for systematic study of the solvation shift although several comprehensive reports on polarization of solvated molecule have been presented.[12,13] In other

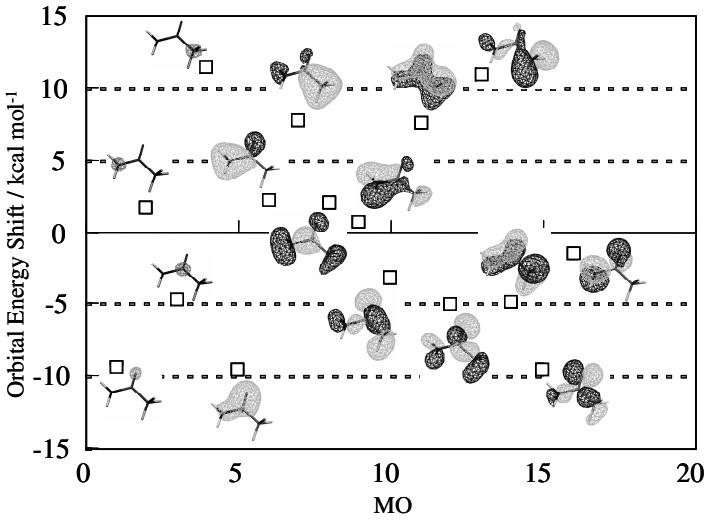

Figure 4.1: Shift of MO energy by solvation effect computed by PCM. HF with 6-311++G** was employed.

words, we can explain the mechanism of the shift neither logically nor comprehensively, and the understanding of the solvation shift of ε has not been systematized at all.

In this study we propose a systematic framework for understanding the orbital-energy shift due to solvation effect. Since the electronic polarization of a molecule is coupled with solvent reaction field, the shift could be understood from the view point of dielectric continuum theory. With the aid of the theory, the shift is systematized and several simple formulae are presented to rationalize it.

4.2 Computational details

All the calculations were carried out at Hartree-Fock (HF) level using 6-311++G** basis set.[14] The computations were carried out with the gas-phase optimized geometries because we would like to exclude the geometrical contribution to the orbital-energy shift. We examined the following 19 organic compounds; Acetamide, Acetic acid, Acetone, Ammonia, Dimethyl ether, Dimethyl sulfide, Formaldehyde, Formamide, Hydrogen sulfide, Methanethiol, Methanol, Methyl amine, N-methyl formamide, Phosphoric acid, Propene, Pyridine, Pyrole, Sulfuric acid, Water. They were taken from reference[15] and supply 265 molecular orbitals (MOs) in-

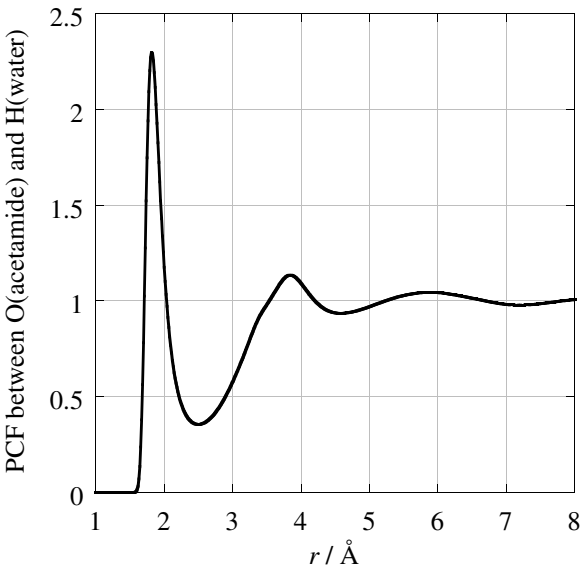

Figure 4.2: PCF between oxygen (acetamide) and hydrogen (solvent water) obtained by RISM-SCF-SEDD computations.

cluding core orbitals (all of them were considered in this study). Several atomic ions (Li^+, Na^+, K^+, F^-, Cl^-, Br^-, I^-) were also studied.

Solvation effect was taken into account by RISM-SCF-SEDD (spatial electron density distribution)[10] and PCM.[11] The RISM-SCF-SEDD is a hybrid method of MO theory and statistical mechanics, an integral equation theory for molecular liquid. Similar to QM/MM, the method determines the electronic structure of a solute as well as the solvent distribution around it in a self-consistent manner, and successfully applied to various chemical processes in solution phase. The method provides microscopic information of the solvation structure in terms of the pair correlation function (PCF). A typical example is illustrated in Figure 4.2. The first peak between O(acetamide)-H(solvent water) found in 2Å represents the hydrogen-bonding. The strong electrostatic field on the oxygen atom in acetamide generated by this localized interaction can be dealt with by RISM-SCF-SEDD method.

The RISM equation was solved with hyper-netted chain (HNC) closure[16] at T=298.15K. On solving the portion of RISM procedure, the Lennard-Jones parameters for the solute molecules were taken from refs.[17–21] SPC-like model of water was employed[22] with a correction of the

Table 4.1: Lennard-Jones parameters.

	σ/Å	ϵ / kcal mol^{-1}
solute		
C	3.296	0.1200
O	3.166	0.1550
N	3.250	0.1700
S	4.000	0.2000
H	1.000	0.0560
Li	1.394	0.3707
Na	2.274	0.3206
K	3.154	0.3060
F	2.720	0.3480
Cl	3.620	0.4480
Br	3.900	0.5290
I	4.320	0.6330

	σ/Å	ϵ / kcal mol^{-1}
H_2O solvent		
O	3.166	0.1550
H	1.000	0.0560
CH_3OH solvent		
Me	3.775	0.2070
O	3.070	0.1700
H	1.000	0.0460
CH_3CN solvent		
Me	3.775	0.2070
C	3.650	0.1500
N	3.200	0.1700

Lennard-Jones parameters of the hydrogen sites (σ=1.0Å, ϵ=0.056 kcal mol^{-1}) under the condition of 1.0 g/cm^3. Acetonitrile[23] and methanol[24,25] were also employed as solvent with 0.786 and 0.792 g/cm^3 of density, respectively. All the parameters are summarized in Table 4.1. PCM computations were performed with the standard parameters implemented in GAMESS program package,[26] while the parameters for atomic species (ions) and acetonitrile solvent were taken from GAUSSIAN 03.[27] RISM-SCF-SEDD calculations also carried out with GAMESS modified by us. It should be emphasized that a general framework of the understanding is independent on the choice of the solvation models as will be shown below, although two different methods, RISM-SCF-SEDD and PCM, were employed to compute the electronic structures of sovlated molecules in this study.

4.3 Theoretical consideration of orbital shift

4.3.1 General theory and electrostatic interaction

The orbital energy in gas phase (ε_i^0) related to MO ψ_i^0 is given by standard Fock operator $\hat{F}^0$ as follows:

$$\varepsilon_i^0 = \left\langle \psi_i^0 \left| \hat{F}^0 \right| \psi_i^0 \right\rangle. \tag{4.1}$$

In solution phase, electrostatic interaction is formed between solute and solvent and the potential field from solvent, $\hat{V}$ is added to the operator.

$$\varepsilon_i = \left\langle \psi_i \left| \hat{F} + \hat{V} \right| \psi_i \right\rangle, \tag{4.2}$$

where ψ_i and ε_i are the MO and its energy of solvated molecule, respectively. It is noted that both of $\hat{F}$ and $\hat{V}$ are the functional of MOs, which change upon transferring from gas phase to solution phase,

$$\hat{F} = \hat{F}^0 + \Delta\hat{F},$$
$$\hat{V} = \hat{V}^0 + \Delta\hat{V},$$

where both of $\hat{F}^0$ and $\hat{V}^0$ are associated with the electronic wave function of the solute molecule in gas phase. Thus, the orbital-energy shift by solvation ($\Delta\varepsilon_i$) is given by

$$\Delta\varepsilon_i = \varepsilon_i - \varepsilon_i^0 = \varepsilon_i^{\mathrm{UV}} + \varepsilon_i^{\mathrm{rlx}} + \varepsilon_i^{\mathrm{ee}} + \varepsilon_i^{\mathrm{wf}}, \tag{4.3}$$

where

$$\varepsilon_i^{\mathrm{UV}} \equiv \left\langle \psi_i^0 \left| \hat{V}^0 \right| \psi_i^0 \right\rangle, \tag{4.4}$$
$$\varepsilon_i^{\mathrm{rlx}} \equiv \left\langle \psi_i^0 \left| \Delta\hat{V} \right| \psi_i^0 \right\rangle, \tag{4.5}$$
$$\varepsilon_i^{\mathrm{ee}} \equiv \left\langle \psi_i^0 \left| \Delta\hat{F} \right| \psi_i^0 \right\rangle. \tag{4.6}$$

$\varepsilon_i^{\mathrm{wf}}$ is all the other contributions arising from the change in wave function, $\psi_i - \psi_i^0 \equiv \Delta\psi_i$. This term can be reduced by using orthogonality of MOs.[28]

$$\begin{aligned}
\varepsilon_i^{\mathrm{wf}} &= \left\langle \psi_i \left| \hat{F} + \hat{V} \right| \psi_i \right\rangle - \left\langle \psi_i^0 \left| \hat{F} + \hat{V} \right| \psi_i^0 \right\rangle \\
&= 2\left\langle \Delta\psi_i \left| \hat{F} + \hat{V} \right| \psi_i \right\rangle - \left\langle \Delta\psi_i \left| \hat{F} + \hat{V} \right| \Delta\psi_i \right\rangle \\
&= 2\varepsilon_i \langle \Delta\psi_i | \psi_i \rangle + \mathcal{O}\{(\Delta\psi_i)^2\} = 2\varepsilon_i \langle \Delta\psi_i | \psi_i^0 \rangle + \mathcal{O}\{(\Delta\psi_i)^2\} \simeq 0.
\end{aligned} \tag{4.7}$$

$\Delta\varepsilon_i$ is then expected to be approximated as follows;

$$\Delta\varepsilon_i \simeq \varepsilon_i^{\mathrm{UV}} + \varepsilon_i^{\mathrm{rlx}} + \varepsilon_i^{\mathrm{ee}}. \tag{4.8}$$

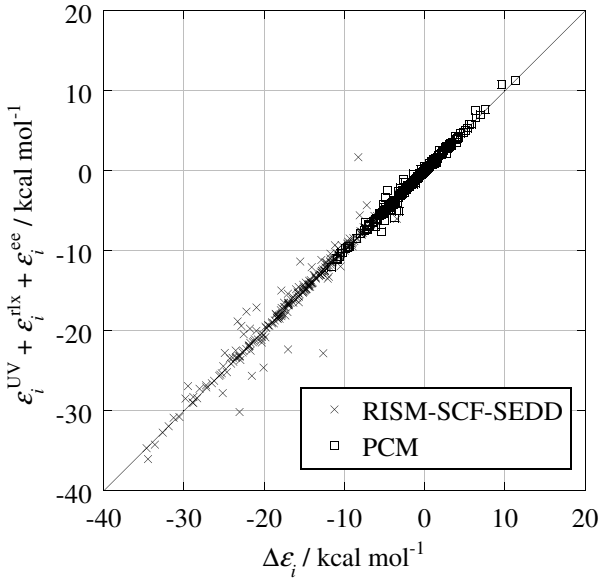

Figure 4.3: Comparison between the exact values ($\Delta\varepsilon_i$) and Eq. (4.8)

The quantities of both sides of this equation were separately obtained for comparison: the left hand side is the difference computed by subtracting gas-phase ε_i^0 from ε_i directly obtained with PCM or RISM-SCF-SEDD methods. The right hand side is the sum of matrix components that are related to PCM or RISM-SCF-SEDD procedure. As shown in Fig.4.3, the contribution from $\varepsilon_i^{\mathrm{wf}}$ is surely negligible and the orbital-energy shift, $\Delta\varepsilon_i$, is well approximated by the sum of the three terms, namely, right hand side of Eq. (4.8) in almost all cases.

Let us proceed to further simplification of the relation. By expanding about arbitrary point, $\varepsilon_i^{\mathrm{UV}}$ is rewritten as follows,

$$\varepsilon_i^{\mathrm{UV}} = \left\langle \psi_i^0 \left| \hat{V}^0 \right| \psi_i^0 \right\rangle = Q_i V^0 + \boldsymbol{\mu}_i^0 \cdot \mathbf{R}^0 + \cdots, \tag{4.9}$$

where Q_i and $\boldsymbol{\mu}_i^0$ are the total charge and dipole moment associated with i-th MO, respectively.

For charged molecules, the first term in the right hand side ($Q_i V^0$) is dominative. In particular for highly symmetric system, the orbital shift may be simplified only with this $\varepsilon_i^{\mathrm{UV}}$ because of the absence of the contribution from polarization. The other two terms ($\varepsilon_i^{\mathrm{ee}}$ and $\varepsilon_i^{\mathrm{wf}}$) in Eq. (4.8) are not necessary to be considered. Since the occupation number in a MO, corresponding

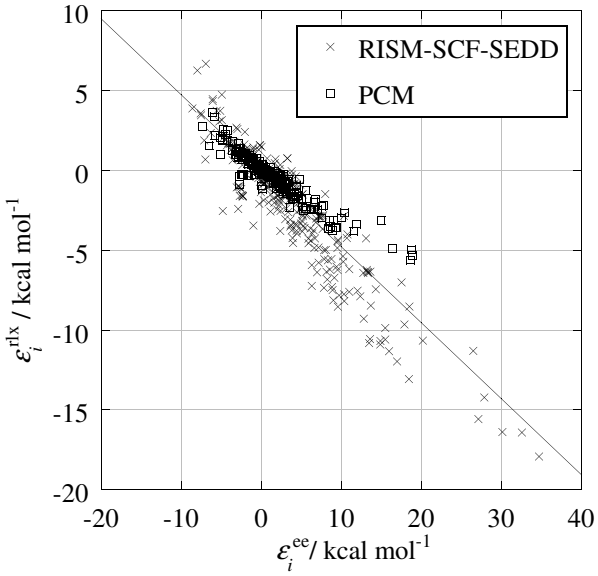

Figure 4.4: Comparison between $\varepsilon_i^{\mathrm{ee}}$ and $\varepsilon_i^{\mathrm{rlx}}$, both of them are computed by PCM and RISM-SCF-SEDD. The slope of the plotted line is -0.476. See the text and Eq. (4.14).

to Q_i is a constant, the energy shift is simply written as (approximation 0),

$$\Delta\varepsilon_i^{\mathrm{approx\ 0}} = V^0. \tag{4.10}$$

Note that the electrostatic potential V^0 is mostly determined from the total charge of the solute molecule as discussed below.

If the solute is neutral molecule, the first term in Eq. (4.9) is vanished and the second term becomes the leading one, in which $\mathbf{R}^0$ is the reaction field corresponding to the total dipole moment of the solute molecule in isolated state ($\boldsymbol{\mu}^0$). To study the two terms neglected in Eq. (4.8)–namely $\varepsilon_i^{\mathrm{rlx}}$ and $\varepsilon_i^{\mathrm{ee}}$–the relationship between them is plotted in Figure 4.4. Both of PCM and RISM-SCF-SEDD computational results clearly show a strong correlation between these two quantities. It should be emphasized that the MOs examined here are gathered from a variety of organic compounds. Within the framework of Onsager's dielectric continuum model, this can be explained as follows; the change of reaction field ($\Delta\mathbf{R}$) come from the density change is given by,[29]

$$\Delta\mathbf{R} = -\frac{2(\epsilon-1)}{2\epsilon+1}\frac{\Delta\boldsymbol{\mu}}{a^3}, \tag{4.11}$$

where ϵ is the dielectric constant of solvent, a is the cavity radius and $\Delta\boldsymbol{\mu}$ is the change in dipole moment of the solute molecule. By comparison of Eq. (4.11) with Eq. (4.5), $\varepsilon_i^{\mathrm{rlx}}$ can be related to the quantity,

$$\varepsilon_i^{\mathrm{rlx}} \sim \boldsymbol{\mu}_i^0 \cdot \Delta\mathbf{R} = -\frac{2(\epsilon-1)}{2\epsilon+1}\frac{\boldsymbol{\mu}_i^0 \cdot \Delta\boldsymbol{\mu}}{a^3}. \tag{4.12}$$

In a similar manner, $\varepsilon_i^{\mathrm{ee}}$ is the change in the Fock operator, which is linked to the change of electronic energy. On the analogy of the expression of the polarization cost using the polarizability of the solute molecule (α),

$$\varepsilon_i^{\mathrm{ee}} \sim \frac{\boldsymbol{\mu}_i^0 \cdot \Delta\boldsymbol{\mu}}{2\alpha}. \tag{4.13}$$

As seen in the definition, the contribution is an expectation value of wave function and not proportional to $(\Delta\boldsymbol{\mu})^2$ because such a contribution is included in $\varepsilon_i^{\mathrm{wf}}$. We then reached the following equation using the relationship.[30]

$$\varepsilon_i^{\mathrm{rlx}} \sim -\frac{4(\epsilon-1)}{2\epsilon+1}\frac{\alpha}{a^3}\varepsilon_i^{\mathrm{ee}} = -\frac{4(\epsilon-1)}{2\epsilon+1}\frac{n^2-1}{n^2+2}\varepsilon_i^{\mathrm{ee}}. \tag{4.14}$$

Note that the solute-dependent parameters, α and a, can be removed from the equation. The proportional constant involves just two parameters, n and ϵ, where n is the refractive index of the solute molecule and typically about 1.4 for almost all organic compounds.[31] Both of the parameters are then virtually regarded as constant values, independent on the choice of solute molecule. From Eq. (4.14) with n=1.4 and ϵ=80.0, the slope is determined as -0.476. As seen in the figure, this value coincides with the distribution for examined 265 MOs. Using this relationship, Eq. (4.8) can be then rewritten as an approximated form that is valid for many organic compounds in aqueous solution (approximation I).

$$\Delta\varepsilon_i^{\text{approx I}} \simeq \varepsilon_i^{\mathrm{UV}} + \left\{1 - \frac{2\epsilon+1}{4(\epsilon-1)}\frac{n^2+2}{n^2-1}\right\}\varepsilon_i^{\mathrm{rlx}} = \varepsilon_i^{\mathrm{UV}} + C_{\mathrm{I}}\varepsilon_i^{\mathrm{rlx}}, \tag{4.15}$$

where C_{I} equals to -1.102 for organic compounds in aqueous solution. Alternatively we can derive (Approximation II),

$$\Delta\varepsilon_i^{\text{approx II}} \simeq \varepsilon_i^{\mathrm{UV}} + \left\{-\frac{4(\epsilon-1)}{2\epsilon+1}\frac{n^2-1}{n^2+2} + 1\right\}\varepsilon_i^{\mathrm{ee}} = \varepsilon_i^{\mathrm{UV}} + C_{\mathrm{II}}\varepsilon_i^{\mathrm{ee}}. \tag{4.16}$$

$C_{\rm II}$ equals $+0.524$ for the same conditions.

Since the increase of the dipole moment by solvation is given by the Onsager's model,

$$\Delta\boldsymbol{\mu} = \left\{ \frac{(n^2+2)(2\epsilon+1)}{3(2\epsilon+n^2)} - 1 \right\} \boldsymbol{\mu}^0 = \frac{2}{3}\frac{(n^2-1)(\epsilon-1)}{2\epsilon+n^2}\boldsymbol{\mu}^0, \tag{4.17}$$

and the reaction field is proportional to this quantity, the orbital-energy shift might be further simplified only with using $\varepsilon_i^{\rm UV}$ (approximation III),

$$\begin{aligned} \Delta\varepsilon_i^{\text{approx III}} &\simeq \left[1 + \left\{ 1 - \frac{2\epsilon+1}{4(\epsilon-1)}\frac{n^2+2}{n^2-1} \right\} \frac{2}{3}\frac{(n^2-1)(\epsilon-1)}{2\epsilon+n^2} \right] \varepsilon_i^{\rm UV} \\ &= \frac{(2\epsilon+1)(n^2+2)}{6(2\epsilon+n^2)}\varepsilon_i^{\rm UV} = C_{\rm III}\varepsilon_i^{\rm UV}, \end{aligned} \tag{4.18}$$

where $C_{\rm III}$=0.656. In this form the shift can be estimated only from the information of gas-phase electronic structure. Remember that Gao, Luque and Orozco discussed induced dipole moment of molecules in aqueous solution based on QM/MM simulations.[13] They found that the dipole moment of organic compound in aqueous solution is about 1.3 times larger than that in gas phase for a variety of organic compounds. Actually, the prefactor of the right-hand side of Eq. (4.17) is 0.31 by using $n = 1.4$ and $\epsilon = 80.0$, which shows excellent agreement with their report.

4.4 Computational results and discussions

4.4.1 Ionic species in aqueous solution

Winter *et al.*[3] recently observed the IP of several ions in aqueous solution. Here we consider ionization of several atomic species in aqueous solution as follows;

$$\begin{aligned} M^+ &\rightarrow M^{2+} + e^- \quad (M = \text{Li, Na, K}) \\ A^- &\rightarrow A + e^- \quad (A = \text{F, Cl, Br, I}). \end{aligned}$$

According to the Koopmans' theorem, the orbital energies computed by RISM-SCF-SEDD and PCM are regarded as the reversed sign of IPs. The change of IPs by solvation (ΔIP) is calculated as the difference between the orbital energies computed by both of the methods.

$$-\Delta\text{IP} = \Delta\varepsilon_i^{\rm PCM} \quad \text{or} \quad -\Delta\text{IP} = \Delta\varepsilon_i^{\rm RISM-SCF}. \tag{4.19}$$

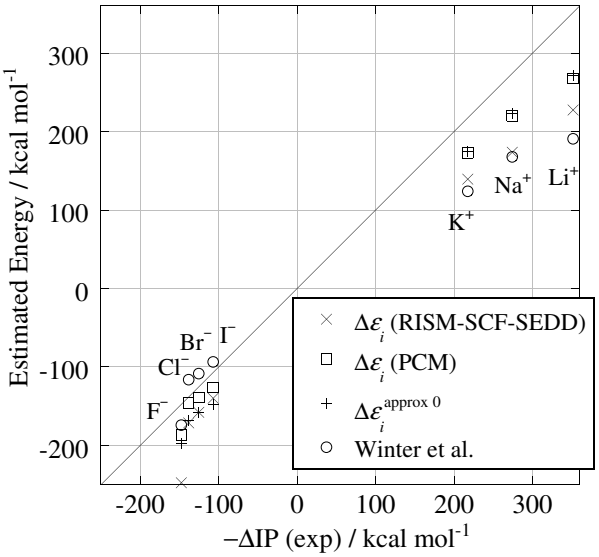

Figure 4.5: The shift computed by PCM, RISM-SCF-SEDD as well as the approximation formula of Eq. (4.20), in comparison with the experimental values, together with the values reported by Winter *et al*.[3]

As an example, computed IPs of Cl^- in gas phase are 4.1 eV (Koopmans) and 3.2 eV (ΔMP2),[32] respectively. In aqueous solution, the evaluated values are 11.7 eV (Koopmans) and 10.9 eV (ΔMP2), indicating the difference between the two methods is similar in magnitude to the gas phase. This trend is also found in polyatomic molecular systems. The most important is the difference is much smaller than the effect from solvation, especially for ionic species, and the discussion based on the Koopmans' theorem is expected to provide correct understanding in semi-quantitative sense.

In the present simplest system, an equivalent quantity can be evaluated from the above mentioned "approximation 0." By using Born approximation with ionic radius a, the shift is written as,

$$\Delta\varepsilon_i^{\text{approx }0} = V^0 \simeq \left(1 - \frac{1}{\epsilon}\right)\frac{Q}{a}, \tag{4.20}$$

where Q is total charge of the ionic species. a's are taken from the PCM parameters. Figure 4.5 compares Eq. (4.20) with corresponding experimental values. A good agreement is seen in all data; *ab initio* RISM-SCF-SEDD and PCM can reproduce the experimental data while

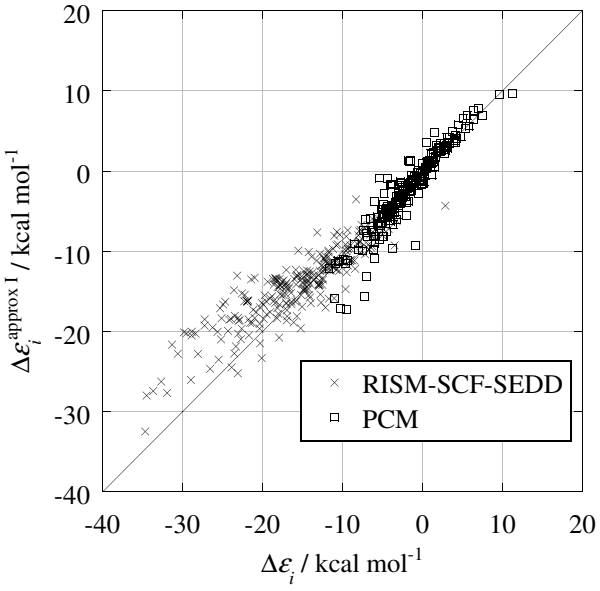

Figure 4.6: Comparison between the exact values ($\Delta\varepsilon_i$) and the approximation formula of Eq. (4.15).

the simplest formula also shows good accordance with experiments and highly sophisticated theoretical methods. Some of the plots evaluated from Eq. (4.20) coincide with PCM values very well because both of them are based on the dielectric continuum theory. The present estimations also show an excellent agreement with the values reported by Winter et al.[3]

4.4.2 Verification of the Approximations

We would like to check accuracy of the introduced approximations for other ordinary polyatomic molecules. Similar to the treatment on Eq. (4.8), the exact value of the shift ($\Delta\varepsilon_i$) is compared with the formulae, $\Delta\varepsilon_i^{\text{approx I}}$(Figure 4.6), $\Delta\varepsilon_i^{\text{approx II}}$(Figure 4.7) and $\Delta\varepsilon_i^{\text{approx III}}$(Figure 4.8). In all the figures, results from PCM and RISM-SCF-SEDD are plotted all together. In any cases, the approximated formulae work well and the shift can be understood over a variety of MOs. The approximation II looks slightly better than I presumably because $\varepsilon_i^{\text{ee}}$ used in this expression is a direct quantity related to the electronic structure of solute molecule whilst $\varepsilon_i^{\text{rlx}}$ is the electrostatic interaction from solvent field, which indirectly associated with the orbital property. III is the lowest level of approximation that uses just single-species matrix elements,

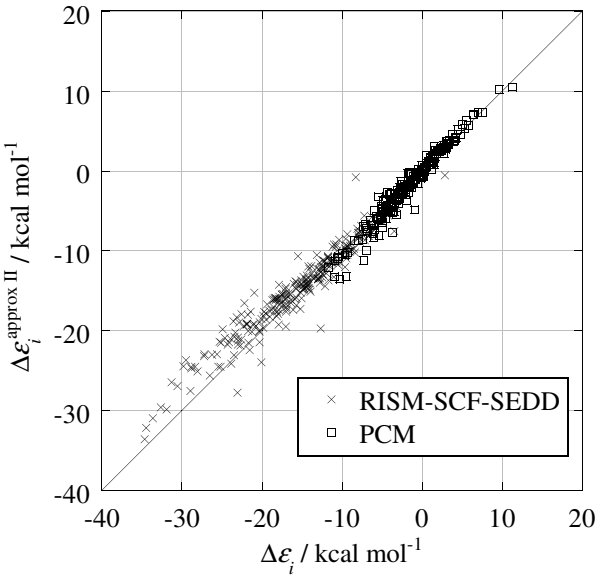

Figure 4.7: Comparison between the exact values ($\Delta\varepsilon_i$) and the approximation formula of Eq. (4.16).

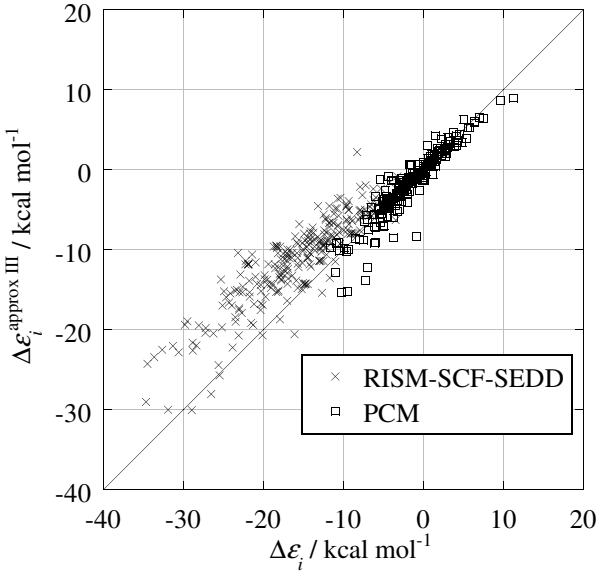

Figure 4.8: Comparison between the exact values ($\Delta\varepsilon_i$) and the approximation formula of Eq. (4.18).

$\varepsilon_i^{\mathrm{UV}}$. Even with this simple expression, the estimated shifts are satisfactory, strongly indicating that the orbital-energy shift is essentially derived from the electrostatic interaction acting on MO. Good agreement between the two solvation methods indicates that the derived approximations are universal and applicable to other type of solvation theories.

4.4.3 Orbital energy shift in various solvents

The obtained relationships are also valid for other solvents. Figure 4.9 shows the exact shifts in methanol (upper panel) and in acetonitrile (lower panel) compared to the approximation III formula. The dielectric constants are 32.62 (methanol) and 36.64 (acetonitrile), leading to 0.651 and 0.652 of C_{III}, respectively. Again, good agreements are found in all the cases: the orbital energy shifts in methanol computed from the two methods are plotted in narrow confine. The result in acetonitrile solvent is also similar, but somewhat interesting. The values computed by RISM-SCF-SEDD tend to be distributed at the right hand side of the line, suggesting that the electrostatic solute-solvent interactions evaluated by RISM-SCF-SEDD are slightly stronger than those by the dielectric continuum theory. We would like to remind the readers that it makes sense that the PCM results are closer to the line because the approximated formula is derived with the aid of dielectric continuum model. It would be possible that the RISM-SCF-SEDD results are closer to the 'experimental' values —which are not available at this moment— because RISM-SCF-SEDD is based on the atomic level interaction between molecules, and specific coordination and local structure such as hydrogen bonding are explicitly treated. There is still controversy over the liquid structure of acetonitrile but it is very plausible that strong electric field is generated in this highly polar solvent.

The main difference between PCM and RISM-SCF-SEDD is usually attributed to the capability to describe such specific solvation structure. As seen in Eq. (4.18), the shift is predictable if the electrostatic interaction is known.

$$C_{\mathrm{III}}\varepsilon_i^{\mathrm{UV}} = C_{\mathrm{III}}\left\langle \psi_i^0 \left| \hat{V}^0 \right| \psi_i^0 \right\rangle. \tag{4.21}$$

Note that all the information in the last term contains only gas-phase quantities, meaning that the shift can be estimated, in principle, only from the electronic structure obtained by standard

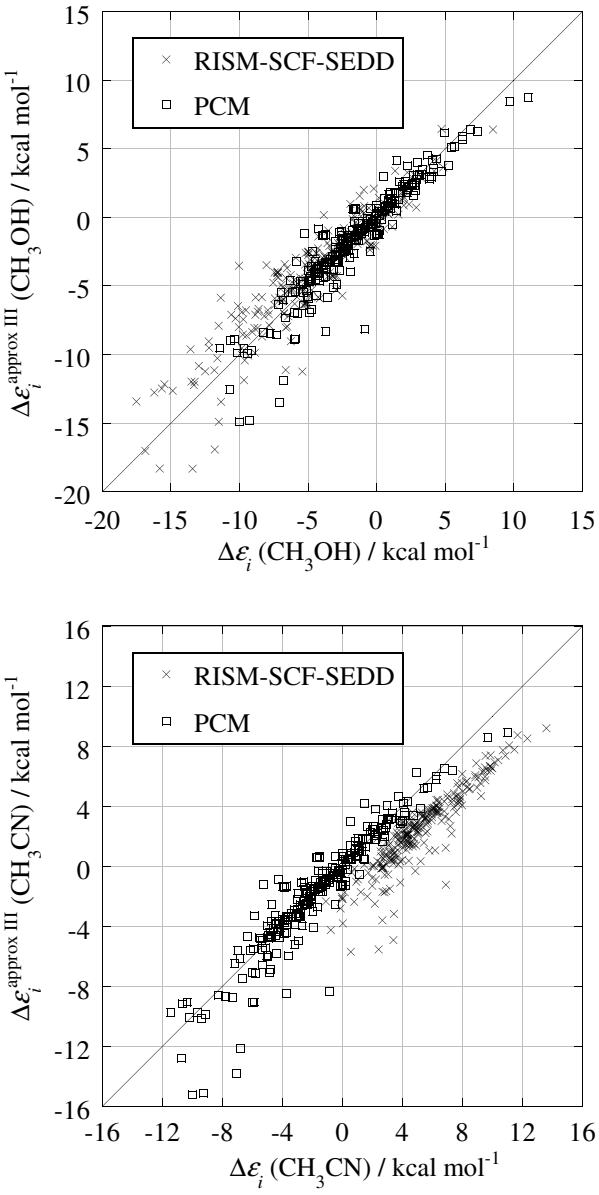

Figure 4.9: The energy shift in methanol (upper panel) and acetonitrile (lower panel). The exact values ($\Delta\varepsilon_i$) and the approximation formula of Eq. (4.18) are compared.

MO method. However, in practice, determination of $\hat{V}^0$ is not simple and depends on the solvation methods.[33,34] In the RISM-SCF-SEDD theory, the potential operator of solvation effect is evaluated from PCFs between the solute site A and solvent s, $g_{As}(r)$.

$$\hat{V}_{(\mathrm{RISM-SCF})} = \sum_A \hat{b}_A \sum_s \rho \int_0^\infty 4\pi r^2 g_{As}(r) \frac{q_s}{r} dr, \tag{4.22}$$

where $\hat{b}_A$ is an appropriate population operator on atom A.[8] In evaluation of $\hat{V}^0$, PCFs were evaluated from the electronic structure fixed to isolated molecule ($g^0_{As}(r)$). The corresponding operator in PCM theory is evaluated from the effective charges of each tesserae on the boundary surface, σ_t,

$$\hat{V}_{(\mathrm{PCM})} = \sum_t^{\mathrm{tesserae}} \frac{\sigma_t}{|\mathbf{r} - \mathbf{r}_t|}. \tag{4.23}$$

In a similar manner, effective charge corresponding to the electronic structure in gas phase is σ^0_t. All the quantities could be computed if $\{\psi^0_i\}$ are available, but actual treatment of $\hat{V}^0$ differs in both methods. It is interesting that complicated modern computational results can be explained by unified formulas based on the simplest Onsager's theory. The dipole-moment based expression can reasonably represent the solute–solvent interaction at least in the present set of molecules.

4.4.4 Solvation structure and energy shift

Finally, we would like to get back to the orbital-energy shifts of acetamide shown in Sec. 4.1. As shown in Fig. 4.1, the orbital number 1 (oxygen core), 5 (σ-bond) and 15 (lone pair) are greatly affected by solvation. Based on Eqs. (4.9) and (4.18), the shift must be attributed to the interaction between the i-th orbital dipole moment ($\boldsymbol{\mu}_i$)[35] and total dipole moment of the molecule ($\boldsymbol{\mu}^0$),

$$\varepsilon_i^{\mathrm{UV}} \simeq \boldsymbol{\mu}_i^0 \cdot \mathbf{R}^0 = -\frac{2(\epsilon-1)}{2\epsilon+1} \frac{\boldsymbol{\mu}_i^0 \cdot \boldsymbol{\mu}^0}{a^3} = -\frac{2(\epsilon-1)}{2\epsilon+1} \frac{|\boldsymbol{\mu}_i^0|\,|\boldsymbol{\mu}^0| \cos\theta_i}{a^3}, \tag{4.24}$$

where θ_i is the angle between $\boldsymbol{\mu}_i$ and the total dipolemoment. $\boldsymbol{\mu}_i$ for the three orbitals are 8.9, 6.4 and 6.7 D, respectively. As seen in Fig. 4.1, larger amplitudes in the 1st, 5th and 15th orbitals are found near oxygen atom, which is one of the keys to make the orbital shifted.

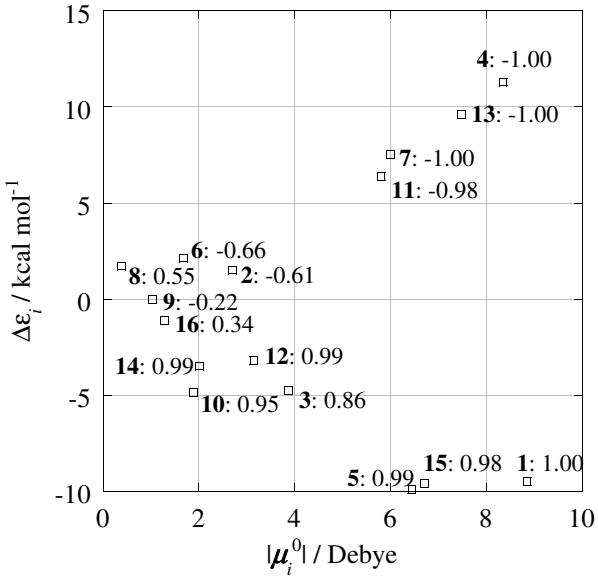

Figure 4.10: Orbital energy shift in acetamide compared with the absolute value of dipole moment attributed to each MO ($\boldsymbol{\mu}_i^0$). The orbital number and $\cos\theta_i$ are also shown.

Another important aspects drawn from the equation is the relative directions of the two dipole moments (see Fig. 4.10). For example, $|\boldsymbol{\mu}_4|$ is large enough (8.4 D) but its direction is almost opposite to that of the total dipole moment of the molecule, $\boldsymbol{\mu}^0$. As a result, the orbital energy is positively shifted. In summary, combination of spatial extension of the MO and electrostatic field generated by surrounding solvent governs the energy shift of MOs.

4.5 Conclusions

We present a systematic understanding for energy shift of MO by solvation effect. With the aid of dielectric continuum theory, several simple formulae are developed to rationalize the orbital energy shifts. For charged system, Born-type treatment is acceptable to estimate the orbital shift. At the same time, approximated formulae based on the Onsager-type model are satisfactory for examined 265 MOs of neutral species. We found that both of the spatial distribution of MO and electrostatic field generated by surrounding solvent are important to determine the orbital energy shift. The developed formulae are valid to explain both for PCM and RISM-SCF-SEDD computations, strongly indicating the discussion in this study is a common

consequence to understand the electronic structure of solvated molecule, being independent of the choice of solvation theories.

The orbital shift is not a direct observable but deeply related to IP and/or electron affinity via the Koopmans' theorem. In the forthcoming paper, the relationship between the experimental measurements and computational evaluation for solvated molecule will be extensively discussed.

Bibliography

[1] A. Szabo and N. S. Ostlund, *Modern Quantum Chemistry* (MacMillan,New York, 1982).

[2] B.Winter, R. Weber, W. Widdra, M. Dittmar, M. Faubel, I.V. Hertel, J. Chem. Phys., **108**, 2625 (2004).

[3] B. Winter, R. Weber, I. V. Hertel, M. Faubel, P. Jungwirth, E. C. Brown, S. E. Bradforth, J. Am. Chem. Soc., **127**, 7203 (2005).

[4] K. Iida, D. Yokogawa, H. Sato, S. Sakaki, Chem. Phys. Lett., **443**, 264 (2007).

[5] R. R. Conteras, A. J. Aizman Inter. J. Quan. Chem., **24**, 89 (1990).

[6] G. Alagona, C. Ghio, J. Igual, Jacopo. Tomasi J. Mol. Struc. (Theochem), **204**, 253 (1990).

[7] E. S. Marcos, J. Maraver, M. F. Ruiz-Lopez, J. Bertran, Can. J. Chem, **64**, 2353 (1986).

[8] S. Ten-no, F. Hirata, S. Kato, J. Chem. Phys., **100**, 7443 (1994).

[9] H. Sato, F. Hirata, S. Kato, J. Chem. Phys., **105**, 1546 (1996).

[10] D. Yokogawa, H. Sato, S. Sakaki, J. Chem. Phys., **126**, 244504 (2007).

[11] J. Tomasi, M. Persico, Chem. Rev, **94**, 2027 (1994).

[12] J. Gao, X. Xia, *Science*, **258**, 631 (1992).

[13] J. Gao, F. J. Luque, M. Orozo, J. Chem. Phys., **98**, 2975 (1993).

[14] For Br, L. A. Curtiss, M. P. McGrath, J.-P. Blaudeau, N. E. Davis, R. C. Binning, Jr., L. Radom, J. Chem. Phys., **103**, 6104 (1995)and For I, M. N. Glukhovtsev, A. Pross, M. P. McGrath, L. Radom, J. Chem. Phys., **103**, 1878 (1995).

[15] D. Elking, T. Darden, R. J. Woods, J. Comput. Chem., **28**, 1261 (2007).

[16] S.J. Singer, D. Chandler, Mol. Phys., **55**, 621 (1985).

[17] S.J. Weiner, P.A. Kollman, D.A. Case, U.C. Singh, C. Ghio, G. Alagona, S. Profeta, Jr, P. Weiner, J. Am. Chem. Soc., **106**, 765 (1984).

[18] S.J. Weiner, P.A. Kollman, D.T. Nguyen, D.A. Case, J. Comput. Chem., **7**, 230 (1986).

[19] R. C. Rizzo, W. L. Jorgensen, J. Am. Chem. Soc., **121**, 4827 (1999).

[20] M. Kinoshita, F. Hirata, J. Chem. Phys., **106**, 5202 (1997).

[21] B. M. Pettitt, P. J. Rossky, J. Chem. Phys., **84**, 5836 (1986).

[22] H.J.C. Berendsen, J.P.M. Postma, W.F. van Gunsteren, J. Hermans, in B. Pullman (Ed.), *Intermolecular Forces*, Reidel, Dordrecht, 1981.

[23] W. L. Jorgensen, J. M. Briggs, Mol. Phys., **63**, 547 (1988).

[24] W. L. Jorgensen, J. Phys. Chem., **90**, 1276 (1986).

[25] W. L. Jorgensen, J. D. Madura, C. J. Swenson, J. Am. Chem. Soc., **106**, 6638 (1984).

[26] M. W. Schmidt, K. K. Baldridge, J. A. Boatz, S. T. Elbert, M.S. Gordon, J. H. Jensen, S. Koseki, N. Matsunaga, K. A. Nguyen, S. Su, T. L. Windus, M. Dupuis, J. A. Montgomery, J. Comput. Chem., **14**, 1347 (1993).

[27] M. J. Frisch, G. W. Trucks, H. B. Schlegel, et al., Gaussian 03, Revision C.02; Gaussian Inc., Wallingford, CT, 2004.

[28] F. J. Luque, J. M. Bofill, M. Orozco, J. Chem. Phys., **103**, 10183 (1995).

[29] C. J. F. Bottcher, *Theory of Electric Polarization*, Elsevier, Amsterdam (1983).

[30] J. N. Wilson, *Chem. Rev.*, **25**, 377 (1939).

[31] K. Sharp, A. Jean-Charles, B. Honig, J. Phys. Chem., **96**, 3822 (1992).

[32] The energy difference between the two states were computed by MP2 and UMP2 method. When applying ΔSCF methods, computed values were 2.5 eV (gas) and 10.2 eV (aqueous). The good agreement with ΔMP2 comes from the well-known cancellation of electron correlation and the orbital relaxation in the Koopmans' theorem,[1] which does not occur in ΔSCF.

[33] B. Mennucci, R. Cammi (Editors), *Continuum Solvation Models in Chemical Physics: From Theory to Applications*, Wiley (2007).

[34] H. Sato, S. Sakaki, J. Phys. Chem. A, **108**, 1629 (2004).

[35] The origin was set to the center of nuclear charges.

Chapter 5

Theoretical study on ionization process in aqueous solution

5.1 Introduction

Ionization energy is a fundamental quantity characterizing electronic structure. It is classified in terms of the presence of relaxation process, namely adiabatic ionization energy and vertical ionization energy. The former in the gas phase has been measured by photoelectron spectroscopy[1,2] and the value in the solution phase has been also estimated from redox potential.[3] On the other hand, vertical ionization energy had been measured only in the gas phase because of experimental difficulty in solution phase. Winter et al. recently measured the vertical ionization energy of various molecules (*e.g.* water, halogen anion, alkali cation, and transition metal complex) in aqueous solution.[4–9] They show that the energy in aqueous solution is significantly different from the gas-phase value. The spectral width of vertical ionization is also reported, indicating that the width in the solution phase is significantly broadened caused by thermal fluctuation of solvent molecule.

The difference between vertical and adiabatic ionization in the gas phase is simply attributed to the molecular structure. Upon the ionization, the structure remains unchanged (vertical ionization), and then relaxes toward the equilibrium structure in the ionized state (adiabatic ionization). On the other hand, because a molecule in solution phase strongly interacts with the surrounding solvent molecules, the ionization is deeply related to their thermal fluctuation, *i.e.* solvation structure. Marcus is the first to realize the importance of the fluctuation of solvent molecules upon electron transfer reaction, and proposed the concept of free energy sur-

face.[10,11] In this concept, the thermal fluctuation is expressed along the "solvation coordinate", on which the free energy of the system is projected. Note that because the ionization corresponds to the oxidative half-reaction of electron transfer, the concept is also valid to treat the ionization process. While a simple dielectric continuum model was employed in the original Marcus scheme, the same concept has been utilized in the molecular level computations such as molecular dynamics (MD) simulation,[12–15] and the procedures[16–20] based on the reference interaction site model (RISM) theory.[21,22] A related quantity such as solvent reorganization energy (λ) is also adequately computed.[23] These numerous studies show that the free energy surface is often well described by the linear response regime in spite of the complexity caused by a huge number of solvent molecules.[12–15,24–26] But a direct comparison with experimental knowledge is still very limited, presumably because of the lack of related experimental data.

In this paper, we report a theoretical study of ionization process in solution phase. Based on the Marcus-like free energy surface, the ionization and following relaxation processes are discussed in connection with the role of solvation through the comparison with experimental data. To achieve the purpose, an accurate evaluation of free energy upon the ionization is essential. In other words, an appropriate ensemble of solvent configurations that are consistent with the change in the electronic structure of solute molecule is required. RISM-SCF,[27,28] a hybrid method of RISM theory[21,22] and *ab initio* electronic structure theory, is regarded as an alternative to QM/MM. Using RISM-SCF, the electronic structure of solute molecule and solvation structure around it are obtained in a self-consistent manner. RISM theory is statistical mechanics for molecular liquid, and treats an ensemble of an infinite number of solvent molecules. It enables us to obtain the molecular-level insight into the solvation effect. In addition, it is possible to combine with highly sophisticated electronic structure theory because the computational cost of the RISM theory is much lower than that of MD simulation. Recently, RISM-SCF is extended to the new version in which spacial electron density distribution (SEDD) is explicitly taken into account (RISM-SCF-SEDD method).[30]

The article is organized as follows. In Sec. II, a computational procedure for ionization energy in solution phase is explained. A new formula for the vertical ionization energy is

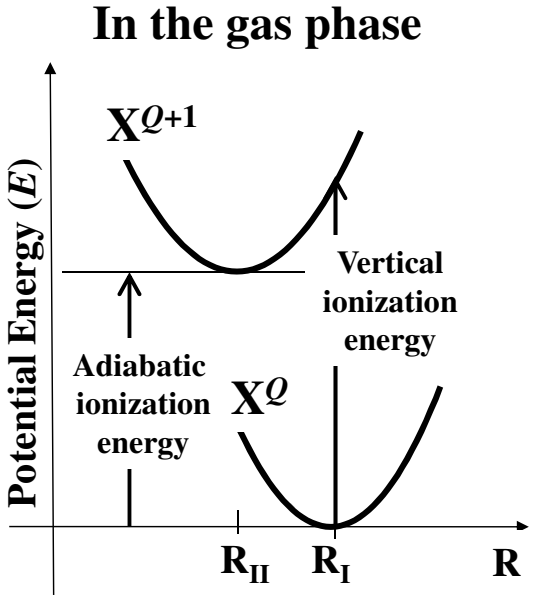

Figure 5.1: Ionization process in the gas phase.

developed with the aid of dielectric continuum theory[31–33] in terms of the solvent relaxation process.[34–39] The computational results are presented in Sec. III and IV, followed by the conclusion in Sec. V.

5.2 Theoretical Method

5.2.1 Ionization Process in the Gas Phase

Let us first review the ionization of a molecule X with total charge Q (X^Q) in the gas phase,

$$\mathrm{X}^Q \rightarrow \mathrm{X}^{Q+1} + e^-. \tag{5.1}$$

The ionization energy is related to the molecular geometry described by a set of all the atomic coordinates ($\{\mathbf{R}\}$). Figure 5.1 shows ionization process in the gas phase. The lower is the potential energy surface of X^Q and the upper one is that of the ionized species (X^{Q+1}) after the electron detachment. $\{\mathbf{R}_\mathrm{I}\}$ is the equilibrium geometry of X^Q. The potential energy difference between X^{Q+1} and X^Q at the fixed geometry corresponds to the vertical ionization energy in the gas phase.

$$I_{\mathrm{ver}}^{\mathrm{g}} = E^+(\{\mathbf{R}_\mathrm{I}\}) - E^0(\{\mathbf{R}_\mathrm{I}\}), \tag{5.2}$$

where superscripts 0 and + respectively denote the state of X^Q and X^{Q+1}, E^0 and E^+ are their total energies. After the ionization, the molecule starts to relax and reaches the new equilibrium geometry ($\{\mathbf{R}_{\rm II}\}$). The adiabatic ionization energy in the gas phase is defined by

$$I_{\rm ad}^{\rm g} = E^+(\{\mathbf{R}_{\rm II}\}) - E^0(\{\mathbf{R}_{\rm I}\}). \tag{5.3}$$

5.2.2 Ionization Process in Solution Phase

In solution phase, a set of all the coordinates of solvent molecule ($\{\mathbf{r}\}$) is also necessary to be considered. Instead of using this huge number of variables, it is convenient to introduce solvation coordinate S.[12] Free energy surface in the vicinity of equilibrium state is expressed as a function of S.

$$A^x(S) \;=\; A^x_{\rm min} - \frac{1}{\beta}\ln P^x(S), \tag{5.4}$$

where superscript x denotes the charge-state 0 or +, $\beta = 1/k_BT$, and k_B is the Boltzmann constant. $A^x_{\rm min}$ corresponds to the minimum of the free energy curvature.[25] $P^x(S)$ is the probability to find the system where S equals the difference in the total energy of the system between the neutral and ionized states ($\Delta E \equiv \Delta E(\{\mathbf{R}\},\{\mathbf{r}\})$).

$$\begin{aligned} P^x(S) &= \langle \delta\left[S - \Delta E(\{\mathbf{R}\},\{\mathbf{r}\})\right]\rangle_x \\ &= \frac{\displaystyle\int \delta\left[S - \Delta E(\{\mathbf{R}\},\{\mathbf{r}\})\right] \exp\left\{-\beta[E^x(\{\mathbf{R}\},\{\mathbf{r}\})]\right\} \mathrm{d}\{\mathbf{R}\}\mathrm{d}\{\mathbf{r}\}}{\displaystyle\int \exp\left\{-\beta[E^x(\{\mathbf{R}\},\{\mathbf{r}\})]\right\} \mathrm{d}\{\mathbf{R}\}\mathrm{d}\{\mathbf{r}\}}, \end{aligned} \tag{5.5}$$

where δ is delta function, and $\langle \ldots \rangle_x$ denotes the ensemble average with state x. It is often approximated with gaussian function,[26]

$$P^x\left(S\right) = \frac{1}{\sqrt{2\pi}\sigma_x} \exp\left\{-\frac{\left(S - \langle \Delta E\rangle_x\right)^2}{2\sigma_x^2}\right\}, \tag{5.6}$$

The variance σ_x is directly related to the spectral width of $I_{\rm ver}$.[5,6] Figure 5.2 illustrates the ionization process in solution. Different from the gas phase phenomena shown in Figure 5.1, the horizontal and vertical axes respectively represent solvation coordinate S and free energy.

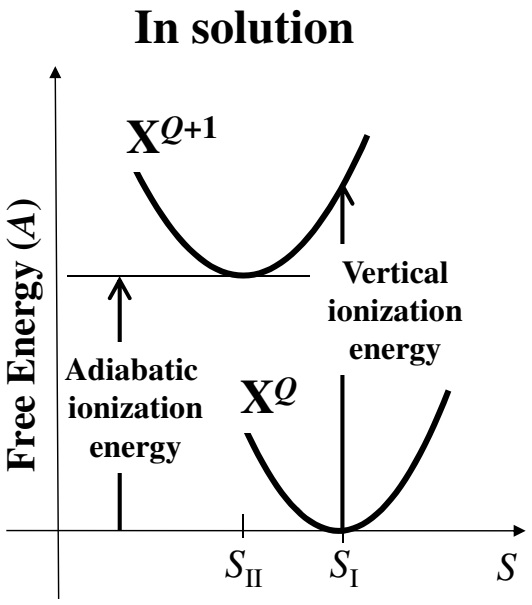

Figure 5.2: Ionization process in solution.

The surface of X^Q has the minimum at S_I. Since the vertical ionization process occurs at the solvation of S_I with the highest probability, the observed I_{ver} is given by

$$I_{ver} = A^+(S_I) - A^0(S_I) = \langle \Delta E \rangle_0 . \tag{5.7}$$

After the vertical ionization, S is changed through the relaxation of solvent configuration. The surface of X^{Q+1} has the minimum at S_{II}. Adiabatic ionization energy is obtained as the free energy difference between the two minimum.[24,25,40]

$$I_{ad} = A^+(S_{II}) - A^0(S_I). \tag{5.8}$$

5.2.3 Vertical Ionization Energy

RISM-SCF-SEDD is an efficient method as far as equilibrium process is concerned and I_{ad} is directly evaluated from Eq. (5.8). However, I_{ver} cannot be calculated with the original procedure because X^{Q+1} at S_I is not in equilibrium state. In the present study, the generalization is considered based on the charging formula with the aid of generalized Born theory.[32,33] The analogous procedure is applied to PCM method based on the similarity in the treatment of electrostatic interaction between solute and solvent.[23,41]

Let us first consider a set of vectors ($\mathbf{Q}^0$ and $\mathbf{Q}^+$), respectively corresponding to neutral and ionized states. The vector component is the charge assigned to each atom (site) in the focused solute molecule. The solute-solvent electrostatic interaction potential generated on this site is also represented as a vector ($\mathbf{V}$). It is noted that the following discussion is applicable to any kind of theoretical framework, and an extension to treat continuous electronic distribution of the solute molecule is straightforward. To treat the vertical ionization, $\mathbf{V}$ is divided into two components in terms of the relaxation time,

$$\mathbf{V} = \mathbf{V}_{\rm f} + \mathbf{V}_{\rm s}. \tag{5.9}$$

The first term of the right hand side is fast component that immediately responds to the ionization. The second term corresponds to the slow component that remains unchanged just after the ionization. With Eq. (5.9), $I_{\rm ver}$ is given as the so-called charging formula with respect to a set of charges ($\mathbf{Q}$),

$$\begin{aligned} I_{\rm ver} &= A^+(S_{\rm I}) - A^0(S_{\rm I}) \\ &= \left\{U^+(S_{\rm I}) - U^0(S_{\rm I})\right\} + \int_{\mathbf{Q}^0}^{\mathbf{Q}^+} \left\{\mathbf{V}_{\rm f}(S_{\rm I}) + \mathbf{V}_{\rm s}(S_{\rm I})\right\} d\mathbf{Q}, \end{aligned} \tag{5.10}$$

where U^+ and U^0 are the internal energies of solute molecule. respectively. Because of the difference in the response of the field, $\mathbf{V}_{\rm f}$ and $\mathbf{V}_{\rm s}$, the integrations are separately performed. The slow component $\mathbf{V}_{\rm s}$ remains in the first state ($\mathbf{V}_{\rm s}^0$) just after the vertical ionization, the integration over $\mathbf{V}_{\rm s}$ yields

$$\int_{\mathbf{Q}^0}^{\mathbf{Q}^+} \mathbf{V}_{\rm s}(S_{\rm I}) d\mathbf{Q} \simeq \left\{\mathbf{Q}^+(S_{\rm I}) - \mathbf{Q}^0(S_{\rm I})\right\} \cdot \mathbf{V}_{\rm s}^0(S_{\rm I}). \tag{5.11}$$

$\mathbf{V}_{\rm s}^0$ is the slow part of the potential for the neutral state ($\mathbf{Q}^0$). On the other hand, the fast component $\mathbf{V}_{\rm f}$ could change during the vertical ionization. If the linear dependency of $\mathbf{V}_{\rm f}$ on $\mathbf{Q}$ is assumed on the vertical ionization, then the integration of $\mathbf{V}_{\rm f}$ yields

$$\int_{\mathbf{Q}^0}^{\mathbf{Q}^+} \mathbf{V}_{\rm f}(S_{\rm I}) d\mathbf{Q} \simeq \frac{1}{2}\left\{\mathbf{Q}^+(S_{\rm I}) \cdot \mathbf{V}_{\rm f}^+(S_{\rm I}) - \mathbf{Q}^0(S_{\rm I}) \cdot \mathbf{V}_{\rm f}^0(S_{\rm I})\right\}. \tag{5.12}$$

From Eqs. (5.9)–(5.12), the following formula is obtained.

$$\begin{aligned} I_{\rm ver} &= \left\{U^+(S_{\rm I}) - U^0(S_{\rm I})\right\} + \left\{\mathbf{Q}^+(S_{\rm I}) - \mathbf{Q}^0(S_{\rm I})\right\} \cdot \mathbf{V}_{\rm s}^0(S_{\rm I}) \\ &\quad + \frac{1}{2}\left\{\mathbf{Q}^+(S_{\rm I}) \cdot \mathbf{V}_{\rm f}^+(S_{\rm I}) - \mathbf{Q}^0(S_{\rm I}) \cdot \mathbf{V}_{\rm f}^0(S_{\rm I})\right\}. \end{aligned} \tag{5.13}$$

With the aid of dielectric continuum theory, a further simple and practical equation is obtained based on Eq. (5.13). In the theory, the electrostatic potential ($\mathbf{V}^{\mathrm{dielec}}$)[35,42] is divided into fast and slow components as follows.

$$\mathbf{V}_{\mathrm{f}}^{\mathrm{dielec}} = k_{\mathrm{f}}\mathbf{V}^{\mathrm{dielec}}, \quad \mathbf{V}_{\mathrm{s}}^{\mathrm{dielec}} = k_{\mathrm{s}}\mathbf{V}^{\mathrm{dielec}}, \tag{5.14}$$

where k_{f} and k_{s} are the constants given by

$$k_{\mathrm{f}} = \left(1 - \frac{1}{\epsilon_\infty}\right)\left(1 - \frac{1}{\epsilon}\right)^{-1}, \quad \text{and} \quad k_{\mathrm{s}} = \left(\frac{1}{\epsilon_\infty} - \frac{1}{\epsilon}\right)\left(1 - \frac{1}{\epsilon}\right)^{-1}. \tag{5.15}$$

ϵ is dielectric permittivity, and ϵ_∞ is optical dielectric permittivity. In dielectric continuum theory, the slow component is considered to be the orientational polarization of solvent as well as a part of electronic polarization of solvent. The fast component is related to the electronic polarization due to the change in the electrostatic field created by the solute.[33,43] Since the electrostatic potential $\mathbf{V}$ is a common quantity among various theoretical frameworks, Eqs. (5.14) and (5.15) might be applicable to treat $\mathbf{V}$ in general.

$$\mathbf{V}_{\mathrm{f}} = k_{\mathrm{f}}\mathbf{V}, \quad \mathbf{V}_{\mathrm{s}} = k_{\mathrm{s}}\mathbf{V}. \tag{5.16}$$

Eq. (5.13) is then rewritten as

$$\begin{aligned} I_{\mathrm{ver}} &= \left\{U^+(S_{\mathrm{I}}) - U^0(S_{\mathrm{I}})\right\} + k_{\mathrm{s}}\left\{\mathbf{Q}^+(S_{\mathrm{I}}) - \mathbf{Q}^0(S_{\mathrm{I}})\right\}\cdot\mathbf{V}^0(S_{\mathrm{I}}) \\ &+ \frac{1}{2}k_{\mathrm{f}}\left\{\mathbf{Q}^+(S_{\mathrm{I}})\cdot\mathbf{V}^+(S_{\mathrm{I}}) - \mathbf{Q}^0(S_{\mathrm{I}})\cdot\mathbf{V}^0(S_{\mathrm{I}})\right\}. \end{aligned} \tag{5.17}$$

In this equation, only $\mathbf{V}$ is necessary, and neither $\mathbf{V}_{\mathrm{f}}$ nor $\mathbf{V}_{\mathrm{s}}$ is required. It should be mentioned that $\mathbf{V}$ is, indeed, well evaluated with non-polarizable solvent model such as SPC model.[44] This is because the model implicitly treats the electronic polarizability of solvent.

According to Åqvist et al., the variance (σ_x, $x = 0, +$) is calculated based on Eq. (5.6) as follows:[26]

$$\beta\sigma_x^2 = \mid \langle\Delta E\rangle_0 - \langle\Delta E\rangle_+ \mid. \tag{5.18}$$

The first term ($\langle\Delta E\rangle_0$) is directly computed with Eqs. (5.7) and (5.17), and the second term is evaluated in a similar manner.

$$\langle -\Delta E\rangle_+ = A^0(S_{\mathrm{II}}) - A^+(S_{\mathrm{II}})$$

$$
\begin{aligned}
&= \left\{U^0(S_{\mathrm{II}}) - U^+(S_{\mathrm{II}})\right\} + k_{\mathrm{s}}\left\{\mathbf{Q}^0(S_{\mathrm{II}}) - \mathbf{Q}^+(S_{\mathrm{II}})\right\}\cdot\mathbf{V}^+(S_{\mathrm{II}}) \\
&+ \frac{1}{2}k_{\mathrm{f}}\left\{\mathbf{Q}^0(S_{\mathrm{II}})\cdot\mathbf{V}^0(S_{\mathrm{II}}) - \mathbf{Q}^+(S_{\mathrm{II}})\cdot\mathbf{V}^+(S_{\mathrm{II}})\right\}. \qquad (5.19)
\end{aligned}
$$

σ_x can be then computed as the sum of these two terms. Therefore the free energy surface within the linear response regime is fully elucidated from a set of information at the specific states.

5.2.4 RISM-SCF-SEDD method

In the present study, the original RISM-SCF-SEDD[27,28,30] was employed to calculate I_{ad} while the extended formula of RISM-SCF-SEDD was used to obtain I_{ver}, as is noted in the previous section. RISM theory is given as follows:[21,22]

$$
\boldsymbol{\rho}\mathbf{h}\boldsymbol{\rho} = \boldsymbol{\omega} * \mathbf{c} * \boldsymbol{\omega} + \boldsymbol{\omega} * \mathbf{c} * \boldsymbol{\rho}\mathbf{h}\boldsymbol{\rho}, \qquad (5.20)
$$

where $*$ denotes convolution integral. The matrix element of $\boldsymbol{\rho}$ is number density, $\boldsymbol{\omega}$ represents intramolecular correlation function defining the molecular geometry, $\mathbf{c}$ is the direct correlation function, and $\mathbf{h}$ is the total correlation function, respectively. Because two unknown functions (i.e. $\mathbf{h}$ and $\mathbf{c}$) are included in Eq. (5.20), another equation relating these functions is required. A typical one is hyper-netted chain (HNC) closure,

$$
c_{\alpha\lambda}(r) = \exp\left[-\beta u_{\alpha\lambda}(r) + h_{\alpha\lambda}(r) - c_{\alpha\lambda}(r)\right] - \left\{h_{\alpha\lambda}(r) - c_{\alpha\lambda}(r)\right\} - 1. \qquad (5.21)
$$

α and λ are solute and solvent sites respectively, $u_{\alpha\lambda}(r)$ is interaction between the sites α and λ. Using Eqs. (5.20) and (5.21), an unique solvation structure is determined with respect to the given intermolecular interaction potential. The excess chemical potential (solvation free energy), $\Delta\mu$, is analytically calculated with the obtained $\mathbf{h}$ and $\mathbf{c}$.[45]

$$
\Delta\mu = -\sum_{\alpha\lambda}\frac{\rho_\lambda}{\beta}\int \mathrm{d}\mathbf{r}\left[c_{\alpha\lambda}(r) - \frac{1}{2}h^2_{\alpha\lambda}(r) + \frac{1}{2}h_{\alpha\lambda}(r)c_{\alpha\lambda}(r)\right]. \qquad (5.22)
$$

In RISM-SCF-SEDD, total free energy of the solution system is defined as

$$
A = E + \Delta\mu, \qquad (5.23)
$$

where E is the energy of solute molecule given as

$$E = \left\langle \Phi \left| \hat{H} \right| \Phi \right\rangle . \tag{5.24}$$

Here $\hat{H}$ is the standard electronic Hamiltonian of the solute molecule in the isolated state. Φ is the electronic wave function in solution phase, and is obtained based on the variational condition with respect to A,[27,28,30]

$$\left\langle \delta\Phi \left| \hat{F} - \hat{V}^{\mathrm{R}} \right| \Phi \right\rangle = 0, \tag{5.25}$$

where $\hat{F}$ is Fock operator, $\hat{V}^{\mathrm{R}}$ is the solute-solvent electrostatic interaction operator in the framework of RISM-SCF-SEDD. Note that E in solution is generally different from that in the gas phase because the electrostatic field created by solvent induces the electronic polarization of solute molecule. The mean electrostatic interaction energy between solute and solvent is written as follows:[30]

$$\left\langle \Phi \left| \hat{V}^{\mathrm{R}} \right| \Phi \right\rangle = \sum_i D_i V_i^{\mathrm{R}} = \mathbf{D} \cdot \mathbf{V}^{\mathrm{R}}. \tag{5.26}$$

Here, D_i is expansion coefficients of charge density $\rho(\mathbf{r})$ defined as

$$\rho(\mathbf{r}) = \sum_i^{N_{\mathrm{ABS}}} D_i f_i(\mathbf{r}), \tag{5.27}$$

where $f_i(\mathbf{r})$ is auxiliary basis sets (ABSs) centered on each solute site, N_{ABS} is the number of ABSs. $\mathbf{D}$ is uniquely determined by the wave function Φ. Here, the Gaussian function is employed as $f_i(\mathbf{r})$ to describe the electron distribution, and the delta function is employed to describe nucleus charge distribution. The element D_i would be thus regarded as the net population of electron or nucleus charge belonging to i-th auxiliary basis. The effective electrostatic interaction potential between $f_i(\mathbf{r})$ and solvent is given by

$$V_i^{\mathrm{R}} = \sum_\lambda \rho_\lambda \int \frac{f_i(\mathbf{r}' - \mathbf{r}_\alpha)}{|\mathbf{r}' - \mathbf{r}|} h_{\alpha\lambda}(|\mathbf{r}' - \mathbf{r}|) d\mathbf{r} d\mathbf{r}', \qquad (i \in \alpha). \tag{5.28}$$

In standard RISM-SCF-SEDD procedure, Φ and $\mathbf{V}^{\mathrm{R}}$ at the equilibrium state are determined in a self-consistent manner by iteratively solving RISM part (Eqs. (5.20) and (5.21)) and

electronic structure calculation part (Eq. (5.25)). It should be stressed that $\mathbf{V}$ is computed based on Eq. (5.28) and molecular-level information of solvation ($h_{\alpha\lambda}(r)$) is necessary for the evaluation.

The adiabatic ionization energy in solution phase ($I_{\rm ad}$) can be calculated with the two separated standard RISM-SCF-SEDD calculations, *i.e.* for the neutral and cation species in the equilibrium state. On the other hand, it is generally difficult to compute $I_{\rm ver}$ with the standard procedure, because X^{Q+1} at $S_{\rm I}$ does not correspond to equilibrium state, and the electronic polarizability of solvent has non-negligible contribution. However, the analogous procedure based on Eq. (5.17) is possible to apply in RISM-SCF-SEDD method. In the equation, $\mathbf{V}$ and $\mathbf{Q}$ are respectively replaced with $\mathbf{V}^{\rm R}$ and $\mathbf{D}$. The internal energies, U^+ and U^0, are replaced with the total energies of the solute molecule (E^+ and E^0).

$$\begin{aligned} I_{\rm ver} &= \left\{E^+(S_{\rm I}) - E^0(S_{\rm I})\right\} + k_{\rm s}\left\{\mathbf{D}^+(S_{\rm I}) - \mathbf{D}^0(S_{\rm I})\right\}\cdot\mathbf{V}^{\rm R,0}(S_{\rm I}) \\ &+ \frac{1}{2}k_{\rm f}\left\{\mathbf{D}^+(S_{\rm I})\cdot\mathbf{V}^{\rm R,+}(S_{\rm I}) - \mathbf{D}^0(S_{\rm I})\cdot\mathbf{V}^{\rm R,0}(S_{\rm I})\right\}. \end{aligned} \tag{5.29}$$

Because the electronic structure of the solute molecule for X^{Q+1} depends on the generated electrostatic field, the variational condition is given as follows.

$$\left\langle \delta\Phi \left| \hat{F} - \left(k_{\rm f}\hat{V}^{\rm R,+}(S_{\rm I}) + k_{\rm s}\hat{V}^{\rm R,0}(S_{\rm I})\right)\right| \Phi\right\rangle = 0. \tag{5.30}$$

$\mathbf{V}^{\rm R,+}(S_{\rm I})$ and $\mathbf{D}^+(S_{\rm I})$ are computed self-consistently by iteratively solving the RISM part (Eqs. (5.20) and (5.21)) and the electronic structure part (Eq. (5.30)). $I_{\rm ver}$ is thus computed with E^0, $\mathbf{D}^0(S_{\rm I})$ and $\mathbf{V}^{\rm R,0}(S_{\rm I})$ obtained from the standard RISM-SCF-SEDD procedure. It is therefore determined only with two additional parameters (ϵ and ϵ_∞) using the analogous procedure to the standard RISM-SCF-SEDD method. The spectral density (σ_x) is similarly expressed as follows.

$$\begin{aligned} \beta\sigma_x^2 &= \Big| \left\{E^+(S_{\rm I}) - E^0(S_{\rm I})\right\} + k_{\rm s}\left\{\mathbf{D}^+(S_{\rm I}) - \mathbf{D}^0(S_{\rm I})\right\}\cdot\mathbf{V}^{\rm R,0}(S_{\rm I}) \\ &+ \frac{1}{2}k_{\rm f}\left\{\mathbf{D}^+(S_{\rm I})\cdot\mathbf{V}^{\rm R,+}(S_{\rm I}) - \mathbf{D}^0(S_{\rm I})\cdot\mathbf{V}^{\rm R,0}(S_{\rm I})\right\} \\ &+ \left\{E^0(S_{\rm II}) - E^+(S_{\rm II})\right\} + k_{\rm s}\left\{\mathbf{D}^0(S_{\rm II}) - \mathbf{D}^+(S_{\rm II})\right\}\cdot\mathbf{V}^{\rm R,+}(S_{\rm II}) \\ &+ \frac{1}{2}k_{\rm f}\left\{\mathbf{D}^0(S_{\rm II})\cdot\mathbf{V}^{\rm R,0}(S_{\rm II}) - \mathbf{D}^+(S_{\rm II})\cdot\mathbf{V}^{\rm R,+}(S_{\rm II})\right\}\Big|. \end{aligned} \tag{5.31}$$

Table 5.1: Lennard-Jones parameters.

	σ / Å	ϵ / kcal mol^{-1}
Li	1.394	0.128
Na	2.274	0.116
K	3.154	0.111
F	2.720	0.348
Cl	3.620	0.448
Br	3.900	0.658
I	4.320	0.806
O	3.166	0.155
H	1.000	0.056

A further simplified expression without dividing into the fast and slow components is available by setting $\epsilon_\infty = 1$ in Eq. (5.29),

$$I_{\rm ver}^{\rm wd} = \left\{E^+(S_{\rm I}) - E^0(S_{\rm I})\right\} + \left\{\mathbf{D}^+(S_{\rm I}) - \mathbf{D}^0(S_{\rm I})\right\} \cdot \mathbf{V}^{\rm R,0}(S_{\rm I}). \tag{5.32}$$

This formula is essentially the same as previously used one to deal with the vertical excitation in solution phase.[16–18,20]

5.3 Computational Detail

In this study, we examined the ionization of cations,

$Li^+ \rightarrow Li^{2+} + e^-$, $Na^+ \rightarrow Na^{2+} + e^-$, $K^+ \rightarrow K^{2+} + e^-$,

anions,

$F^- \rightarrow F + e^-$, $Cl^- \rightarrow Cl + e^-$, $Br^- \rightarrow Br + e^-$, $I^- \rightarrow I + e^-$.

and water molecule,

$H_2O \rightarrow H_2O^+ + e^-$.

Geometry optimization of H_2O was performed by B3LYP/6-311++G**. Energy calculations were then carried out at MP2/6-311++G** level. For ionized open shell species, the unrestricted treatment (UB3LYP, UHF, UMP2) were adopted. Solvation effect was taken into account using RISM-SCF-SEDD method and polarizable continuum model (PCM).[33] Non-equilibrium PCM[35] was employed for the calculations of $I_{\rm ver}$. Gas phase and PCM calcula-

Table 5.2: Vertical ionization energy in the gas phase ($I^{\rm g}_{\rm ver}$) by MP2 and experimental methods.[50,51] The difference from the experimental value is also listed together with the root-mean-square deviation (RMSD). The unit is eV.

	Exp.[50,51]	MP2	deviation
$Li^+ \rightarrow Li^{2+}$	75.6	75.0	0.6
$Na^+ \rightarrow Na^{2+}$	47.3	47.0	0.3
$K^+ \rightarrow K^{2+}$	31.6	31.3	0.3
$F^- \rightarrow F$	3.4	3.2	0.2
$Cl^- \rightarrow Cl$	3.6	3.2	0.4
$Br^- \rightarrow Br$	3.4	3.1	0.3
$I^- \rightarrow I$	3.1	3.0	0.1
$H_2O \rightarrow H_2O^+$	12.6	12.6	0.0
RMSD (calc. from exp.)			0.3

tions were performed by Gaussian 03 program package[46] while RISM-SCF-SEDD calculations were done by GAMESS package[47] modified by us.

In the RISM procedure, the density of solvent water was set to 1.00 g/cm^3 at T =298.15 K, and HNC closure[45] was employed. The Lennard-Jones parameters of the solutes were taken from Refs.[48,49] and SPC-like water was employed for the solvent.[44] All of them are summarized in Table 5.1. Dielectric permittivity and optical dielectric permittivity of water solvent were set to $\epsilon = 78.390$ and $\epsilon_\infty = 1.776$.[46]

5.4 Results and discussions

5.4.1 Ionization Energy

Table 5.2 shows ionization energy in the gas phase ($I^{\rm g}_{\rm ver}$) and the difference from the experimental value.[50,51] Although the computed values are slightly greater than the experimental ones, the root-mean-square of the deviations (RMSD) is 0.3 eV, showing a reasonable agreement. Table 5.3 shows the change of ionization energy caused by solvation, $\Delta I_{\rm ver}$ ($= I_{\rm ver} - I^{\rm g}_{\rm ver}$) and $\Delta I_{\rm ad}$ ($= I_{\rm ad} - I^{\rm g}_{\rm ad}$), which are the central results in this study. The corresponding experimental values[3–5] and $\Delta I^{\rm wd}_{\rm ver}$ (Eq. (5.32)) are also listed. It is noted that the contributions from the solvation ($\Delta I_{\rm ver}$ and $\Delta I_{\rm ad}$) are much greater than the deviations found in Table 5.2. Clearly, the computational results on the solvation show good agreement with

Table 5.3: The change of ionization energy by solvation in eV.

	Experiment		RISM − SCF − SEDD			PCM		
	$\Delta I_{\rm ver}$[4,5]	$\Delta I_{\rm ad}$[3]	$\Delta I_{\rm ver}^{\rm wd}$	$\Delta I_{\rm ver}$	$\Delta I_{\rm ad}$	$\Delta I_{\rm ver}^{\rm wd}$	$\Delta I_{\rm ver}$	$\Delta I_{\rm ad}$
$Li^+ \rightarrow Li^{2+}$	-15.2		-10.5	-13.5	-16.4	-11.5	-14.2	-17.4
$Na^+ \rightarrow Na^{2+}$	-11.9		-8.0	-10.3	-12.6	-9.4	-11.6	-14.3
$K^+ \rightarrow K^{2+}$	-9.4		-6.5	-8.3	-10.1	-7.4	-9.1	-11.2
$F^- \rightarrow F$	(6.4)[1]	4.8	11.2	8.6	5.4	8.0	6.2	4.0
$Cl^- \rightarrow Cl$	6.0	3.5	7.6	5.8	3.8	6.7	5.2	3.1
$Br^- \rightarrow Br$	5.4	3.2	7.0	5.4	3.5	6.1	4.7	2.9
$I^- \rightarrow I$	4.6	2.8	6.2	4.8	3.2	5.5	4.2	2.6
$H_2O \rightarrow H_2O^+$	-1.5		0.8	-1.0	-3.0	-0.3	-1.9	-3.9
RMSD (w.r.t. exp.)			-	1.2	0.4	-	0.6	0.5

[1]: The experimental value of $\Delta I_{\rm ver}$ of F^- is the estimated value.[5,52]

experimental values and well reproduce the dependencies on the solute size: As large the size of molecule, the absolute value of $\Delta I_{\rm ver}$ and $\Delta I_{\rm ad}$ decreases. It is negative for cation whereas positive for anion.

By definition, the values of $\Delta I_{\rm ad}$ are a few eV lower than those of $\Delta I_{\rm ver}$, because of the stabilization caused by the relaxation of solvent configuration. This is well illustrated in the pair correlation functions (PCFs) shown in Fig. 5.3. The first peak between Na^+ and water oxygen (O_W) at r=2 Å gets higher after the ionization due to increase of the charge ($Na^+ \rightarrow Na^{2+}$). On the other hand, the first peak between Cl^- and water hydrogen (H_W) at r=2 Å corresponding to Cl^--H_W hydrogen bond completely disappears after the ionization, *i.e.*, the detachment of electron from Cl^- ($Cl^- \rightarrow Cl$). These remarkable changes of solvation structure are consistent with the dominant stabilization by orientational polarization.

5.4.2 Solute–Solvent Electrostatic Interaction

The first two terms in Eqs. (5.29) and (5.32), corresponding to the polarization of solvent, comprise only less than 5% of total $\Delta I_{\rm ver}$. For example, the first two terms of Cl^- is 0.02 eV, which is much smaller than the total energy (5.8 eV). In other words, $\Delta I_{\rm ver}$ is mainly determined by the remaining component that originates from the changing in the solute-solvent electrostatic interaction energy.

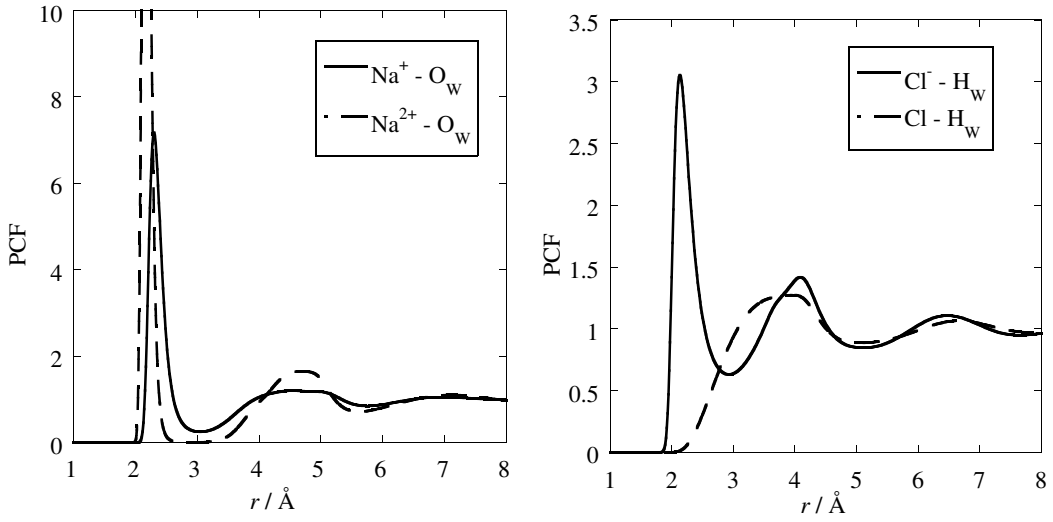

Figure 5.3: PCF between Na^+ and O_W, Na^{2+} and O_W (left hand panel), Cl^- and H_W, Cl and H_W (right hand panel) before ionization (solid line) and after ionization (dashed line).

In general, electrostatic interaction energy is expanded by multipole moments. For a charged molecule ($Q \neq 0$), the monopole term (QV) is dominative. Based on Eq. (5.29), $\Delta I_{\rm ver}$ is approximated as

$$\Delta I_{\rm ver} \simeq k_{\rm s} \left\{ Q^+ - Q^0 \right\} V^0(S_{\rm I}) + \frac{1}{2} k_{\rm f} \left\{ Q^+ V^+(S_{\rm I}) - Q^0 V^0(S_{\rm I}) \right\}, \tag{5.33}$$

where Q^x (x = 0 or +) is the solute charge in the state x, and V_x is the electrostatic field generated by the solvent with this state. According to the dielectric continuum theory, the reaction field V^x is given as follows:[31]

$$V^x = -\left(1 - \frac{1}{\epsilon}\right) \frac{Q^x}{a}, \tag{5.34}$$

where a is solute radius. Using this equation, Eq. (5.33) is rewritten as an explicit function of Q^0 and Q^+. $\Delta I_{\rm ver}^{\rm wd}$ is also in accord with the experimental value and rewritten as

$$\Delta I_{\rm ver}^{\rm wd} = \left(Q^+ - Q^0\right) V^0(S_{\rm I}) = -\left(Q^+ - Q^0\right) \left(1 - \frac{1}{\epsilon}\right) \frac{Q^0}{a}. \tag{5.35}$$

This simple equation may be useful to understand the computational results shown in Table 5.3, which are obtained from highly sophisticated theory. Equation (5.35) of cation ($Q^0 = 1$ and $Q^+ = 2$) becomes negative whereas that of anion ($Q^0 = -1$ and $Q^+ = 0$) is positive, and

Table 5.4: FWHM of vertical ionization energy in aqueous solution. The bottom is RMSD of the calculated values from the experimental values. The unit is eV.

		RISM − SCF − SEDD		PCM	
	Experiment[4,5]	$\epsilon_\infty = 1.000$	$\epsilon_\infty = 1.776$	$\epsilon_\infty = 1.000$	$\epsilon_\infty = 1.776$
$Li^+ \rightarrow Li^{2+}$	1.4 ± 0.2	1.3	1.0	1.3	1.0
$Na^+ \rightarrow Na^{2+}$	1.1 ± 0.3	1.1	0.9	1.2	0.9
$K^+ \rightarrow K^{2+}$	1.4 ± 0.2	1.0	0.8	1.0	0.8
$F^- \rightarrow F$		1.2	0.9	1.1	0.8
$Cl^- \rightarrow Cl$	0.6 ± 0.2	1.0	0.8	1.0	0.8
$Br^- \rightarrow Br$	0.9 ± 0.2	1.0	0.7	0.9	0.7
$I^- \rightarrow I$	0.8 ± 0.3	0.9	0.7	0.9	0.7
$H_2O \rightarrow H_2O^+$	1.45	1.0	0.8	1.0	0.8
RMSD (calc. from exp.)		0.3	0.4	0.3	0.4

the absolute value of $\Delta I_{\rm ver}$ decreases as increase of a. Because of the neutrality, Eq. (5.34) for H_2O ($Q^0 = 0$) becomes zero, and actually the absolute value of $\Delta I_{\rm ver}^{\rm wd}$ is much smaller than those of the ions. The difference between $\Delta I_{\rm ver}$ and $\Delta I_{\rm ver}^{\rm wd}$ allows us to estimate the polarization energy.

$$\Delta I_{\rm ver}^{\rm wd} - \Delta I_{\rm ver} = \left(1 - \frac{1}{\epsilon_\infty}\right) \frac{\left(Q^+ - Q^0\right)^2}{2a}. \tag{5.36}$$

The quantity is always positive by definition.

5.4.3 Spectral width of vertical ionization energy

Table 5.4 shows the full width at half maximum (FWHM) of $I_{\rm ver}$ ($2\sqrt{2\ln 2}\sigma_0 \simeq 2.35\sigma_0$). The computed values are mostly within the limit of accuracy of the experimental values. The accordance is consistent with the result of MD simulation by Åqvist et al.,[26] showing that the free energy surfaces of the molecules investigated in the present study are well described by the linear response regime. Also, the free energy curvatures computed by the present method are similar to those by simulations. Based on Eqs. (5.33) and (5.34), σ_0 is approximated as

$$\sigma_0 = \sqrt{\frac{1}{\beta}\left(\frac{1}{\epsilon_\infty} - \frac{1}{\epsilon}\right) \frac{\left(Q^+ - Q^0\right)^2}{a}}. \tag{5.37}$$

This equation indicates the width increases as the decrease of the solute size (a). Although the difference originated from the size dependency is here in the range of experimental error bar, the size dependency given by Eq. (5.37) is consistent with the theoretical results.

Equation (5.37) is also rewritten as follows.

$$\sigma_0 = \sqrt{k_\mathrm{s}} \sqrt{\frac{1}{\beta}\left(1 - \frac{1}{\epsilon}\right)\frac{\left(Q^+ - Q^0\right)^2}{a}}. \tag{5.38}$$

If the fast and the slow component are not divided, $\sqrt{k_\mathrm{s}}$ equals 1 and the width is represented only with the second square-root part. If $\epsilon_\infty = 1.776$ is assumed, $\sqrt{k_\mathrm{s}}$ equals 0.747. This suggests that the contribution from fast component makes the spectra width narrower.

5.5 Conclusion

Ionization process in aqueous solution was studied using hybrid-type electronic structure theories, RISM-SCF-SEDD method and PCM. The vertical and adiabatic ionization were evaluated based on the free energy surface, and thereon the role of solvation was discussed. The computed values show well agree with experimental measurements.

With the aid of dielectric continuum theory, the ionization energy was further analyzed. A semi-empirical formula, which allows us to divide the solute-solvent interaction into fast and slow components, was proposed. The solvation before ionization mainly determines the change of vertical ionization energy. However, the fast polarization of solvent induced by the ionization also has non-negligible contribution. In particular, the change of ionization energy of H_2O is mainly determined by the fast polarization. On the other hand, the relaxation of solvent configuration, namely the change of solvation structure, is the main origin of the change of the adiabatic ionization energy. The spectral width of the vertical ionization was also studied. The calculated widths were well in accord with the experimental values.

Bibliography

[1] K. M. Ervin, Chem. Rev., **101**, 391 (2001).

[2] K. M.-Dethlefs, E. W. Schlag, Annu. Rev. Phys. Chem., **42**, 109 (1991).

[3] R. G. Pearson, J. Am. Chem. Soc., **108**, 6109 (1986).

[4] B. Winter, R. Weber, W. Widdra, M. Dittmar, M. Faubel, I. V. Hertel, J. Phys. Chem. A, **108**, 2625 (2004).

[5] B. Winter, R. Weber, I. V. Hertel, M. Faubel, P. Jungwirth, E. C. Brown, S. E. Bradforth, J. Am. Chem. Soc., **127**, 7203 (2005).

[6] B. Winter, M. Faubel, Chem. Rev., **106**, 1176 (2006).

[7] B. J-Cwiklik, P. Slavíček, L. Cwiklik, D. Nolting, B. Winter, P. Jungwirth, J. Phys. Chem. A, **112**, 3499 (2008).

[8] R. Seidel, M. Faubel, B. Winter, J. Blumberger, J. Am. Chem. Soc., **131**, 16127 (2009).

[9] J. Moens, R. Seidel, P. Geerlings, M. Faubel, B. Winter, J. Blumberger, J. Phys. Chem. B, **114**, 9173 (2010).

[10] R. A. Murcus, J. Chem. Phys., **24**, 966 (1956).

[11] R. A. Murcus, J. Chem. Phys., **24**, 979 (1956).

[12] A. Warshel, W. W. Parson, Annu. Rev. Phys. Chem., **42**, 279 (1991).

[13] K. Ando, S. Kato, J. Chem. Phys., **95**, 5966 (1991).

[14] G. King, A. Warshel, J. Chem. Phys., **93**, 8682 (1990).

[15] E. A. Carter, J. T. Hynes, J. Phys. Chem., **93**, 2184 (1989).

[16] H. Sato, Y. Kobori, S. Tero-Kubota, F. Hirata, J. Chem. Phys., **119**, 2753 (2003).

[17] H. Sato, Y. Kobori, S. Tero-Kubota, F.Hirata, J. Phys. Chem. B, **108**, 11709 (2004).

[18] S. Chong, S. Miura, G. Basu, F. Hirata, J. Phys. Chem., **99**, 10526 (1995).

[19] H. Sato, Y. Kobori, S. Kubota, F. Hirata, J. Phys. Chem. B, **108**, 11709 (2004).

[20] N. Yoshida, T. Ishida, F. Hirata, J. Phys. Chem. B, **112**, 433 (2008).

[21] D. Chandler, H. C. Andersen, J. Chem. Phys., **57**, 1930 (1972).

[22] F. Hirata, P. J. Rossky, Chem. Phys. Lett., **83**, 329 (1981).

[23] M. Caricato, F. Ingrosso, B. Mennucci, H. Sato, J. Phys. Chem. B, **110**, 25115 (2006).

[24] J. Blumberger, M. Sprik, J. Phys. Chem. B, **109**, 6793 (2005).

[25] Y. Tateyama, J. Blumberger, M. Sprik, I. Tavernelli, J. Chem. Phys., **122**, 234505 (2005).

[26] J. Åqvist, T. Hansson, J. Phys. Chem., **100**, 9512 (1996).

[27] S. Ten-no, F. Hirata, S. Kato, J. Chem. Phys., **100**, 7443 (1994).

[28] H. Sato, F. Hirata, S. Kato, J. Chem. Phys., **105**, 1546 (1996).

[29] B. Roux, H. A. Yu, M. Karplus, J. Phys. Chem., **94**, 4683 (1990).

[30] D. Yokogawa, H. Sato, S. Sakaki, J. Chem. Phys., **126**, 244504 (2007).

[31] C. J. F. Bottcher, *Theory of Electric Polarization*, (Elsevier, Amsterdam, 1983).

[32] W. C. Still, A. Tempczyk, R. C. Hawley, T. Hendrickson, J. Am. Chem. Soc., **112**, 6127 (1990).

[33] J. Tomasi, B. Mennucci, R. Cammi, Chem. Rev., **105**, 2999 (2005).

[34] K. Naka, A. Morita, S. Kato, J. Chem. Phys., **111**, 481 (1999).

[35] M. Cossi, V. Barone, J. Chem. Phys., **112**, 2427 (2000).

[36] J. W. Caldwell, P. A. Kollman, J. Phys. Chem., **99**, 6208 (1995).

[37] S. E. Bradforth, P. Jungwirth, J. Phys. Chem. A, **106**, 1286 (2002).

[38] B. J.-Cwiklik, P. Slavíček, L. Cwiklik, D. Nolting, B. Winter, P. Jungwirth, J. Phys. Chem. A, **112**, 3499 (2008).

[39] K. Ando, J. Chem. Phys., **115**, 5228 (2001).

[40] R. W. Zwanzig, J. Chem. Phys., **22**, 1420 (1954).

[41] H. Sato, S. Sakaki, J. Phys. Chem. A, **108**, 1629 (2004).

[42] H. J. Kim, J. T. Hynes, J. Chem. Phys., **93**, 5194 (1990).

[43] M. A. Aguilar, J. Phys. Chem. A, **105**, 10393 (2001).

[44] H. J. C. Berendsen, J. P. M. Postma, W. F. van Gunsteren, J. Hermans, *Intermolecular Forces*, edited by B. Pullman, (Reidel, Dordrecht, 1981).

[45] S. J. Singer, D. Chandler, Mol. Phys., **55**, 621 (1985).

[46] Gaussian 03, Revision C.02; Gaussian Inc., Wallingford, CT, 2004.

[47] M. W. Schmidt, K. K. Baldridge, J. A. Boatz, S. T. Elbert, M. S. Gordon, J. H. Jensen, S. Koseki, N. Matsunaga, K. A. Nguyen, S. Su, T. L. Windus, M. Dupuis, J. A. Montgomery, J. Comput. Chem., **14**, 1347 (1993).

[48] M. Kinoshita, F. Hirata, J. Chem. Phys., **106**, 5202 (1997).

[49] B. M. Pettitt, P. J. Rossky, J. Chem. Phys., **84**, 5836 (1986).

[50] *Handbook of Chemistry and Physics*, 78th ed., edited by D. R. Lide, (CRC Press, Boca Raton, Florida, 1997).

[51] M. S. Banna, B. H. McQuaide, R. Malutzki, V. Schmidt, J. Chem. Phys., **84**, 4739 (1986).

[52] M. Faubel, *Photoionization and Photodetachment*, edited by C. Y. Ng (World Scientific, Singapore, 2000), Vol. 10A, Part 1, p 634.

Chapter 6

A two-dimensional-reference interaction site model theory for solvation structure near solid-liquid interface

6.1 Introduction

Solvation near solid-liquid interface has been a subject of numerous studies, and recently, the molecular or atomic level information is gradually being clarified.[1–6] For example, Fukuma et al. investigated mica-water interface with atomic force microscopy (AFM) and visualized water distribution near the interface.[1,2] Schultz et al. investigated Ag(100)-water interface with sum frequency generation (SFG) spectroscopy and showed that water orientation is dependent upon the applied electric potential.[3]

Theoretical or computational methods also provide valuable knowledge of the solvation structure near the interface, usually considering a solid as an atomistic wall. Molecular dynamics (MD) simulation is a representative and there are numerous studies of solid-liquid interface.[7–14] The atomic-level knowledge that cannot be obtained with experimental methods is accumulated. The reference interaction site model (RISM) theory is the statistical mechanics for molecular liquids, and can be regarded as an alternative to MD simulation. The distinguishing feature of the RISM theory is to analytically treat an ensemble average of an infinite number of solvent molecules.[15–19] The applicability of the theory is not limited to bulk liquid, and the theory has been extended to various solution systems. The polymer RISM theory treats the atomistic wall consisting of a virtually infinite number of atomic sites arranged in a periodic array.[20–23] Akiyama and Hirata studied orientation of liquid water molecules near

the wall with the polymer-RISM theory.[24] Kovalenko et al. reported three-dimensional (3D) density-distribution of solvent near an atomistic wall with the 3D-RISM theory.[17,25,26] Woelki et al. proposed the singlet-RISM theory where a solid is treated as an atomic site of infinite radius.[27,28]

In this study, we develop a new equation to describe solvation structure near solid-liquid interface at the atomic-level. The new equation belongs to the RISM family, and thus analytically treats an ensemble of infinite number of solvent molecules. The remarkable feature of the equation is focusing on the inherent feature near the interface, namely, anisotropy of solvation structure. The equation describes the anisotropic solvation structure as two-dimensional (2D) density distribution in a cylindrical coordinate system. The 2D distribution is along two directions, one of which is perpendicular to the interface and the other is parallel to the interface. The distribution along the perpendicular direction represents solvation shells near the interface. The distribution along the parallel direction is governed by atomistic features of the wall. The 2D-RISM equation is then combined with the polymer-RISM equation. The combined equation describes solvation structure around the wall consisting of atomic sites arranged in a 2D-periodic array. We apply the combined equation to the system in which an atomistic wall is immersed in solvent water. Solvation structure near the wall-water interface is discussed at the atomic-level. For example, adsorption position of water onto the wall and water orientation near the wall are discussed.

6.2 Theory

6.2.1 2D-RISM equation

Solvation structure is in general described with the six-dimensional Ornstein-Zernike (6D-OZ) equation.[18,19] In this study, the system consists of an atomistic wall and a solvent, where the wall is fixed in the system. The 6D-OZ equation for this system is given as

$$\begin{aligned} &h(\mathbf{r}_{12}, \mathbf{\Omega}_2) \\ &= c(\mathbf{r}_{12}, \mathbf{\Omega}_2) + n^V \left\langle \int d\mathbf{r}_3 c(\mathbf{r}_{13}, \mathbf{\Omega}_3) h^V(\mathbf{r}_{32}, \mathbf{\Omega}_3, \mathbf{\Omega}_2) \right\rangle_{\mathbf{\Omega}_3}, \end{aligned} \tag{6.1}$$

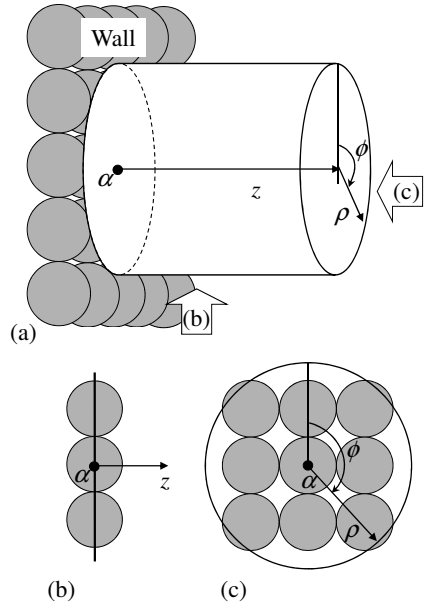

Figure 6.1: (a); Cylindrical coordinate system. (b); View from the direction perpendicular to z-axis. (c); View from the direction parallel to z-axis.

where 1 indicates the wall, 2 and 3 indicate the solvent molecules, respectively. $\mathbf{r}_{12}$ is defined as $\mathbf{r}_{12} = \mathbf{r}_2 - \mathbf{r}_1$, where $\mathbf{r}_1$ is an arbitrary position in the wall and $\mathbf{r}_2$ is a center-of-mass of solvent molecule 2. In Eq. (6.1) and thereafter, we define $\mathbf{r}_{AB}$ as a 3D vector from a position of a particle A ($\mathbf{r}_A$) to that of a particle B ($\mathbf{r}_B$). $\mathbf{\Omega}_A$ is the orientation of a particle A and $\langle\,\rangle_{\mathbf{\Omega}_A}$ denotes the averaging over $\mathbf{\Omega}_A$. c is the direct correlation function between the wall and solvent, and h is the total correlation function between the wall and solvent. The superscript V denotes solvent, n^V is the number density of solvent, and h^V is the total correlation function of solvent. In Eq. (6.1), the orientation of the wall ($\mathbf{\Omega}_1$) is omitted because here $\mathbf{\Omega}_1$ is fixed in the system. In the reciprocal space, h is written as

$$\begin{aligned} h(\mathbf{k}, \mathbf{\Omega}_2) &= \int h(\mathbf{r}_{12}, \mathbf{\Omega}_2) e^{i\mathbf{k}\cdot\mathbf{r}_{12}} d\mathbf{r}_{12} \\ &= c(\mathbf{k}, \mathbf{\Omega}_2) + n^V \left\langle c(\mathbf{k}, \mathbf{\Omega}_3) h^V(\mathbf{k}, \mathbf{\Omega}_3, \mathbf{\Omega}_2) \right\rangle_{\mathbf{\Omega}_3} . \end{aligned} \tag{6.2}$$

To derive the equation for the 2D distribution from the 6D-OZ equation, let us then introduce the cylindrical coordinate system shown in Fig. 6.1. An origin of the coordinate system is defined as a position of an arbitrary wall site α, an axis perpendicular to the wall is defined

as z-axis, ρ is the distance from the z-axis on a plane parallel to the wall, and ϕ is an angle along the wall. In this coordinate system, the position of a solvent site η is defined as $\mathbf{r}_{\alpha\eta} = \{\rho_{\alpha\eta}, z_{\alpha\eta}, \phi_{\alpha\eta}\}$. The 2D total correlation function between the sites α and η, $h_{\alpha\eta}(\rho_{\alpha\eta}, z_{\alpha\eta})$, can be given by averaging over $\phi_{\alpha\eta}$ and $\mathbf{\Omega}_2$ as

$$h_{\alpha\eta}(\rho_{\alpha\eta}, z_{\alpha\eta}) = \left\langle \int h(\mathbf{r}_{12}, \mathbf{\Omega}_2)\delta(\mathbf{r}_{12} - \mathbf{r}_{1\alpha} - \mathbf{r}_{\eta 2} - \mathbf{r}_{\alpha\eta})d\mathbf{r}_{12} \right\rangle_{\phi_{\alpha\eta}, \mathbf{\Omega}_2}, \tag{6.3}$$

where δ is the δ-function, and the integral over $\mathbf{r}_{12}$ is to change the variable from $\mathbf{r}_{12}$ to $\mathbf{r}_{\alpha\eta}$.[17,18]

Using Eqs. (6.2) and (6.3), $h_{\alpha\eta}$ in the reciprocal space is given as

$$\begin{aligned} h_{\alpha\eta}(k^\rho, k^z) &= \int h_{\alpha\eta}(\rho_{\alpha\eta}, z_{\alpha\eta}) e^{i\mathbf{k}\cdot\mathbf{r}_{\alpha\eta}} d\mathbf{r}_{\alpha\eta} \\ &= \left\langle c(\mathbf{k}, \mathbf{\Omega}_2) e^{-i\mathbf{k}\cdot\mathbf{r}_{1\alpha}} e^{-i\mathbf{k}\cdot\mathbf{r}_{\eta 2}} \right\rangle_{\phi_{\alpha\eta}, \mathbf{\Omega}_2} \\ &\quad + n^V \left\langle c(\mathbf{k}, \mathbf{\Omega}_3) h^V(\mathbf{k}, \mathbf{\Omega}_3, \mathbf{\Omega}_2) e^{-i\mathbf{k}\cdot\mathbf{r}_{1\alpha}} e^{-i\mathbf{k}\cdot\mathbf{r}_{\eta 2}} \right\rangle_{\phi_{\alpha\eta}, \mathbf{\Omega}_2, \mathbf{\Omega}_3}, \end{aligned} \tag{6.4}$$

where k^ρ and k^z are the ρ-component and z-component of $\mathbf{k}$, respectively. To perform the averaging, we then assume that the direct correlation function, c, can be written as the superposition of 2D site-site direct correlation functions, $\{\tilde{c}_{\alpha\eta}\}$, as follows:

$$c(\mathbf{r}_{12}, \mathbf{\Omega}_2) = \sum_{\alpha\eta} \tilde{c}_{\alpha\eta}(\rho_{\alpha\eta}, z_{\alpha\eta}). \tag{6.5}$$

This assumption (Eq. (6.5)) is analogous to that employed to derive the RISM equation and the 3D-RISM equation.[17,19,26] In the reciprocal space, Eq. (6.5) is written as

$$\begin{aligned} c(\mathbf{k}, \mathbf{\Omega}_2) &= \int c(\mathbf{r}_{12}, \mathbf{\Omega}_2) e^{i\mathbf{k}\cdot\mathbf{r}_{12}} d\mathbf{r}_{12} \\ &= \sum_{\alpha\eta} \tilde{c}_{\alpha\eta}(k^\rho, k^z) e^{i\mathbf{k}\cdot\mathbf{r}_{1\alpha}} e^{i\mathbf{k}\cdot\mathbf{r}_{\eta 2}}, \end{aligned} \tag{6.6}$$

where the integral over $\mathbf{r}_{12}$ is for fixed orientation of 1 and 2, i.e., for the fixed intramolecular vectors ($\mathbf{r}_{1\alpha}$ and $\mathbf{r}_{\eta 2}$), and, thus, the integral variable is transformed as $d\mathbf{r}_{12} = d\mathbf{r}_{\alpha\eta}$. This transformation is applied to derive the RISM equation.[19]

If the direct correlation function, c, in Eq. (6.4) is replaced with the superposition (Eq. (6.6)), then the following equation is obtained.

$$h_{\alpha\eta}(k^\rho, k^z) = \sum_{\alpha'\eta'} e^{i\mathbf{k}\cdot\mathbf{r}_{\alpha\alpha'}} \tilde{c}_{\alpha'\eta'}(k^\rho, k^z) \left[\omega^V_{\eta'\eta}(|\mathbf{k}|) + n^V h^V_{\eta'\eta}(|\mathbf{k}|)\right]. \tag{6.7}$$

Here α' and η' are wall and solvent sites respectively, and $\left\langle e^{i\mathbf{k}\cdot\mathbf{r}_{\alpha\alpha'}}\right\rangle_{\phi_{\alpha\eta}} = e^{i\mathbf{k}\cdot\mathbf{r}_{\alpha\alpha'}}$ is applied because $e^{i\mathbf{k}\cdot\mathbf{r}_{\alpha\alpha'}}$ is not dependent on $\phi_{\alpha\eta}$. $\omega^V_{\eta'\eta}$ is the intramolecular correlation function of solvent. In the reciprocal space, $\omega^V_{\eta'\eta}$ is given as

$$\omega^V_{\eta'\eta}(|\mathbf{k}|) = \frac{\sin(|\mathbf{k}||\mathbf{r}_{\eta'\eta}|)}{|\mathbf{k}||\mathbf{r}_{\eta'\eta}|}, \tag{6.8}$$

where $\mathbf{r}_{\eta'\eta}$ is the vector from the site η' to the site η in one solvent molecule. $h^V_{\eta'\eta}$ in Eq. (6.7) is the site-site total correlation function of bulk solvent. Because of the isotropy of bulk solvent, $h^V_{\eta'\eta}(\mathbf{k})$ can be reduced to $h^V_{\eta'\eta}(|\mathbf{k}|)$. $\omega^V_{\eta'\eta}$ and $h^V_{\eta'\eta}$ have the same meanings as those used in the RISM equation.[15–19]

Because Eq. (6.7) includes $e^{i\mathbf{k}\cdot\mathbf{r}_{\alpha\alpha'}}$ ($\mathbf{r}_{\alpha\alpha'} = \{\rho_{\alpha\alpha'}, z_{\alpha\alpha'}, \phi_{\alpha\alpha'}\}$), the solution of Eq. (6.7) could be dependent on $\phi_{\alpha\alpha'}$ besides $\rho_{\alpha\alpha'}$ and $z_{\alpha\alpha'}$. However, the solution in the real space, $h_{\alpha\eta}(\rho_{\alpha\eta}, z_{\alpha\eta})$, is not dependent on $\phi_{\alpha\alpha'}$. This is clearly seen by rewriting $e^{i\mathbf{k}\cdot\mathbf{r}_{\alpha\alpha'}}$ using the Jacobi-Anger expansion,

$$e^{i\mathbf{k}\cdot\mathbf{r}_{\alpha\alpha'}} = e^{ik^z z_{\alpha\alpha'}} \sum_{m=-\infty}^{\infty} i^m J_m(k^\rho \rho_{\alpha\alpha'}) e^{im\phi_{\alpha\alpha'}}, \tag{6.9}$$

where i is the imaginary unit, and J_m is the m-th Bessel function. Applying Eq. (6.9), the terms of Eq. (6.7) other than the one corresponding to $m = 0$ vanish by the inverse Fourier transformation because here $h_{\alpha\eta}$ and $\tilde{c}_{\alpha\eta}$ are not functions of ϕ. That is to say, only the $m = 0$ term gives a non-vanishing contribution in the real space. Eq. (6.7) is, thus, rewritten to the equation named the 2D-RISM equation,

$$h_{\alpha\eta}(k^\rho, k^z) = \sum_{\alpha'\eta'} \mathrm{w}_{\alpha\alpha'}(k^\rho, k^z)\, \tilde{c}_{\alpha'\eta'}(k^\rho, k^z) \left[\omega^V_{\eta'\eta}(|\mathbf{k}|) + n^V h^V_{\eta'\eta}(|\mathbf{k}|)\right], \tag{6.10}$$

where $\mathrm{w}_{\alpha\alpha'}$ is the 2D-intramolecular correlation function of the wall written as follows:

$$\mathrm{w}_{\alpha\alpha'}(k^\rho, k^z) = e^{ik^z z_{\alpha\alpha'}} J_0(k^\rho \rho_{\alpha\alpha'}). \tag{6.11}$$

$\mathrm{w}_{\alpha\alpha'}$ describes the molecular structure of the wall.

6.2.2 Combining with the polymer-RISM equation

As is seen from Eq. (6.10), the equation to be solved is a matrix equation and the size of matrix becomes larger as the number of wall sites increases. It thus becomes cumbersome to

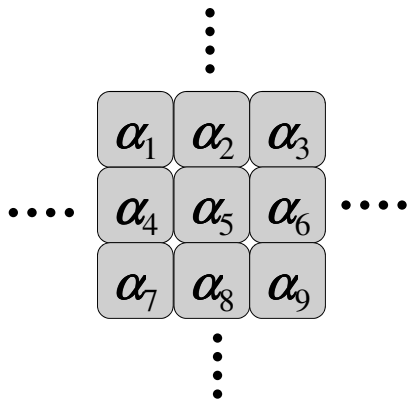

Figure 6.2: Wall consisting of units arranged in a 2D periodic array.

obtain the solution of the matrix equation as the wall size increases. However, by combining with the polymer-RISM equation,[20–24] we can drastically reduce the size of the matrix for a system, the wall of which is represented as shown in Fig. 6.2. The wall consists of identical units arranged in a 2D periodic array. Each unit labeled as $\boldsymbol{\alpha}_i$ ($i = 1, ..., N$) is a finite set of atomic sites $\{\alpha_i, \alpha_i', ..., \alpha_i^{(M)}\}$. Using these notations, Eq. (6.10) is rewritten as follows:

$$\begin{aligned} h_{\alpha_i\eta}(k^\rho, k^z) &= \sum_j^N \sum_{\alpha'\eta'} \mathrm{w}_{\alpha_i\alpha_j'}(k^\rho, k^z)\tilde{c}_{\alpha_j'\eta'}(k^\rho, k^z) \\ &\qquad \times \left[\omega^V_{\eta'\eta}(|\mathbf{k}|) + n^V h^V_{\eta'\eta}(|\mathbf{k}|)\right]. \end{aligned} \tag{6.12}$$

If the total number of unit N is large enough, all units are virtually identical to each other, and thus,

$$\begin{aligned} h_{\alpha_1\eta}(k^\rho, k^z) &= h_{\alpha_2\eta}(k^\rho, k^z) = \cdots = h_{\alpha_N\eta}(k^\rho, k^z) \\ &= \frac{1}{N}\sum_i^N h_{\alpha_i\eta}(k^\rho, k^z) \equiv h_{\alpha\eta}(k^\rho, k^z). \end{aligned} \tag{6.13}$$

Here, because of the identity, the index i is dropped and $h_{\alpha_i\eta}(k^\rho, k^z)$ is rewritten as $h_{\alpha\eta}(k^\rho, k^z)$ in the last equation. Similarly, $\tilde{c}_{\alpha_i\eta}(k^\rho, k^z)$ is also rewritten as $\tilde{c}_{\alpha\eta}(k^\rho, k^z)$. Equation (6.12) is then rewritten as

$$\begin{aligned} h_{\alpha\eta}(k^\rho, k^z) = \sum_{\alpha'\eta'} \mathrm{W}_{\alpha\alpha'}(k^\rho, k^z)\tilde{c}_{\alpha'\eta'}(k^\rho, k^z) \\ \times \left[\omega^V_{\eta'\eta}(|\mathbf{k}|) + n^V h^V_{\eta'\eta}(|\mathbf{k}|)\right], \end{aligned} \tag{6.14}$$

where $\mathrm{W}_{\alpha\alpha'}$ is the new intramolecular correlation function defined by

$$\mathrm{W}_{\alpha\alpha'}(k^{\rho}, k^{z}) = \frac{1}{N}\sum_{ij}^{N} \mathrm{w}_{\alpha_i\alpha'_j}(k^{\rho}, k^{z}). \tag{6.15}$$

Now, according to Eq. (6.14), the size of the matrix depends on the number of sites in one unit (M) and *does not* on N. The summation over the units is required only once to solve Eq. (6.15). Although the solution of Eq. (6.14) is dependent on N, the dependency is in practice negligibly small when N is large enough as demonstrated in Sec. 6.4.

6.2.3 Closure

The two unknown functions, $\tilde{c}_{\alpha\eta}$ and $h_{\alpha\eta}$, appear in Eq. (6.14), and thus, another equation called $closure$ relating these functions is needed. In this study, the following KH-type closure[17,26] is adopted:

$$\begin{aligned} \mathrm{g}_{\alpha\eta}(\rho_{\alpha\eta}, z_{\alpha\eta}) &= \begin{cases} \exp\{\chi_{\alpha\eta}(\rho_{\alpha\eta}, z_{\alpha\eta})\} & (\text{for} \quad \chi_{\alpha\eta}(\rho_{\alpha\eta}, z_{\alpha\eta}) \le 0), \\ \chi_{\alpha\eta} + 1 & (\text{for} \quad \chi_{\alpha\eta}(\rho_{\alpha\eta}, z_{\alpha\eta}) > 0), \end{cases} \\ \chi_{\alpha\eta}(\rho_{\alpha\eta}, z_{\alpha\eta}) &= -\beta u_{\alpha\eta}(\rho_{\alpha\eta}, z_{\alpha\eta}) + h_{\alpha\eta}(r_{\alpha\eta}, z_{\alpha\eta}) - \tilde{c}_{\alpha\eta}(\rho_{\alpha\eta}, z_{\alpha\eta}), \end{aligned} \tag{6.16}$$

where $\mathrm{g}_{\alpha\eta}(\rho_{\alpha\eta}, z_{\alpha\eta}) = h_{\alpha\eta}(\rho_{\alpha\eta}, z_{\alpha\eta}) + 1$ is 2D pair correlation function (2D-PCF) between the wall site α and the solvent site η. $\beta = 1/k_{\mathrm{B}}T$, k_{B} is Boltzmann's constant. The interaction potential between α and η, $u_{\alpha\eta}$, is given as the sum of Coulombic and Lennard-Jones terms as

$$u_{\alpha\eta}(\rho_{\alpha\eta}, z_{\alpha\eta}) = 4\epsilon_{\alpha\eta}\left[\left(\frac{\sigma_{\alpha\eta}}{|\mathbf{r}_{\alpha\eta}|}\right)^{12} - \left(\frac{\sigma_{\alpha\eta}}{|\mathbf{r}_{\alpha\eta}|}\right)^{6}\right] + \frac{q_{\alpha}q_{\eta}}{|\mathbf{r}_{\alpha\eta}|}, \tag{6.17}$$

where q_{α} and q_{η} are charges on α and η, respectively. $\sigma_{\alpha\eta}$ and $\epsilon_{\alpha\eta}$ are the Lennard-Jones parameters.

The procedure of the present theory is summarized as follows. $\omega^{V}_{\eta'\eta} + n^{V}h^{V}_{\eta'\eta}$ is first calculated with the RISM equation for bulk solvent. The intramolecular correlation function, $\mathrm{W}_{\alpha\alpha'}$, is then calculated with Eq. (6.15). In the final step, $h_{\alpha\eta}$ and $\tilde{c}_{\alpha\eta}$ are iteratively calculated with Eqs. (6.14) and (6.16) until the convergence is achieved.

6.3 Computational detail

To solve the present equations, the 2D Fourier transform in the cylindrical coordinate system is required. The transform consists of the Hankel transform with respect to ρ and the 1D Fourier transform with respect to z. The Hankel transform is performed with the logarithmic grids using Talman's algorithm.[29] The number of grid points along ρ is 512 and the grid spacing is $\Delta \ln(\rho/\rho_0)$ = 0.02, where ρ_0 is 1 Bohr. The minimum of ρ, $\rho_{\min}$, is set as $\ln(\rho_{\min}/\rho_0) = -5.12$. The 1D Fourier transform is performed with the fast Fourier transform algorithm. The number of grid points along z is 4096 and the spacing is Δz = 0.02 Bohr. To apply our theory to a charged wall, Ng's method[30] is employed.

As the first application of the theory, we treat the model system where a single wall is immersed in aqueous solution. The atomic sites of the wall are arranged in accord with the face of a cubic lattice. The lattice constant (a) is 1.5 Å and the Lennard-Jones parameters of the atomic sites are σ = 1.500 Å and ϵ = 0.101 kcal mol^{-1}. The lattice constant and the LJ parameters of the wall are the same as the system investigated by Crozier et al. using MD simulation,[7] and are close to that by Woelki et al. using the singlet-RISM theory.[27,28] For solvent water molecule, simple-point-charge-like model is employed (oxygen site: σ_{O} = 3.166 Å and ϵ_{O} = 0.155 kcal mol^{-1}; hydrogen site: σ_{H} = 1.000 Å and ϵ_{H} = 0.056 kcal mol^{-1}).[31] Calculations are carried out at 298.15 K and the number density of solvent water of n^V = 0.033426 Å^{-3}.

In the following, we rewrite $\mathrm{g}_{\alpha\eta}(\rho_{\alpha\eta}, z_{\alpha\eta})$ as $\mathrm{g_O}(\rho, z)$ or $\mathrm{g_H}(\rho, z)$ for simplicity, where $\mathrm{g_O}(\rho, z)$ is 2D-PCF between the wall site and the oxygen site and $\mathrm{g_H}(\rho, z)$ is 2D-PCF between the wall site and the hydrogen site.

6.4 Results and discussions

Figure 6.3 shows the dependency on the total number of unit N, where $\mathrm{g_O}$(ρ=0.9 Å, z=2.0 Å) and $\mathrm{g_H}$(ρ=0.9 Å, z=2.8 Å) are plotted along N. These positions correspond to peak tops in the case of $N = 625$ (= 25^2). The values of $\mathrm{g_O}$ and $\mathrm{g_H}$ are almost unchanged when N is larger

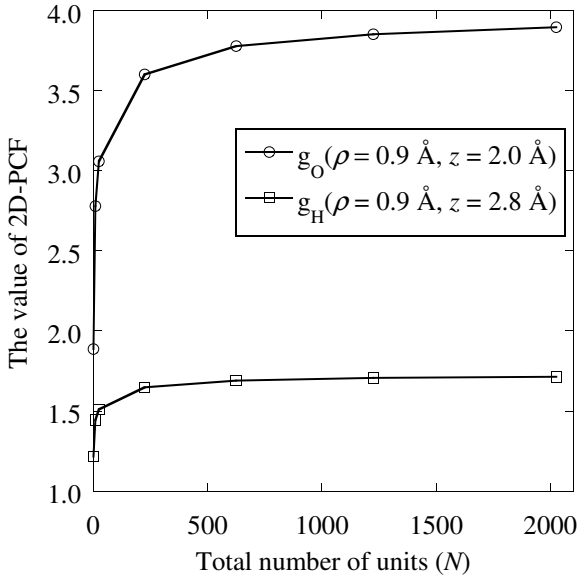

Figure 6.3: Dependency on N of $g_O(\rho = 0.9$ Å, $z = 2.0$ Å) and $g_H(\rho = 0.9$ Å, $z = 2.8$ Å) .

than 625. N is, thus, fixed at 625 in the following discussion.

Figure 6.4(a) shows the contour map of $g_O(\rho, z)$. In the vicinity of $z = 0$ Å, any distinct peak is not found because the wall excludes solvent water from this area. The distribution increases with increasing distance from the wall (z) and reaches the maximum at $z = 2.0$ Å. This area corresponds to the first solvation shell where water molecules are in contact with the wall. The maximum of g_O is 3.8, which is reasonably agree with the previous studies employing analogous model system: 3.2 (singlet-RISM)[28] and 4.0 (MD).[7] Note that the distributions of the previous studies are averaged over ρ, namely, the definition of g_O is slightly different from that in the present study where the dependency on ρ is also illustrated. The small distribution around $z = 0.0$ Å ~ 1.0 Å and ρ=2.25 Å seems to be an artifact, probably caused by the adopted closure that affects the description of the short-range region.[32] Further careful investigations would be necessary to confirm it, but it is noted that the present theory yields the first solvation shell that is reasonably agree with the previous studies, as is described in the following discussion.

g_O at $z \sim 2$ is especially dependent on ρ. The maximum of g_O is at $\rho = 0.9$ Å, $z = 2.0$ Å, and the distribution expands from $\rho = 0.6$ Å to 1.2 Å, where g_O is larger than 3.6. Fig.

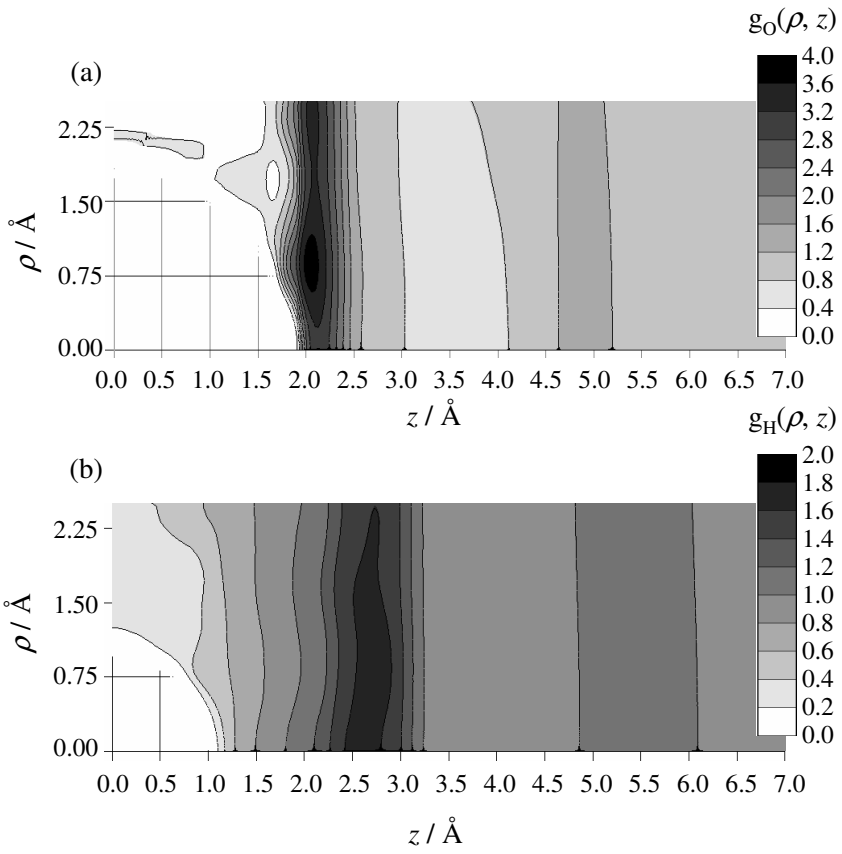

Figure 6.4: Contour map of 2D-PCF between the wall site and the oxygen site (a), and the hydrogen site (b). The wall is neutral.

6.5 illustrates this area, which includes bridge positions ($a/2$ = 0.75 Å) and hollow positions ($a/\sqrt{2}$ = 1.06 Å). It is also noted that the height of g_O at the on-top position ($\rho = 0.0$ Å, $z = 2.0$ Å) is lower by about 0.7 compared to the maximum. In other words, water molecules are preferably adsorbed on bridge and/or hollow positions compared to on-top positions.

We found another maximum at $z \sim 5$ Å, corresponding to the second solvation shell. Different from the first solvation shell ($z \sim 2$ Å), the profile of the second solvation shell is virtually independent of ρ, indicating that the effect of atomistic feature of the wall is negligibly small at this area.

Figure 6.4(b) shows the contour map of $g_H(\rho, z)$. The distinct peak is found in the area from z = 2.5 Å to 3.0 Å, which is slightly distant from the first solvation shell of the oxygen site ($z \sim 2$ Å). $g_O(\rho, z)$ and $g_H(\rho, z)$, therefore, show that the hydrogen site tends to be located

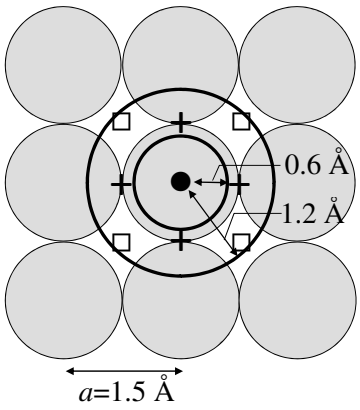

Figure 6.5: Relationship between the area from ρ = 0.6 Å to 1.2 Å and the molecular structure of the wall. •: on-top position (ρ = 0 Å); +: bridge position ($\rho = a/2$); □: hollow position ($\rho = a/\sqrt{2}$).

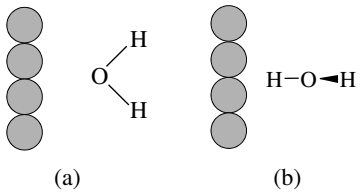

Figure 6.6: (a) and (b) Orientation of water molecule near the wall.

further from the wall than the corresponding oxygen site as depicted in Fig. 6.6(a).

The solvation structures change by charging the wall. Fig. 6.7(a) shows the contour map of $g_O(\rho, z)$, where all atomic sites of the wall are charged to $-0.04213\ |e|$. The applied charges correspond to $-0.3\ \mathrm{C{\cdot}m^{-2}}$. This surface charge density is chosen to be the same as the previous works.[7,28] The profile of g_O looks similar to that around the neutral wall at a glance. However, the peak top at ρ = 0.9 Å, z = 2.0 Å slightly increases from 3.8 (neutral) to 4.0 (charged). This increase may be interesting because the oxygen site is more preferably adsorbed on the negatively charged wall in spite of the electrostatic repulsion between the oxygen site and the wall.

The increase is attributed to strong attractive interaction between the hydrogen site and the wall. Fig. 6.7(b) shows the contour map of $g_H(\rho, z)$ near the negatively charged wall. The probability becomes slightly higher especially near **B** to form a ridge, and a distinct peak is

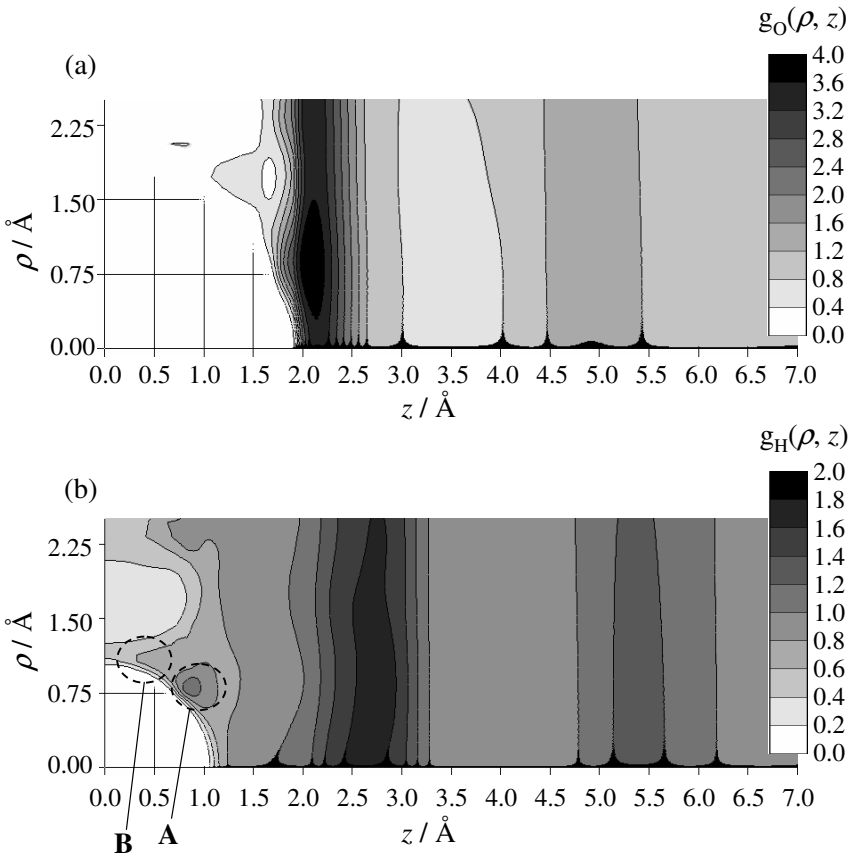

Figure 6.7: Contour map of 2D-PCF between the wall site and the oxygen site (a), and the hydrogen site (b). The wall is negatively charged.

found at **A**. Based on the geometrical consideration, **A** includes bridge positions and **B** includes hollow positions, respectively (cf. Fig. 6.5). These changes are consistent with the previous works.[7,28] As illustrated in Fig. 6.6(a), the distribution, in which two hydrogen atoms are further than the oxygen atom, is dominative before the charging. The aforementioned changes in **A** and **B** indicate that a mixing ratio of another configuration displayed in Fig. 6.6(b) becomes greater, namely one of O-H bond is directed perpendicular to the wall. The attractive interaction between the hydrogen site and the negatively charged wall is consistent with the above-mentioned increase of g_O in the area of the first solvation shell.

6.5 Conclusion

In this study, we developed the 2D-RISM equation for solvation structure near solid-liquid interface. The developed equation focuses on the anisotropy of solvation structure near the interface by using the 2D density distribution in the cylindrical coordinate system. The 2D-RISM equation was then combined with the polymer-RISM equation to treat the solvation near the wall consisting of atomic sites in a 2D-periodic array. The model system was studied as the first application, and we found that water molecules in the first solvation shell are preferably adsorbed on hollow and/or bridge positions than on-top positions, whereas those in the second solvation shell do not show any specific preference. A new peak appears in the first solvation shell upon charging the wall, indicating that the contribution from another orientational configuration also becomes visible by the applied electric field. This change is assigned as follows: O-H bond is directed perpendicular to the negatively charged wall. The interaction between the hydrogen site and the negatively charged wall is consistent with the increase of g_O.

Bibliography

[1] T. Fukuma, K. Kobayashi, K. Matsushige, H. Yamada, Appl. Phys. Lett., **87**, 034101 (2005).

[2] T. Fukuma, Sci. Technol. Adv. Mater, **11**, 033003 (2010).

[3] Z. D. Schultz, S. K. Shaw, A. A. Gewirth, J. Am. Chem. Soc., **127**, 15916 (2005).

[4] H. Noguchi, T. Okada, K. Uosaki, Faraday Discuss., **140**, 125 (2008).

[5] M. F. Toney, J. N. Howard, J. Richer, G. L. Borges, J. G. Gordon, O. R. Melroy, D. G. Wiesler, D. Yee, L. B. Sorensen, Nature, **368**, 444 (1994).

[6] M. F. Toney, J. N. Howard, J. Richer, G. L. Borges, J. G. Gordon, O. R. Melroy, D. G. Wiesler, D. Yee, L. B. Sorensen, Surf. Sci., **335**, 326 (1995).

[7] P. S. Crozier, R. L. Rowley, D. Henderson, J. Chem. Phys., **113**, 9202 (2000).

[8] P. S. Crozier, R. L. Rowley, D. Henderson, J. Chem. Phys., **114**, 7513 (2001).

[9] D. A. Rose, I. Benjamin, J. Chem. Phys., **95**, 6856 (1991).

[10] S. K. Reed, O. J. Lanning, P. A. Madden, J. Chem. Phys., **126**, 084704 (2007).

[11] E. Spohr, J. Phys. Chem., **93**, 6171 (1989).

[12] E. Spohr, K. Heinzinger, Chem. Phys. Lett., **123**, 218 (1986).

[13] G. D. Smith, O. Borodin, S. P. Russo, R. J. Rees, A. F. Hollenkamp, Phys. Chem. Chem. Phys., **11**, 9884 (2009).

[14] P. Zarzycki, S. Kerisit, K. M. Rosso, J. Phys. Chem. C, **114**, 8905 (2010).

[15] D. Chandler, H. C. Andersen, J. Chem. Phys., **57**, 1930 (1972).

[16] F. Hirata, P. J. Rossky, Chem. Phys. Lett., **83**, 329 (1981).

[17] *Molecular Theory of Solvation*, ed. F. Hirata, Kluwer: Dordrecht, The Netherlands, 2003.

[18] J. -P. Hansen, I. R. McDonald, *Theory of Simple Liquids*, 3nd Ed. Academic, London, 2006.

[19] C. G. Gray, K. E. Gubbins, *Theory of Molecular Fluids*, Vol. 1, Oxford University Press, New York, 1984.

[20] D. Chandler, Y. Singh, D. M. Richardson, J. Chem. Phys., **81**, 1975 (1984).

[21] K. S. Schweizer, J. G. Curro, Phys. Rev. Lett., **58**, 246 (1987).

[22] J. G. Curro, K. S. Schweizer, J. Chem. Phys., **87**, 1842 (1987).

[23] F. Hirata, R. M. Levy, Chem. Phys. Lett., **136**, 267 (1987).

[24] R. Akiyama, F. Hirata, J. Chem. Phys., **108**, 4904 (1998).

[25] A. Kovalenko, F. Hirata, Chem. Phys. Lett., **290**, 237 (1998).

[26] A. Kovalenko, F. Hirata, J. Chem. Phys., **110**, 10095 (1999).

[27] S. Woelki, H.-H. Kohler, H. Krienke, J. Phys. Chem. B, **111**, 13386 (2007).

[28] S. Woelki, H.-H. Kohler, H. Krienke, J. Phys. Chem. B, **112**, 3365 (2008).

[29] J. D. Talman, J. Comp. Phys., **29**, 35 (1978).

[30] K.-C. Ng, J. Chem. Phys., **61**, 2680 (1974).

[31] H. J. C. Berendsen, J. P. M. Postma, W. F. van Gunsteren, J. Hermans. In: B. Pullman (Ed.), Intermolecular Forces, Reidel, Dordrecht, 1981.

[32] A. Kovalenko, F. Hirata, J. Chem. Phys., **133**, 2793 (2000).

General conclusion

In this thesis, the author theoretically studied the chemical process in solution in terms of molecular property of solute and solvent. The process was accordingly discussed from the two point of view. One is the change of electronic structure of solute molecule. The electronic structure is mainly characterized by orbital energy and resonance structure. The other is solvation structure, which successfully reveals the role of solvent at the molecular-level. The important conclusions are summarized as follows.

In chapter 1, the origin of the reaction barrier between carbon dioxide and hydroxide anion was studied using RISM-SCF as well as PCM. The computed total energy monotonically decreases without barrier in the gas phase. On the other hand, both RISM-SCF and PCM calculations surely show the barrier in aqueous phase, which is consistent with the experimental knowledge. Within the framework of the frontier orbital theory, the orbital energy changes of π^* orbital at $\mathrm{CO_2}$ moiety and lone pair orbital at $\mathrm{OH^-}$ were investigated to account for the barrier origin. It was found that the energy of the π^* orbital of $\mathrm{CO_2}$ moiety is not affected by the solvation so much, while that of $\mathrm{OH^-}$ orbital is considerably lowered. In consequence the energy gap increases in solution than that in the gas phase, causing the reduction of the reactivity. The free energy profile was then investigated in terms of solvation structure. The peak heights dramatically change as the reaction progresses: the peak of $\mathrm{O_{hydrx}}$–$\mathrm{H_W}$ is rapidly lowered and that of $\mathrm{O_{crbn}}$–$\mathrm{H_W}$ is enhanced as the two species approach each other. The interplay of hydration and dehydration plays important roles governing the free energy change along the reaction.

In chapter 2, the bonding mechanism between carbon dioxide and monoethanolamine was studied. In gas phase, the energy monotonically increases at shorter region due to the repulsive

interaction derived from *Pauli*'s principle. On the other hand, in aqueous solution, after the formation of intermediate similar to gas phase, stable structure is found at bonding region via the transition state. To clarify the mechanism of bond formation, the change of electronic structure was analyzed in terms of resonance structure. It was found that the bond formation significantly affects the electronic structure. The ionic character of CO_2 moiety is especially enhanced by the bond formation while the double bond character is considerably reduced. In terms of molecular orbital, the change corresponds to the electron transfer from N lone pair to CO_2 π^* orbital. The character of C$\cdots$N bond is remarkably changes by solvation: the C^+ N^- ionic weight is the most dominant in gas phase whereas (C–N) is the most dominant in aqueous solution. This result indicates that solvation effect induces the bond formation. The change of solvation structure was then investigated to clarify the role of solvation. It was found that the bond formation step is understood as an interplay between the solvation around O_{cdx} and the desolvation around N. The strong solvation around O_{cdx} is surely consistent with the charge transfer to O_{cdx}, suggesting that solvation promotes the bond formation.

In chapter 3, the proton transfer after the bond formation was studied. It was shown that MEA acts as the base. By investigating the role of solvation, it is found that the hydration around O_{cdx} significantly drives the stabilization of the final product. The strong interaction between O_{cdx} and H_W could be understood by the dominative resonance character of C^+_{cdx} O^-_{cdx}.

In chapter 4, the orbital energy shift by solvation effect was studied to systematically understand the mechanism of the shift. With the aid of dielectric continuum theory, several simple formulae were developed to rationalize the orbital energy shifts. The developed formulae are valid to explain both for PCM and RISM-SCF-SEDD computations, indicating the discussion in this study is a common consequence to understand the electronic structure of solvated molecule, being independent of the choice of theory for solvation. For charged system, Born-type treatment is acceptable to estimate the energy shift. At the same time, approximated formulae based on the Onsager-type model are satisfactory for examined 265 molecular orbitals of neutral species. It was found that both of the spatial distribution of molecular orbital

and electrostatic field generated by surrounding solvent are important to determine the orbital energy shift. Ionization potential of several atomic species in aqueous solution was investigated based on the Born-like approximated formula with Koopmans' theorem. The derived formula shows good accordance with experiments although there is a few deviation. By further simplification, it is clarified that the shift must be attributed to the interaction between the i-th orbital dipole moment ($\boldsymbol{\mu}_i$) and total dipole moment of the molecule ($\boldsymbol{\mu}^0$),

In chapter 5, ionization in solution phase was studied. To clarify the ionization process in solution phase, the free energy surface was introduced, and the role of solvation was discussed based on the surface. To treat the vertical ionization, fast component and slow component of solute-solvent interaction was divided with the aid of dielectric continuum theory, and thereby a semi-empirical formula was proposed. The computed values of ionization energy are well agree with experimental measurements. The solvation before ionization mainly determines the change of vertical ionization energy. However, the fast component of solvent induced by the ionization also has non-negligible contribution. Especially, the change of ionization energy of H_2O is mainly determined by the fast component. On the other hand, the change of solvation structure significantly contributes to the change of the adiabatic ionization energy.

The dielectric continuum theory was then utilized to obtain the insight into the change of energy in terms of the property of solute. The obtained equation well rationalizes the experimental results in terms of dependency on solute size and charge. The spectral width of the vertical ionization was also studied using the linear response approximation. The calculated widths were well in accord with the experimental values. The simple equation based on Born's formula for the width was then proposed. This equation indicates the width should be increased as the decrease of the solute size. The size dependency given by the equation is, to say the least, well consistent with the theoretical results.

In chapter 6, the 2D-RISM equation for solvation structure near solid-liquid interface was developed in order to grasp the feature of solvation near the interface, namely anisotropy. The derived equation describes the anisotropic solvation structure by using the 2D density distribution in the cylindrical coordinate system. The 2D-RISM equation was then combined with the

polymer-RISM equation to treat the solvation near the wall consisting of atomic sites in a 2D-periodic array. The model system was studied as the first application. It was shown that water molecules in the first solvation shell are preferably adsorbed on hollow and/or bridge positions than on-top positions whereas those in the second solvation shell do not show any specific preference. A new peak appears in the first solvation shell upon charging the wall, indicating that the contribution from another orientational configuration also becomes visible by the applied electric field. This change is assigned as follows: O-H bond is directed perpendicular to the negatively charged wall.

In this thesis, the author studied chemical process in solution focusing on the molecular orbital and solvation structure. The mechanism of the process was then systematically understood in terms of the molecular property of solute and solvent. The author believes that the insight obtained in this study will contribute as the guideline to understand the process in solution for a long time.

List of Publications

Publications included in this thesis

Chapter 1

”The barrier origin on the reaction of CO_2+OH^- in aqueous solution”

Kenji Iida, Daisuke Yokogawa, Hirofumi Sato, Shigeyoshi Sakaki

Chem. Phys. Lett. **2007**, *443*, 264-268.

Chapter 2

”Carbon dioxide capture at the molecular level”

Kenji Iida, Daisuke Yokogawa, Atsushi Ikeda, Hirofumi Sato, Shigeyoshi Sakaki

Phys. Chem. Chem. Phys. **2009**, *11*, 8556-8559.

Chapter 3

”Proton Transfer Step in the Carbon Dioxide Capture by Monoethanol Amine: A Theoretical Study at the Molecular Level”

Kenji Iida, Hirofumi Sato

J. Phys. Chem. B, *in press*.

Chapter 4

”A systematic understanding of orbital energy shift in polar solvent”

Kenji Iida, Daisuke Yokogawa, Hirofumi Sato, Shigeyoshi Sakaki

J. Chem. Phys. **2009**, *130*, 044107.

Chapter 5

”Theoretical study on ionization process in aqueous solution”

Kenji Iida, Hirofumi Sato

Submitted.

Chapter 6

”A two-dimensional-reference interaction site model theory for solvation structure near solid-liquid interface”

Kenji Iida, Hirofumi Sato

J. Chem. Phys. **2011**, *135*, 244702.